THE UNIVERSITY OF MANITOBA

POWER METHODS OF INVESTIGATING BILINEAR HYSTERESIS

by

K. H. MA

A Thesis

SUBMITTED TO THE FACULTY OF GRADUATE STUDIES
IN PARTIAL FULFILMENT OF THE REQUIREMENTS FOR THE DEGREE OF

DOCTOR OF PHILOSOPHY

DEPARTMENT OF CIVIL ENGINEERING

WINNIPEG, MANITOBA

AUGUST 1980

POWER METHODS OF INVESTIGATING BILINEAR HYSTERESIS

by

KING HUNG MA

A thesis submitted to the Faculty of Graduate Studies of
the University of Manitoba in partial fulfillment of the requirements
of the degree of

DOCTOR OF PHILOSOPHY

ACKNOWLEDGEMENTS

The author would like to express his sincere appreciation to his adviser, Dr. A.H. Shah, for his encouragement and suggestions rendered during the preparation of this thesis.

The suggestions and assistance given by Dr. K.R. McLachlan were invaluable. Discussion with him is always inspirational. His profound interest in this work is gratefully acknowledged.

Thanks are also due to Dr. N. Popplewell, who at various stages, gave the author valuable ideas and comments.

The author would like also to thank his wife, Ellen, for her understanding and moral support.

Appreciation is also extended to Mr. J. Clark, machinist, and Mrs. V. Ring for typing this manuscript.

Finally, the author wishes to thank the University of Manitoba for the financial support in the form of a post-graduate fellowship.

TO

E L L E N

TABLE OF CONTENTS

LIST OF TABLES

LIST OF FIGURES

LIST OF SYMBOLS

a_i	accelerometer
A_i	Amplifier
B	magnetic flux density
c, c_i	viscous damping coefficients
c_{ij}	viscous damping influence coefficient
C_i	modal viscous damping coefficient
C_o	effective damping coefficient
C_i^*	function of modal damping coefficient
D_i	diode
erf,erfc	error and complementary error functions
E	expected value of
f, f_i	frequencies in Hertz
f_c	central frequency
f_o	small amplitude natural frequency
f^*	mean frequency of yielding
F_{12}	bandwidth ratio
$g(y,\dot{y})$	bilinear hysteretic restoring force
$g(y)$	bilinear nonhysteretic restoring force
g_o	yield force level of bilinear hysteretic element
G	Covariance matrix of system responses
$H(j\omega)$	complex frequency response function
Hz	Hertz (cycle/second)
i	integer, current
j	integer, $\sqrt{-1}$

k, k_i	spring constants, integer
K_i	modal stiffness coefficient
l	integer
L	total length of wire in magnetic field
m, m_i	masses
M_i	generalized mass of the i-th mode
n	number of degrees of freedom
p, p_i	forcing functions
p_o	$\equiv g_o$ in the case of an hysteretic element
P_i	generalized force of the i-th mode
$pr( )$	probability density function
r	integer
R	resistance
$R_{yy(\tau)}$	autocorrelation function (of displacement)
$R_{p\dot{y}(\tau)}$	cross-correlation function (of force and velocity)
S	constant power spectral density
t, t_i	time
T	matrix transposition when used as a superscript
v	voltage
VR_i	variable resistance
W	power ratio
y, y_i	displacements
Y_i	generalized displacement of the i-th mode
$\dot{y}, \dot{y}_i$	velocities
$\dot{Y}_i$	generalized velocity of the i-th mode
$\ddot{y}, \ddot{y}_i$	accelerations

$\ddot{Y}_i$	generalized acceleration of the i-th mode
y_o	yield displacement
y^*	mean peak values beyond y_o for a Gaussian process
$\ddot{y}_G$	ground acceleration
α	ratio of yielding state stiffness to non-yielding state stiffness of a bilinear hysteretic element
ϵ	a small parameter specifying the degree of nonlinearity
Δf	bandwidth of signal from idealized filter; effective bandwidth
$\overline{\Delta f}$	filter bandwidth
η	loss factor
ξ	damping ratio
σ	root-mean-square value; standard deviation
τ	delay time
ϕ_{ij}	element of free vibration undamped mode shape matrix
ψ_{ij}	element of the inverted mode shape matrix
ω, ω_i	radian frequencies
ω_c	central frequency in radian/sec
ω_o	small amplitude natural radian frequency
$\{\ \}$	vector
$[\ ]$	matrix
$\overline{\quad}$	time average

ABSTRACT

The study of a bilinear hysteretic system subjected to stationary random excitation in the highly nonlinear region with special regard to the system's energy loss behavior is presented. Traditional methods such as the treatment of a system as an equivalent linear system with viscous damping have been avoided. Recognizing the fact that the energy loss parameter of an hysteretic system is response dependent, the power ratio is introduced as a measure of loss. The power ratio is defined as the true power dissipation to the apparent power supplied to the system, thus involving the forcing function and the response in its definition. As only a ratio of power is involved, it may be applied with equal validity to linear and nonlinear systems to express a measure of loss similar to that of the damping ratio.

The relationship between the power ratio and damping ratio is first established with the aid of several linear systems. Results for a nonlinear nonhysteretic system are given to show that useful results can be obtained in a strongly nonlinear case with known viscous damping. Theoretical results are validated with results from a physical model.

The essence of hysteresis is discussed using an isolated bilinear hysteretic element. In this case, displacement is the input and the restoring force of the element is the response. Theoretical results of power ratio are shown validated by means of both a physical-analog model and a digital simulation program. Plots of power ratio versus different element parameters and input parameters are presented for periodic and

random input waveforms. The dependence of the hysteretic element upon the form factor of the input displacement waveform is indicated. The meaning of power ratio as a lost effectiveness factor is also established.

Extension of the hysteretic element to include a single mass, thus forming a single degree of freedom bilinear hysteretic system is made. The input quantity in this case is the force acting on the mass. Plots of power ratio obtained by digital simulation of the system are presented. Owing to the addition of an inertia force, the effect of force waveform dependency is less significant. In this case, a peak power ratio is obtained which corresponds to resonance of the system. It is shown that the natural frequency of the small amplitude response has a significant effect on the performance of a system subjected to narrow-band excitation. For broad-band excitation, this effect is less pronounced.

The work outlined in this thesis explored the energy loss behavior of a bilinear hysteretic mechanism with the use of power ratio, over a wide range of input and output parameters. Such a mechanism governs the performance of a system under structural overload, hence, the understanding of the hysteretic mechanism may find application in the design of force limiting and loss producing elements in civil engineering structures. Such elements may be installed at suitable locations to provide controllable and self repairing yielding. In this way, major damage in the structure may be avoided.

CHAPTER I

INTRODUCTION

1.1 INTRODUCTION

In structural dynamics the three elements which govern the performance of a system are mass, stiffness and damping. The mass (inertia) and stiffness (elastic) elements alone permit the storage of energy in kinetic and potential form and the process of exchange between these two forms of energy under dynamic conditions is the basis of much of our understanding of vibrating systems. This exchange of energy is, of course, loss-less and the total energy in the vibrating system at any time will depend solely on the amount gained from an external source. The addition of damping elements allows us to account for energy loss from the system and brings the analysis into accord with the physical behavior of linear vibrating structural systems. Energy loss may take place through losses into the surrounding medium (ambient damping), internal damping (material damping) and friction at connections (interface damping). While the properties of the mass and stiffness elements of a system can be estimated readily from a knowledge of geometrical configuration, material properties and system natural frequencies, the property of the energy loss element is not so clear-cut and is still the subject of extensive investigation [1,2,3].

Most analytical work in structural dynamics has assumed the systems to be linear so that the principle of superposition is valid and modal analysis of multi-degree of freedom systems can be performed. In

line with these assumptions, the damping elements are often ascribed the "linear viscous" form in which the velocity in an element is proportional to the force applied to that element. This idealization offers great mathematical simplicity and, in most cases, gives a satisfactory description of the performance of a system as long as the amplitude of vibration is small. In civil engineering, cases of severe excitation such as earthquake, blast and wind, occur and a structure may be driven beyond its linear limit at large amplitudes of vibration. Such nonlinear behavior may be due to the nonlinear stress-strain relationship of the material, or a similar phenomenon arising from Coulomb friction between sliding surfaces. Furthering the understanding of the behavior of structures under such nonlinear conditions is the primary objective of the work reported in this thesis.

If the nonlinearity in the structure is small, the system can be modelled adequately as an equivalent linear system having "equivalent viscous damping" [2,4,5]. As the degree of nonlinearity increases, viscous damping alone can no longer describe the energy-loss mechanism of the system because energy loss due to hysteresis becomes significant.

Hysteresis is an energy-loss mechanism which depends on the past history of the system. Hysteresis may be due to the presence of Coulomb friction in the system, or it may be due to the elasto-plastic behavior of the material in the system. One simplified model of hysteresis and one which allows adequate description of this effect is bilinear hysteresis (Figure 1.1). This bilinear model is a good approximation to the energy loss behavior in many civil engineering structures during overload [4].

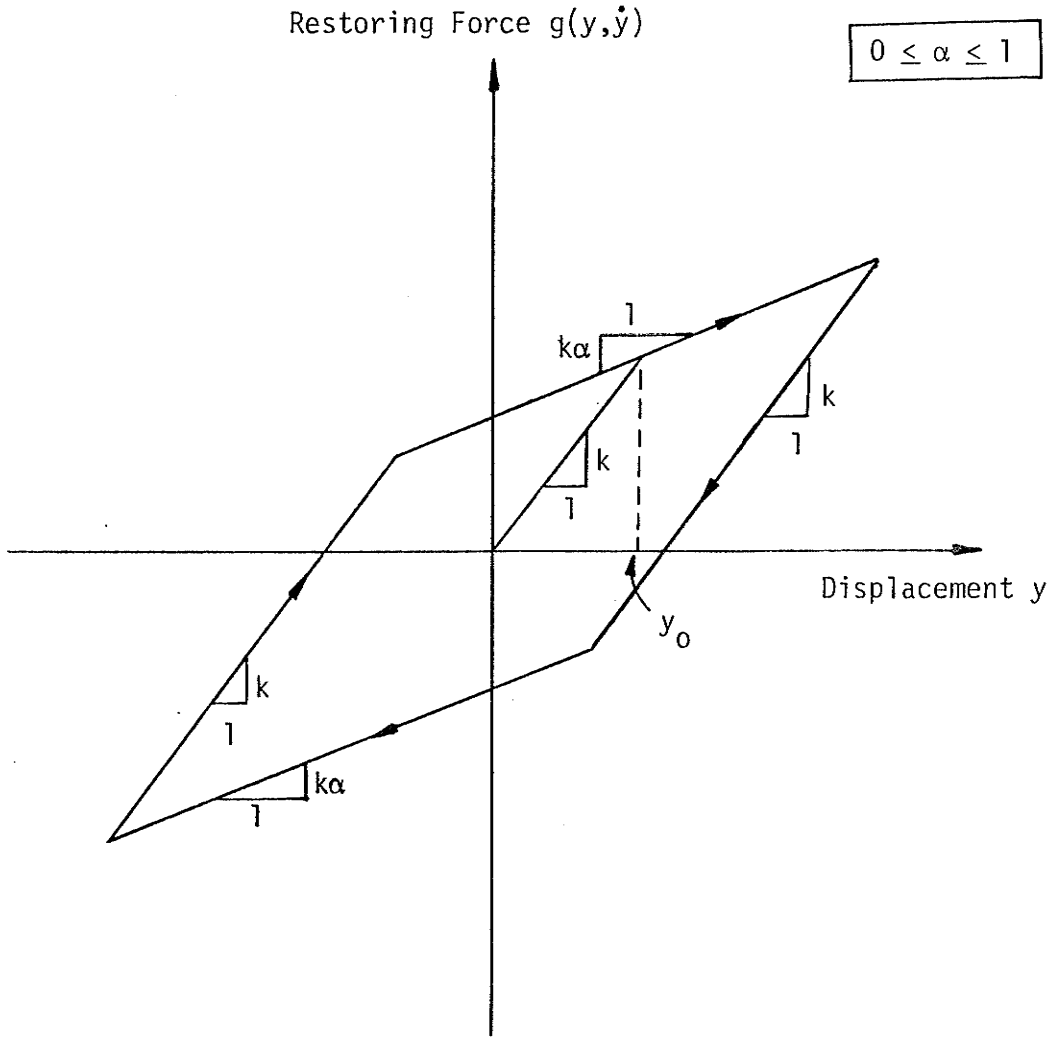

Figure 1.1 Restoring Force-Displacement Relationship of a Bilinear Hysteretic Element

Figure 1.1 shows the restoring force g of a bilinear hysteretic element versus displacement y. The nature of bilinear hysteresis is such that the restoring force-displacement slope relationships will always be either k or kα. The slope k corresponds to a non-yielding state whereas kα corresponds to a yielding state. Which of these two slopes holds under any circumstances depends solely on whether local yield has been or is about to be exceeded. The particular starting point for either slope will depend entirely on the past history of yielding. Accordingly, the element is nonelastic and a loop is described for a complete cycle of oscillation. This loop is called the hysteretic loop. It is interesting to note that the amount of energy dissipated by the element over the cycle is proportional to the area enclosed within the hysteretic loop. Hence, the energy loss in an hysteretic element depends upon how it is forced. All these properties of hysteresis, namely, history dependency, force dependency and the ability to dissipate energy, together with the invalidity of the principle of superposition, make the study of hysteretic system both stimulating and fascinating.

This thesis presents the study of a bilinear hysteretic system in the highly nonlinear region with special regard to the system's energy loss behavior.

1.2 OUTLINE OF METHODS OF ANALYSIS IN STRUCTURAL DYNAMICS

1.2(i) Linear Systems

Perhaps the best known and simplest kind of problem in structural dynamics is the analysis of a lumped-mass, viscously damped, one degree of freedom (1-DOF) linear system subjected to deterministic loading. The

approaches for solving this problem, one in the time domain and one in the frequency domain, are standard [6,7,8,9]. In the time domain, the response (such as displacement) of the system to a unit impulse, generally referred to as the unit-impulse response function, is first established. The system displacement responses are then evaluated by using the Duhamel integral, which is the convolution of the forcing function and the corresponding unit-impulse response function. In the frequency domain approach, the forcing function is first resolved into an infinite sum of harmonic components. The displacement of the system to a unit harmonic component, called the complex frequency response function, is then established. The system displacement responses are obtained by integrating the product of the harmonic force component and the complex frequency response function, over the entire frequency range.

In both of the above approaches, the integration processes are possible because the principle of superposition holds. If the system is strictly linear but has n degrees of freedom (n-DOF), it can be treated, through proper transformation of coordinates, as n, independent, 1-DOF systems, provided that the system exhibits a Rayleigh type of viscous damping [6].

In many cases, such as wind and earthquake loading, the assumption of periodic forcing is unsatisfactory and interest turns to the analysis of linear systems subject to random loading. In these cases, system responses are also random and statistical descriptions of the loading and responses are more meaningful than time-history descriptions. The appropriate statistical descriptions and the techniques for deriving them are well documented [6,10,11,12,13,14], and, hence, only one example is

given here to illustrate these techniques. The chosen example is that of the mean square displacement response to stationary random excitation, using both time domain and frequency domain approaches.

In the time domain, the autocorrelation of displacement, defined as the expected value of the product of displacement at zero time delay and the displacement after delay of τ seconds, is obtained by applying the Duhamel integral twice and taking the expected value of the resulting integral. The autocorrelation of displacement is then expressed in terms of the autocorrelation of the forcing function and the unit-impulse response function of the system. By setting τ to zero in the expression for the autocorrelation of the displacement and integrating twice over the entire time domain, the mean square displacement is obtained.

In the frequency domain approach, the displacement autocorrelation function is decomposed into an infinite sum of frequency components, the amplitude of which is called the displacement power spectral density. The displacement power spectral density and the autocorrelation function form a Fourier transform pair [10]. The former, and hence the latter quantity, can be expressed in terms of the complex frequency response function and the power spectral density of the forcing function. The mean square displacement is obtained by setting τ to zero in the expression for the displacement autocorrelation and integrating over the entire frequency domain.

In addition to the direct process of determining the response of a system from knowledge of its passive parameters and the forcing to which it is subjected, attention has also been given to determining system parameters from measured responses to known forcing functions [15,16].

Interest in this inverse problem stems mainly from the lack of knowledge of the contribution made by the many and varied forms of damping mechanisms that exist in a typical civil engineering structure. As with the direct problem, the inverse solutions may be obtained using either the time domain or the frequency domain approach.

In the frequency domain approach [17,18,19], response data are measured for a collection of frequency points. The system parameters are then evaluated by processing these response measurements, one data point at a time, together with the known system data, using a recursive least square technique. In the time domain approach, the response measurements for some time points are taken, the system parameters are then obtained by processing these response data, one data point at a time, together with the known system data, using either the recursive least square technique [20], or the maximum likelihood technique [21]. In employing the least squares technique, appropriate weighting matrices may be incorporated into the least square algorithm to account for the random nature of test data and the structural model parameters [15]. These techniques involve very large data processing time if a large collection of data points are taken.

1.2(ii) Nonlinear Systems

From the foregoing résumé of techniques for analyzing the vibration of linear structures, the main difficulty in attempting similar analysis for nonlinear structures becomes clear, namely, that the superposition theorem is violated. The ramifications of this violation are, firstly, that the total response of a structure cannot be obtained as a summation of responses to different forcing functions, and, secondly, that

the analysis of multidegree of freedom systems cannot employ modal techniques. Another difficulty in attempting a linear approach for nonlinear structures is the assumption of viscous damping. Viscous damping is described usually by the viscous damping ratio, which is obtained by comparing the energy loss in a cycle with the peak potential energy stored in the system during that cycle. From the performance point of view, the damping ratio is a very important parameter in linear structures because it is this ratio which governs the maximum response of a structure. However, the damping ratio is a constant derived from the parameters of a linear system, hence its application in nonlinear hysteretic structures is limited because the energy loss parameters in such structures are response dependent.

If the excitation is deterministic, a nonlinear structure can be analyzed using either the step-by-step numerical integration [6,7] or the graphical method [7,22]. Step-by-step numerical integration is a widely used technique in solving nonlinear deterministic problems in civil engineering, hence, only this method is illustrated here.

The essence of step-by-step numerical integration is the approximation of the nonlinear system as a sequence of successively changing linear systems, each existing for an equal time step. The system nonlinearity is accounted for by using new properties to correspond with the deformed state at the beginning of each time step. Dynamic equilibrium is established at the beginning of the time step and the motion of the system during the time step is evaluated on the basis of an assumed response mechanism. The responses computed at the end of a time step are used as initial conditions for the next step, thus the process can

be continued step-by-step for any desired time. This technique deals with all kinds of nonlinearities and gives satisfactory results providing the time step is small enough to account for the rate of variation of loading, nonlinear damping and stiffness properties. In general, the variation of material property is not a critical factor in choosing the integration time step; if a significant sudden change takes place, as in the yielding of a hysteretic spring, a special subdivided time step may be introduced to treat this effect accurately. It is found that the time step needs to be much smaller than the vibration period of the system if stable results are to be obtained.

The step-by-step and graphical methods depend upon having a deterministic forcing of the system. Hence, the search for methods of analyzing nonlinear systems subjected to random excitation becomes important when earthquake and similar loadings are of interest. Unfortunately, there appears to be no widely accepted method of analysis in this area which is at all comparable to that developed for the analysis of linear systems. While the techniques for analyzing these nonlinear systems are not yet well developed, there are several approaches available which can treat a small class of problems quite adequately. They are, the Fokker-Planck equation, the perturbation method, the power balance method and the equivalent linearization approach.

In applying the Fokker-Planck equation [23,13], an exact solution can be obtained for a nonlinear nonhysteretic system in which the damping forces are proportional to the velocity. The excitation needs to be a Gaussian white noise. If all of these conditions are satisfied, the solution to the Fokker-Planck equation gives the transitional probability

density function of the velocity and displacement responses. Various response statistics such as the mean square displacement and the frequency of crossing of the displacement across a certain level can be determined. However, the restoring force needs to be a single-valued function of the displacement, hence, this approach cannot be used to treat an hysteretic system.

In the perturbation approach [24,25,22,13], the displacement response is represented as an expansion in powers of a parameter ε (assumed small), which specifies the size of the nonlinearity of the system. Substituting the assumed expansion into the equation of motion of the system and equating coefficients of like powers of ε yields a set of linear differential equations for the terms in the assumed expansion. A first-order approximation is obtained by neglecting terms of order ε^2 and higher in the expansion, hence, only two linear differential equations need be considered. Response statistics of the nonlinear system are obtained from the cross statistics of the linear differential equations. This approach is restricted to a weakly nonlinear system. Also, the system must contain some finite value of viscous damping to make the solution of the first linear differential equation bounded.

The power balance approach [26,27,28], on the other hand, involves a balance of power supplied to the system by the environment and power dissipated in hysteresis effects. The average power input can be readily evaluated [26] for Gaussian, white, broad-band random forcing. The hysteretic power dissipation is obtained by multiplying the average energy dissipation per cycle (area within the hysteretic loop) and the average frequency of the response displacement waveform which is restricted to be a Gaussian narrow-band process with Rayleigh distribution of peaks.

The mean square displacement can then be evaluated from the power balance equation.

The equivalent linearization approach [4,5,29,30,32] is perhaps the most commonly used among the approximate methods of analyzing nonlinear structural systems to random excitations. In [4,5], the method of equivalent linearization of Krylov and Bogoliubov [43] is extended to deal with stationary Gaussian excitation. The nonlinear hysteretic system is rewritten as a linear system having equivalent viscous damping and stiffness parameters. These parameters are chosen to minimize the mean square difference between the nonlinear and linear equations. The motion must be narrow-band with Rayleigh distribution of peaks, so that only lightly damped and weakly nonlinear system can be considered. Alternatively, an equivalent linear system may be chosen such that some statistical measures between the nonlinear and the equivalent linear system are matched. In [29], methods of matching displacement, matching velocity, matching displacement and velocity, and matching response power spectral density are proposed. Highly nonlinear systems may be considered but it appears that different equivalent linear systems are found when different response statistics are considered.

Most work to date in nonlinear structural dynamics assumes the displacement response of the system to Gaussian excitation to be narrow-band, Gaussianly distributed with Rayleigh distribution of peaks. These assumptions become progressively less acceptable as any system is driven into the highly nonlinear response regime. The displacement response in such a highly nonlinear system will in general be non-Gaussian and will cover a bandwidth in excess of the excitation bandwidth. Hence, the ex-

isting methods mentioned are inadequate for the treatment of highly nonlinear systems. Filling this gap in the field of structural dynamics is, of course, a major undertaking and contributions from many sources will be required. Most notably, it is felt that contributions which help to break free from "linear" or "near linear" thinking will be most fruitful in filling this gap. The purpose of the present work, then, is to consider particular problems such as the energy loss behavior of a bilinear hysteretic system, without placing constraints on its degree of nonlinearity.

The consideration of power in structural dynamic systems is not new. Many investigators [33,34,35,36,37] have employed the concept of average power in the evaluation of power flow between resonators. The evaluation of mean square displacement from a knowledge of the power balance in the system was done in [26,27]. In [38], a procedure was formulated for the evaluation of mean square responses when complete system information and average power input are known. All the above work involves the consideration of power or mean square responses. However, these quantities have not been employed in defining the energy-loss property of a nonlinear system. One of the features offered as new in the present work is the introduction of power ratio as an energy loss effectiveness factor in structural systems. Power ratio is obtained by comparing the average power dissipation to the apparent power input to the system, and, hence, it performs a role similar to that of the damping ratio.

CHAPTER II

ANALYSIS OF VISCOUS DAMPING IN LINEAR SYSTEMS USING POWER EQUATIONS

2.1 INTRODUCTION

To gain familiarity with the use of power in considering structural systems, several linear systems with viscous damping were first investigated. In each case, the forcing of the system was assumed to be a random time function. This work offered some interesting insights into the use of the power method generally and, in particular, laid the groundwork for the validation of power ratio in the assessment of linear and nonlinear vibrating systems.

2.2 GENERAL POWER EQUATIONS

Consider an n-DOF linear system as shown in Figure 2.1(a) which is an idealization of the shear structure shown in Figure 2.1(b). The equation of motion of this system is

$$[m]\{\ddot{y}\} + [c]\{\dot{y}\} + [k]\{y\} = \{p\} \ , \qquad (2.1)$$

where [m], [c] and [k] are the system's (n x n) mass, viscous damping and stiffness matrices respectively. The {y}, {$\dot{y}$} and {$\ddot{y}$} are the (n x 1) displacement, velocity and acceleration vector, and {p} is a (n x 1) load vector. Postmultiplying each term of equation (2.1) by the row vector $\{\dot{y}\}^T$ (superscript T denotes transposition) and taking expected value (ensemble average) of the entire ensemble, equation (2.1) becomes

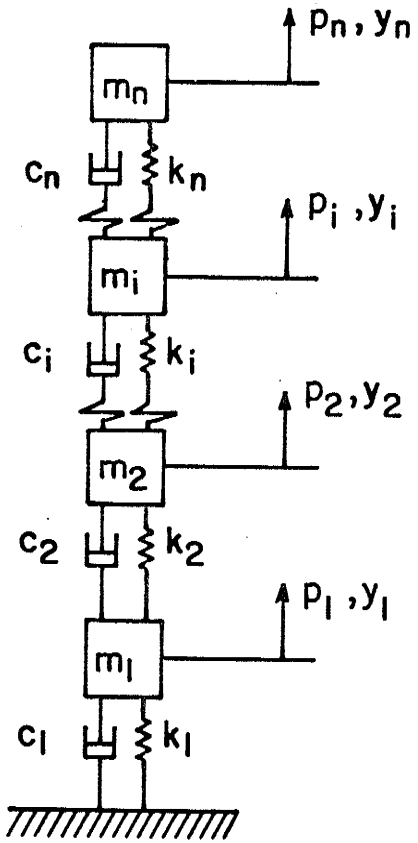

(a) Idealization

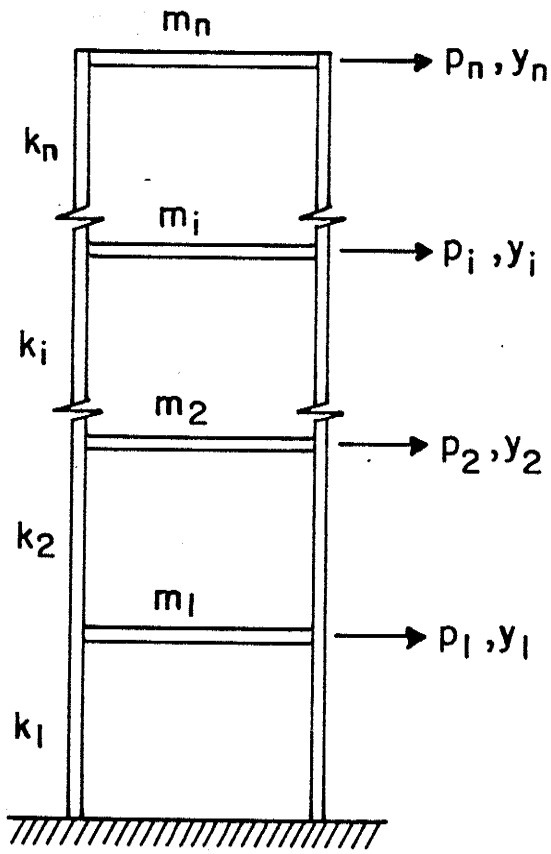

(b) Real Structure (Shear Building)

Figure 2.1 Multi-Degree of Freedom Linear System

$$[m]E[\ddot{y}\dot{y}^T] + [c]E[\dot{y}\dot{y}^T] + [k]E[y\dot{y}^T] = E[p\dot{y}^T] \ , \qquad (2.2)$$

where E denotes expected value; $E[\ddot{y}\dot{y}^T]$, $E[\dot{y}\dot{y}^T]$, $E[y\dot{y}^T]$, and $E[p\dot{y}^T]$ are the system's (n x n) zero-lag covariance matrices. If the loading vector is restricted to be stationary and ergodic, so then are the responses [12]. Hence, replacing the expected values in equation (2.2) by the time averages, equation (2.2) becomes

$$[m]\overline{[\ddot{y}\dot{y}^T]} + [c]\overline{[\dot{y}\dot{y}^T]} + [k]\ \overline{[y\dot{y}^T]} = \overline{[p\dot{y}^T]} \ , \qquad (2.3)$$

where $\overline{}$ denotes a time average quantity.

Each term in equation (2.3) has the dimension of power, hence, equation (2.3) is referred to as the power equation of the system. If the excitation force {p} is assumed to act on one mass then $\frac{n}{2}(3n+1)^{\dagger}$ measurements are required to form the mean product matrices $\overline{[\ddot{y}\dot{y}^T]}$, $\overline{[\dot{y}\dot{y}^T]}$, $\overline{[y\dot{y}^T]}$ and $\overline{[p\dot{y}^T]}$. If [m] and [k] in equation (2.3) are known then [c] can be evaluated if $\overline{[\dot{y}\dot{y}^T]}$ is nonsingular.

In many circumstances it is desirable to eliminate displacement {y} as quantities to be measured, because the direct measurement of displacement in full scale structure is impracticable (see Appendix A). Hence, premultiplying equation (2.3) by $[k]^{-1}$ (assuming the inverse exists), adding to the resulting equation its transposed equation and using the relations,

$$\overline{[y\dot{y}^T]} = - \overline{[\dot{y}y^T]} \ ,$$

$$\overline{[\ddot{y}\dot{y}^T]} = - \overline{[\dot{y}\ddot{y}^T]} \ ,$$

---

† As a result of stationarity [40], $\overline{[y\dot{y}^T]}$ and $\overline{[\ddot{y}\dot{y}^T]}$ are anti-symmetrical and each contains n(n - 1)/2 distinct elements. $\overline{[\dot{y}\dot{y}^T]}$ is symmetrical and contains n(n + 1)/2 distinct elements. $\overline{[p\dot{y}^T]}$ contains n distinct elements.

equation (2.3) becomes

$$[k]^{-1}[c][\overline{\dot{y}\dot{y}^T}] + [\overline{\dot{y}\dot{y}^T}][c][k]^{-1} = [k]^{-1}[\overline{p\dot{y}^T}] + [\overline{\dot{y}p^T}][k]^{-1}$$
$$- [k]^{-1}[m][\overline{\ddot{y}\dot{y}^T}] - [\overline{\dot{y}\ddot{y}^T}][m][k]^{-1} \quad . \tag{2.4}$$

Since the matrix $[\overline{y\dot{y}^T}]$ is eliminated, the required number of measurements are reduced to $n(n+1)$. [c] is symmmetrical and generally contains $n(n+1)/2$ unknowns. The resultant matrix on each side of equation (2.4) is also symmetrical so that $n(n+1)/2$ independent linear equations can be obtained for the evaluation of [c].

A precise evaluation of $[\overline{\ddot{y}\dot{y}^T}]$ may prove difficult in practice because of possible phase shift errors between the acceleration and the derived velocity (see Appendix A), but the need to evaluate these quantities can be avoided by reformulating the equations of motion into the modal power equations.

2.3 MODAL POWER EQUATIONS

2.3(i) Broad-band Excitation

Consider the equations of motion as given by equation (2.1), and let

$$\{y\} = [\phi]\{Y\} \quad , \tag{2.5}$$

be the expression which transforms the generalized coordinates {Y} of the system to the geometrical displacement coordinates {y}. $[\phi]$ is the undamped free vibration mode shape matrix. Substituting equation (2.5) and its derivatives into equation (2.1), premultiplying the resultant eqauation by $[\phi]^T$, and assuming the damping to be Rayleigh [6], the following modal equaitons are obtained.

$$M_i \ddot{Y}_i + C_i \dot{Y}_i + K_i Y_i = P_i \ , \ i = 1,n \ , \tag{2.6}$$

where

$[M] = [\phi]^T[m][\phi]$, $[C] = [\phi]^T[c][\phi]$ and

$[K] = [\phi]^T[k][\phi]$ are diagonal generalized mass, damping and stiffness matrices, respectively, and

$$\{P\} = [\phi]^T\{p\} \ , \tag{2.7}$$

is the generalized load vector.

Multiplying equation (2.6) by $\dot{Y}_i$ and taking time averages, the modal dampings are given as

$$C_i = \frac{\overline{P_i \dot{Y}_i}}{\overline{\dot{Y}_i^2}} \ , \quad i = 1,n \ . \tag{2.8}$$

If the excitation acts only on the r-th mass then, in the geometric coordinates, the modal damping C_i is

$$C_i = \frac{\overline{\phi_{ri} \, p_r \sum_j \psi_{ij} \dot{Y}_j}}{\sum\sum_{jk} \psi_{ij} \psi_{ik} \dot{Y}_j \dot{Y}_k} \ , \ (i,j,k = 1,n) \ , \tag{2.9}$$

where $[\psi] = [\phi]^{-1}$. If the damping is not Rayleigh, then the matrix [C] will not be diagonal and the C_i as given by equation (2.9) is the 'equivalent' modal damping coefficient which causes the same amount of dissipation as the original mode.

The modal damping of equation (2.9) depends only on the matrices $\overline{[\dot{y}\dot{y}^T]}$ and $\overline{[p\dot{y}^T]}$, the number of measurements required is reduced significantly to $n(n+3)/2$. As will be seen in the next sub-section, the number of measurements may further be reduced by exciting a particular mode of the system.

2.3 (ii) Band-Limited Excitation

For an n-DOF system, assume that the system has n distinct modes with modal frequencies $f_1, f_2, \ldots, f_i, \ldots f_n$ as shown in Figure 2.2. Suppose that the system is excited by a force p which has a frequency bandwidth†, Δf, centered at the i-th modal frequency, f_i, such that Δf does not envelop the frequency bands of other modes. This can be considered as an i-th mode excitation. Hence, if the excitation force p acts only on the r-th mass, then from equation (2.5) and (2.7),

$$\left.\begin{aligned} y_r &= \phi_{ri}\, Y_i \\ \text{and} \qquad & \\ P_i &= \phi_{ri}\, p_r \end{aligned}\right\} \quad (2.10)$$

By introducing equation (2.10) and its derivative in equation (2.8), the modal damping of the i-th mode becomes

$$C_i = \phi_{ri}^2 \frac{\overline{p_r\, \dot{y}_r}}{\overline{\dot{y}_r^2}} \quad . \qquad (2.11)$$

In equation (2.11), $\overline{p_r\, \dot{y}_r}$ is the mean power and $\overline{\dot{y}_r^2}$ is the mean square velocity measured at the location of the forcing. Each value of modal damping depends only on two measurements.

It has been shown that structural damping can be evaluated by using various forms of the power equations. All assume stationary ergodic forcing functions. The first of the formualations, equation (2.3), allows the complete damping matrix to be determined but requires

---

† The force is assumed to be ideally filtered so that there is no frequency component outside Δf.

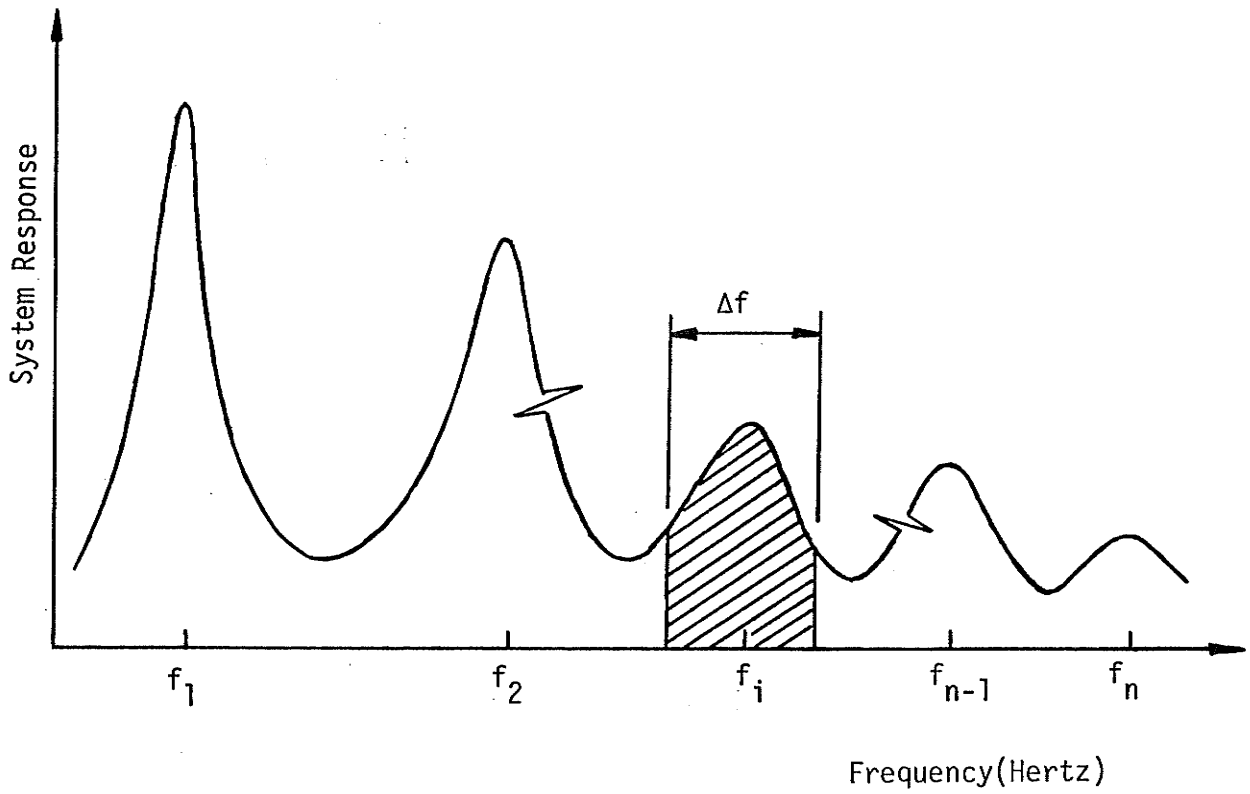

Figure 2.2 System Response Versus Frequency for a Linear System With Distinct Modes

the evaluation of a large number of covariances. Displacement measurements are also required. The second, equation (2.4), eliminates the need for displacement measurements but still relies upon the evaluation of a large number of covariances, and the matrix $[\overline{\ddot{y}\dot{y}^T}]$ which is very sensitive to measurement errors. The third, equation (2.8), eliminates the evaluation of $[\overline{\ddot{y}\dot{y}^T}]$, but yields only the modal damping if the modes are distinct, otherwise it yields 'equivalent' modal damping. The last, equation (2.11), needs only the variance and power measurements for the evaluation of the modal damping, but can be applied meaningfully only to a system which has distinct modes.

2.4 EXPERIMENTAL SET-UP AND DISCUSSIONS

A 3-DOF structural model was constructed and a computer simulation program for linear systems compiled to validate the results of this chapter. Photographs of the model and the measuring system are shown in Figures 2.3 and 2.4. Further reference is made to the model and to the linear simulation program in Appendixes A and B respectively.

The work presented in this chapter offers an alternative to the evaluation of viscous damping parameters in linear systems. What makes it different from other work is the use of power and mean square measurements. It was undertaken to provide a working knowledge of the use of power measurement methods in linear structural systems from which a sound start into the consideration of nonlinear structural systems might be made. For this reason, the practical validation of the theoretical results in this chapter was not prosecuted with the completeness that might be sought in a primary investigation. Nevertheless, for the experiments and digital

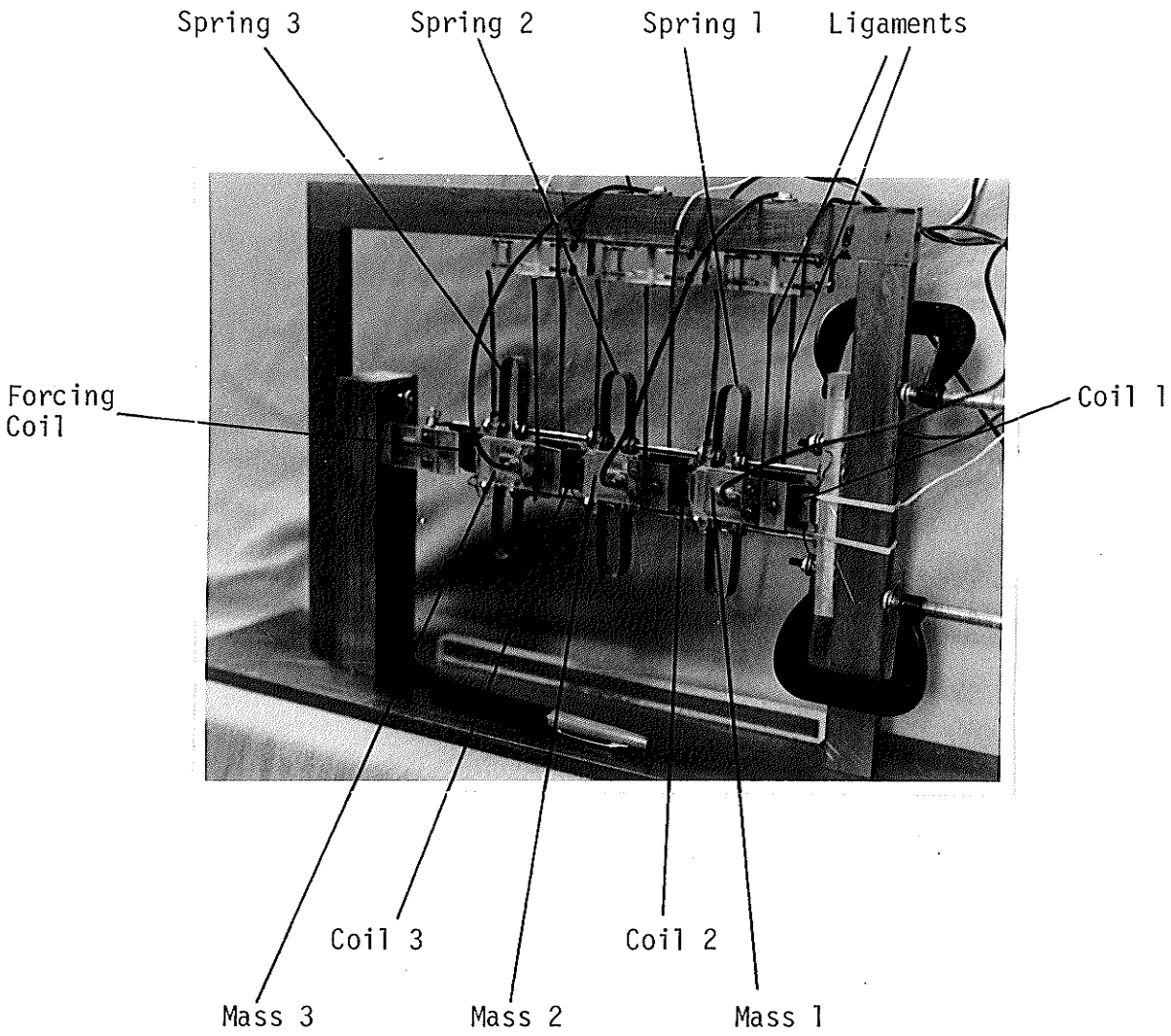

Figure 2.3 Photograph of the 3-DOF Linear Physical Model

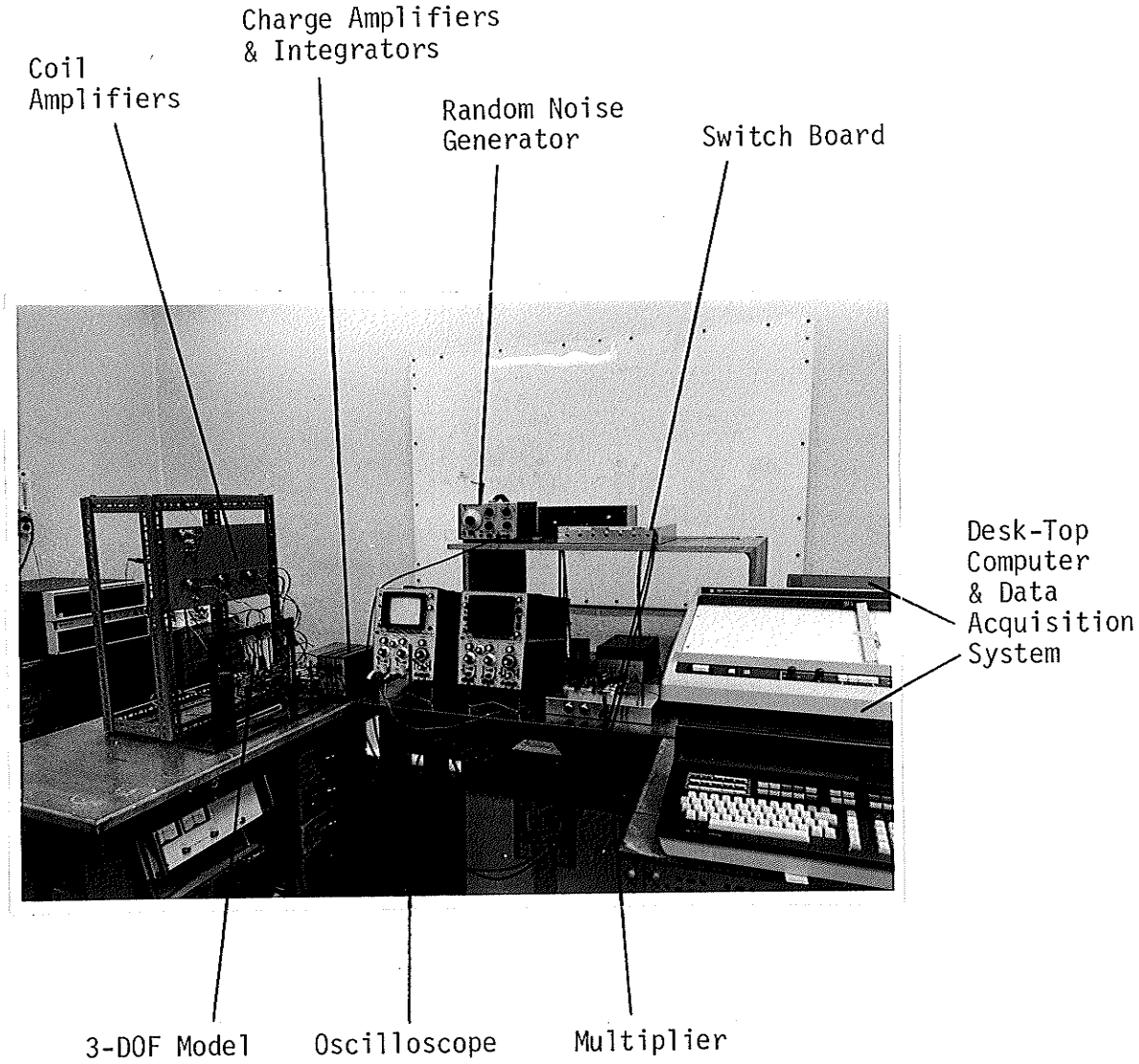

Figure 2.4 Measuring System of the 3-DOF Model

simulations that were performed, agreement generally within ten percent was obtained between the values obtained by the half-power method [6] and the methods enunciated here. A typical set of results from the physical model are shown in Table A.1, Appendix A.

All of the methods in this chapter permit the calculation of the viscous damping coefficients in units of mechanical ohms (N.s/m). They do not, however, give direct insight into the behavior of a structure when under the influence of external forcing. In linear systems the damping ratio or quality factor have been used to succinctly state the overall vibrational performance of a structure. These classical measures for assessing the relationship between the storage and dissipation of energy require that the structure be linear and that all modes be separable. The introduction of a measure that is similar in importance to damping ratio but takes into account the effect of external loading is clearly required if progress is to be made in understanding and analyzing strongly nonlinear vibrating systems. The power ratio is submitted here as such a measure.

CHAPTER III

POWER RATIO AS AN ENERGY LOSS EFFECTIVENESS FACTOR

3.1 INTRODUCTION

The definition of power ratio has its roots in electrical engineering [44] where a similar ratio, called the power factor, has been defined as the actual power dissipation (average of voltage times current) to the apparent power (root-mean-square voltage times root-mean-square current). Hence both are loss effectiveness factors. The power ratio is similarly defined but has been given a different name because it was introduced to deal with random vibration whereas the power factor was introduced to deal with sinusoidal excitation at one frequency.

Let $p(t)$ be a random forcing function with zero mean and $\dot{y}(t)$ be the velocity response of a system taken at the forcing location. The power ratio W is defined as

$$W = \frac{E[p\dot{y}]}{\sqrt{E[pp]} \cdot \sqrt{E[\dot{y}\dot{y}]}}$$

where E[ ] denotes expected values. If both $p(t)$ and $\dot{y}(t)$ can be assumed to be stationary and ergodic, then the power ratio can be defined as

$$W = \frac{\overline{p\dot{y}}}{\sqrt{\overline{pp}} \cdot \sqrt{\overline{\dot{y}\dot{y}}}}, \qquad (3.1)$$

where the bar (—) denotes time averaging, $\overline{p\dot{y}}$ is the actual power dissi-

pation (all sources of power loss included) and $\sqrt{\overline{pp}} \cdot \sqrt{\overline{\dot{y}\dot{y}}}$ is the apparent power supplied to the system (see Appendix C). Interpreted this way, the power ratio is a normalized factor and it indicates what proportion of the apparent input power is actually being dissipated. Hence, it has a meaning similar to that of damping ratio.

From another point of view, the power ratio is the zero-lag correlation coefficient between the forcing function and the velocity. Only when the velocity is directly proportional to the forcing (as in a pure viscous damper), has the power ratio a value of one. When there is no correlation between the forcing and velocity (as in pure mass or pure linear spring), the power ratio is zero. For all other combinations of mass, damper, spring (linear or nonlinear), the power ratio has a value between zero and one.

3.2 LINEAR SYSTEM

Since the viscous damping coefficient (or damping ratio) is a widely recognized relative loss parameter in linear systems, the power ratio is first expressed in terms of the viscous damping coefficient in order to demonstrate its meaning as a factor which indicates the relative loss in a system.

Consider a single degree of freedom (1-DOF) system having mass m, stiffness k, viscous damping coefficient c and that it is subjected to a stationary and ergodic forcing p, as shown in Figure 3.1(a). The

forcing has a constant power spectral density S_{pp} , central radian frequency ω_c, and a bandwidth of $\Delta\omega$, as shown in Figure 3.1(b). The forcing bandwidth $\Delta\omega$ is assumed to cover sufficiently the peak response region of the system curve, which is shown in Figure 3.1(c). It is shown in Section D.1 of Appendix D that the square of the power ratio, W^2,of such a system is given by

$$W^2 = \frac{c}{4m\ \Delta f}\ , \tag{3.2}$$

where $\Delta f = \Delta\omega/2\pi$.

The power ratio clearly depends on the bandwidth of forcing. As the forcing bandwidth Δf increases, the effective power dissipation per unit bandwidth decreases as one would expect.

Equation (3.2) can be readily extended to a multi-degree of freedom system. The band-limited excitation of such a system is first studied.

Consider an n-DOF linear system which is subjected to stationary and ergodic forcing p_r acting on the r-th mass as shown in Figure 3.2(a). The system has a response-frequency curve as shown in Figure 3.2(b). The forcing has a constant power spectral density over a bandwidth Δf_i such that Δf_i is centered at the i-th modal frequency f_i and it does not envelop the frequency band of any other mode. In Appendix D (see Section D.2) it is demonstrated that the square of the power ratio measured at the mass at which the forcing is acting is related to the i-th modal damping C_i as

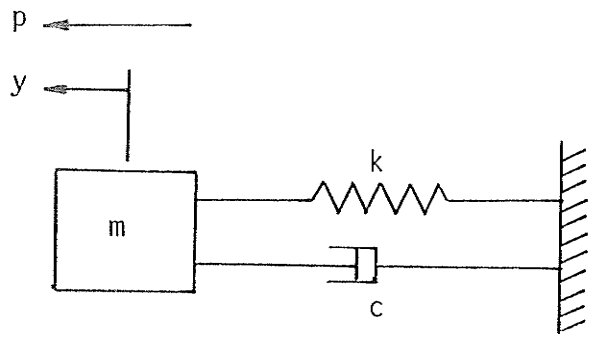

(a) Idealized System

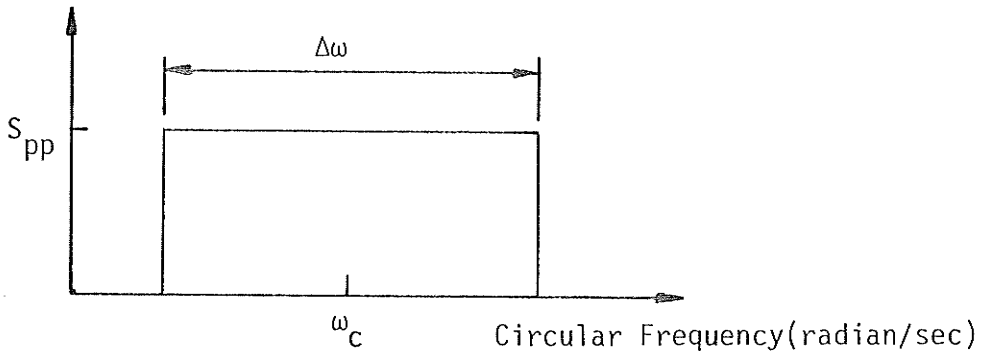

(b) Power Spectral Density of Forcing Versus Frequency

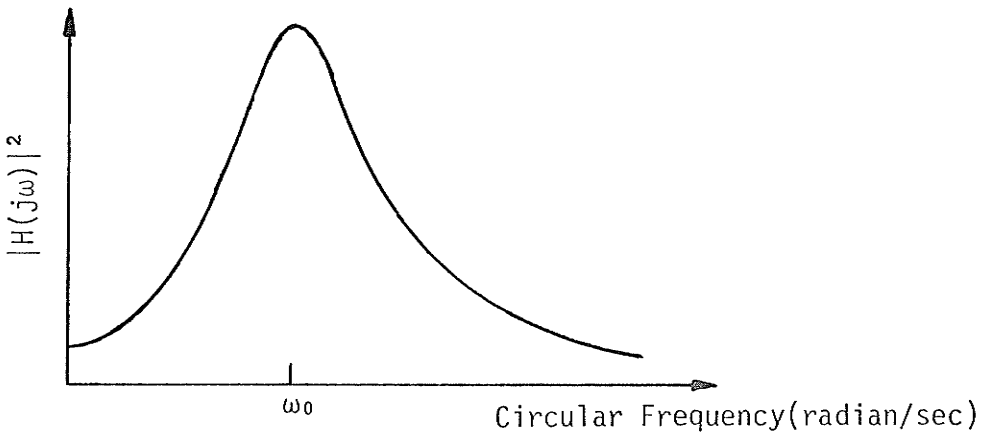

(c) Square of the Absolute Value of System Response Function Versus Frequency

Figure 3.1 1-DOF Linear System

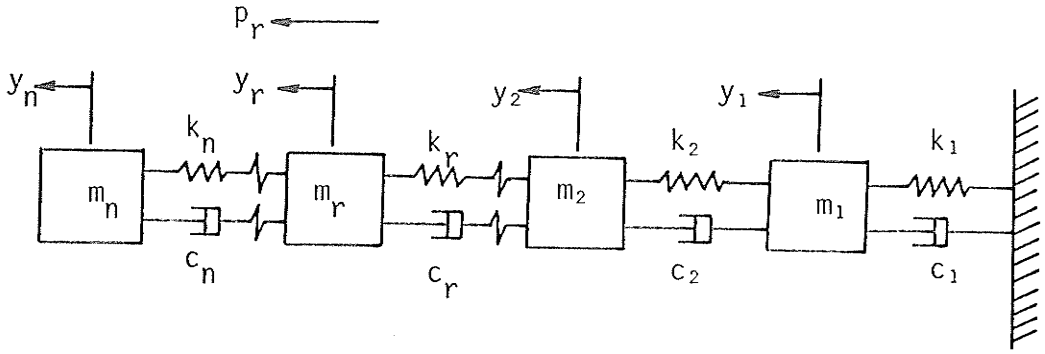

(a) Idealized System

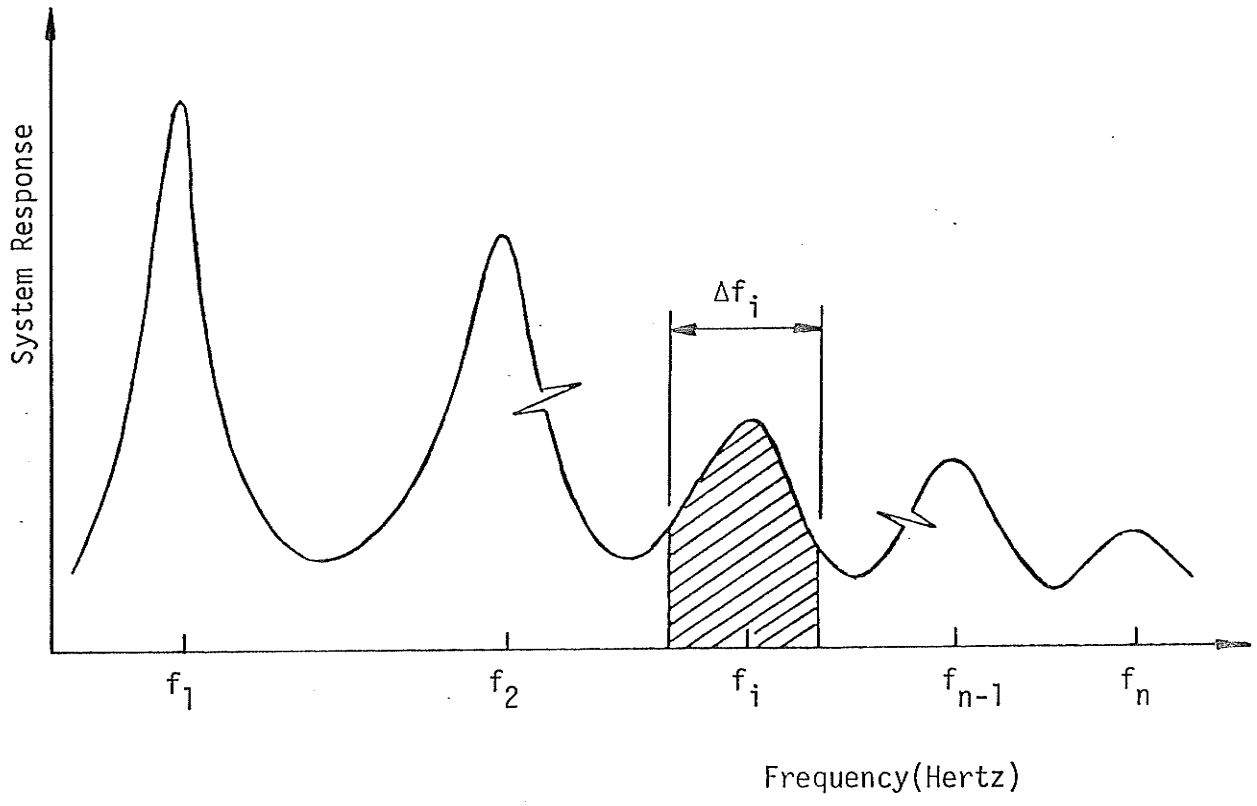

(b) System Response - Frequency Curve

Figure 3.2 n-DOF Linear System

$$W^2 = \frac{C_i}{4\ \Delta f_i} \quad . \tag{3.3}$$

To use this approach the system must possess distinct modes such that the excitation of a particular mode does not interfere with other modes. Equation (3.3) assumes an identity matrix for the generalized mass.

The power ratio can also be related to the damping of various modes by subjecting the system to a broad-band excitation. Consider again the n-DOF linear system of Figure 3.2. The stationary and ergodic forcing, p_r, acts on the r-th mass and has a constant power spectral density over a bandwidth Δf, which is broad enough to cover the entire range of the system response. With reference to Section D.3 of Appendix D, the square of the power ratio, taken at the r-th mass, is of the form

$$W^2 = \frac{C_o}{4\ \Delta f} \ , \tag{3.4}$$

where $C_o = \dfrac{1}{\sum_{j=1}^{n} \dfrac{1}{C_j^*}}$ is the effective damping with respect to the force driving point. C_j^* is a function of modal damping C_j and is given by $C_j^* = L_r^4\ C_j/\phi_{rj}^4$, where $L_r^2 = \sum_{j=1}^{n} \phi_{rj}^2$ and $[\phi]$ is the undamped free vibration mode shape matrix.

It is interesting to note that C_o represents the overall damping of the system having the dampers C_j^* in series. The power ratio, in this case, is the loss effectiveness factor for the entire structure at the point of forcing. In this respect, it is like Lyon's statistical energy analysis [40] in that it summarizes the relative power loss of all modes which would otherwise be impossibly complicated to treat separately if the number of modes is large.

Using this method, starting with the bandwidth from low frequency and enveloping one additional modal frequency at a time, it is possible to calculate modal damping values for as many modes as desired. If the modes are not distinct, then these values will be 'equivalent' modal damping values.

3.3 1-DOF NONLINEAR NONHYSTERETIC SYSTEM

Consider a 1-DOF nonlinear nonhysteretic system as shown in Figure 3.3(a). The system has a mass m, viscous damping coefficient c and is subjected to a stationary and ergodic forcing p. Without loss of generality, the nonlinear spring is assumed to exhibit a bilinear restoring force g(y), as shown in Figure 3.3(b). g(y) has a first slope k_3, and beyond the yield point, a second slope (k_3+k_A). The nonhysteretic characteristic of the spring is such that the same bilinear path in Figure 3.3(b) will be followed by all loading and unloading sequences. The value of g(y) is known therefore for any value of y. Accordingly, no area is enclosed by the path upon loading and unloading, thus defining the spring as nondissipative.

The equation of motion for this system is

$$m\ddot{y} + c\dot{y} + g(y) = p \ . \tag{3.5}$$

The only dissipative element in the system is the viscous damper. g(y) will not dissipate energy and hence the power ratio of this system is given by

$$W^2 = \frac{c}{4\ m\Delta f} \ , \tag{3.6}$$

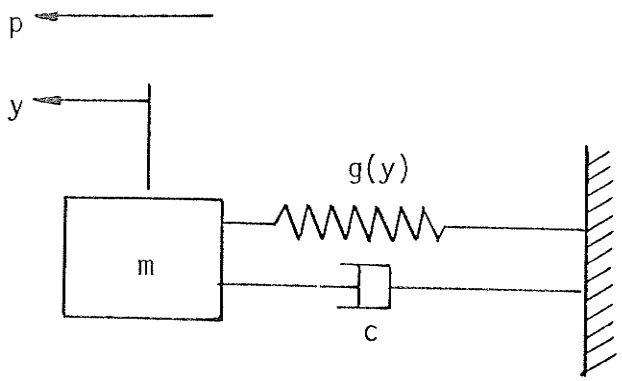

(a) Idealized System

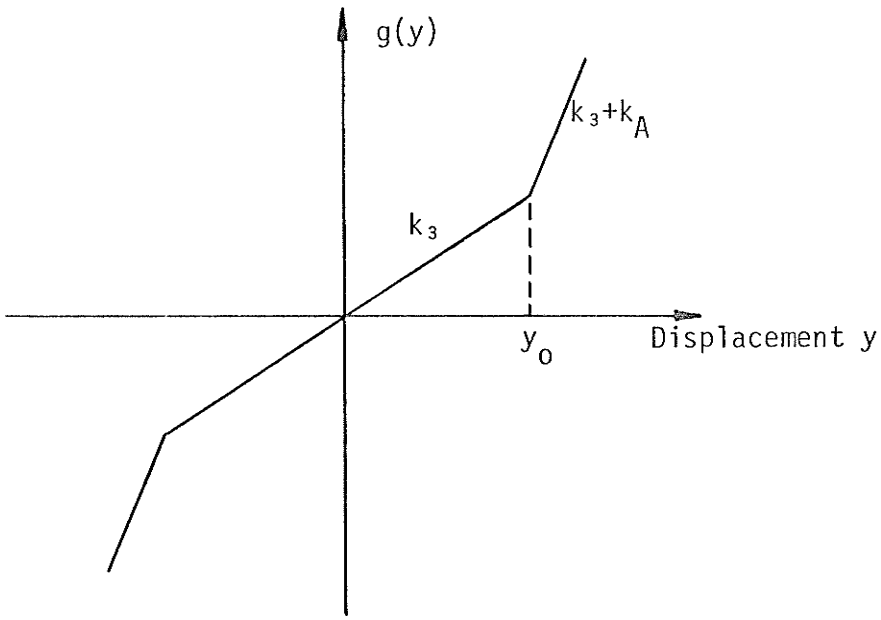

(b) Spring Force Versus Displacement

Figure 3.3 1-DOF Bilinear Nonhysteretic System

which is also the expression for a linear system.

To validate the results shown above, experiments were carried out by using the physical model described in Appendix A.

3.4 NUMERICAL RESULTS AND DISCUSSIONS

To give experimental verification of the methods just enumerated, both 1-DOF and n-DOF systems are required. To provide these, the 3-DOF physical model was used either as such or with mass m_2 blocked, making it effectively infinite, to yield a 1-DOF system comprising m_3 and k_3 (Figure A.1). This resulted in a system having a natural frequency of 9.3 Hertz and a damping coefficient of 0.06 N-s/m, 0.18 N-s/m, 0.55 N-s/m or 1.33 N-s/m depending upon the damping switch position 0, 1, 2 or 3 selected (Figure A.2). These damping coefficients were determined by using the half-power method and are taken as adequate references in the present work.

In the first case, the 1-DOF physical model was used to check the validity of equation (3.2). Measurements of $\overline{p\dot{y}}$, $\overline{pp}$ and $\overline{\dot{y}\dot{y}}$ were taken for the different damping settings and for different excitation bandwidths, $\overline{\Delta f}$, centered at 9.3 Hertz. The power ratio in each case was evaluated and equation (3.2) was used to calculate the viscous damping of the system. These results are given in Table 3.1. It is noted that the power ratio, which is a measure of dissipation per unit excitation bandwidth, is not a constant. The product of the power ratio and the excitation bandwidth is fairly constant, and the viscous damping coefficients evaluated this way are generally accurate to within 10 percent of the reference values.

Effective* Δf (Hertz)	DAMPER SWITCH POSITION					
	1		2		3	
	W	c (N-s/m)	W	c (N-s/m)	W	c (N-s/m)
Reference	-	0.18	-	0.55	-	1.33
9.2	0.24	0.19	0.40	0.53	0.66	1.44
13.7	0.20	0.20	0.34	0.57	0.54	1.44
20.5	0.16	0.19	0.28	0.58	0.44	1.43
27.9	0.14	0.20	0.24	0.58	0.38	1.46

* See Appendix A

TABLE 3.1 Power Ratio and Viscous Damping Coefficients of a 1-DOF Linear Model

To validate equation (3.4), the full 3-DOF physical model was forced at the third mass. The resonant frequencies and undamped free vibration mode shape matrix are those given by equation (A.1).

First, an experiment was performed with all damper settings in switch position 1. The three resulting modal damping values (as determined by half-power method) are given in Table 3.2. When the effective bandwidth is equal to 30 Hz, the power ratio is found to be 0.0966 and the square root of the right-hand-side of equation (3.4) is 0.0952, a difference of about 1.5 percent. When Δf is increased to 45 Hz, the corresponding numbers agree still closer, a result of improving frequency coverage.

An experiment was then performed with the setting of damper 1 in switch position 2, damper 2 in switch position 0, and damper 3 in switch position 1. In this case, the modal dampings were found to be those shown in Table 3.2. The results of power ratio and the corresponding total power loss effect from all modes were found to agree within 1.6 percent. The good agreement obtained in these cases is most likely due to the low damping present in the system, and hence the assumption of separable modes is satisfied.

To validate equation (3.6), a 1-DOF bilinear nonhysteretic model is required. This was provided by inserting the tip of a thin elastic rod with stiffness k_A into a gap in the mass of the 1-DOF linear model. The mass of rod was assumed to be negligible. When the system response amplitude is below a certain level, there is no contact between the rod and the mass, hence, the system remains linear with stiffness k_3. When the amplitude exceeds a certain level, the mass and the rod will come

1st EXPERIMENT - All damper in switch position 1					
C_1 (N-s/m)	C_2 (N-s/m)	C_3 (N-s/m)	Effective Δf	W	$(\frac{C_o}{4\ \Delta f})^{1/2}$
0.320	1.660	4.130	30	0.0966	0.0952
			45	0.0775	0.0777
2nd EXPERIMENT - Switch position of dampers: damper 1:2 damper 2:0 damper 3:1					
0.315	1.806	2.627	30	0.0961	0.0946
			45	0.0768	0.0772

TABLE 3.2 Validation of Equation (3.4)

into contact and the rod, acting as a cantilever, adds stiffness k_A to the system. Under these conditions, the system stiffness becomes (k_3+k_A), see Figure 3.3(b).

Two groups of experiments were performed for the bilinear nonhysteretic model. The first group of experiments used a rod which gave 3.57 as the ratio of $(k_3+k_A)/k_3$. Mean square measurements of $\overline{p\dot{y}}$, $\overline{pp}$ and $\overline{\dot{y}\dot{y}}$ were taken with damping set first to 0.18 N-s/m and then to 1.33 N-s/m. For each of these settings, three different forcing bandwidths were selected. The power ratio was evaluated for each case, and the corresponding viscous damping coefficient was calculated by using equation (3.6). The results are given in Table 3.3(a). The second group of experiments were identical with the first except that $(k_3+k_A)/k_3$ was set equal to 1.63. The corresponding results of power ratio and viscous damping coefficient are given in Table 3.3(b). In both cases, a high level of excitation was maintained to ensure that the model was driven significantly into the nonlinear region such that measurement of damping by the half-power method was not possible.

From Table 3.3, it is noted that the values of power ratio are not affected significantly by the spring stiffness of the system. This is due to, firstly, the value of viscous damping coefficient, being a function of the electro-magnetic property of the model, is invariant to the change of stiffness. Secondly, the added spring has very small loss, hence, the values of power ratio are a function of viscous damping only. The damping coefficients obtained from the power ratio agree with the reference damping, to within 10 percent. In general, as the system frequency-response curve becomes less sharply peaked, as in the case of

Effective Δf (Hertz)	DAMPER SWITCH POSITION			
	1		3	
	W	c (N·s/m)	W	c (N·s/m)
Reference	-	0.18	-	1.33
20.5	0.16	0.19	0.44	1.43
27.9	0.14	0.20	0.37	1.38
45.0	0.11	0.20	0.30	1.46

(a) Strong spring, $(k_3+k_A)/k_3 = 3.57$

Effective Δf (Hertz)	DAMPER SWITCH POSITION			
	1		3	
	W	c (N·s/m)	W	c (N·s/m)
Reference	-	0.18	-	1.33
20.5	0.16	0.19	0.45	1.49
27.9	0.14	0.20	0.38	1.45
45.0	0.11	0.20	0.30	1.46

(b) Weak spring, $(k_3+k_A)/k_3 = 1.63$

TABLE 3.3 Power Ratio and Viscous Damping Coefficients of a 1-DOF Bilinear Nonhysteretic Model

a highly damped system, a larger difference would be expected between the measured and reference values of viscous damping coefficient. Hence, the accuracy thus obtained is quite satisfactory although a possible source of error might be due to the impact which exists between the inserted rod and the mass.

The work presented in this chapter deals with linear systems and a system with a nonlinear, nondissipative spring. Interesting results are noted. Firstly, the power ratio is the effective dissipation per unit excitation bandwidth for a system with a sharply peaked frequency-response curve. Secondly, the effective damping of the whole structure with respect to the driving point can be summarized as a combination of damping from each individual mode. And, lastly, for a system with a nondissipative spring, it is found that the power ratio is not affected significantly by the change of system spring stiffness. Although power ratio may be used in linear systems, it is primarily introduced to deal with nonlinear systems. Many of its interesting characteristics and its usefulness as a loss effectiveness factor can be more clearly visualized when a nonlinear hysteretic element is studied.

CHAPTER IV

POWER RATIO IN BILINEAR HYSTERETIC ELEMENTS

4.1 INTRODUCTION

It has already been suggested that hysteresis is the loss mechanism that is of interest when vibrational overload of a structure takes place and that the power ratio may be a suitable measure of loss effectiveness in hysteretically damped systems. Consequently, the power ratio of a simplified hysteretic element shown in Figure 4.1(a) was studied. It was studied in isolation first to allow for a full ranging enquiry free from the complication of inertial forces.

4.2 BILINEAR HYSTERETIC ELEMENTS

The element of Figure 4.1(a) is assumed to be massless and has a Coulomb slider which starts to move only at a force level of $\pm (1-\alpha)ky_o$, where y_o is the yield displacement of the element. The corresponding yield force at y_o is designated as p_o. The total restoring force $g(y,\dot{y})$ of the hysteretic element, when plotted against displacement y, is depicted in Figure 4.1(b).

In the present analysis, the input quantity is the displacement y, which is assumed to have a Gaussian distribution. The output quantity is the restoring force, the statistical properties of which are unknown. Since $g(y,\dot{y})$ is the only force in the system, it is also referred to as $p(y,\dot{y})$. In order to obtain an expression for the power ratio, it is necessary to know the values of $E[pp]$, $E[p\dot{y}]$ and $E[\dot{y}\dot{y}]$.

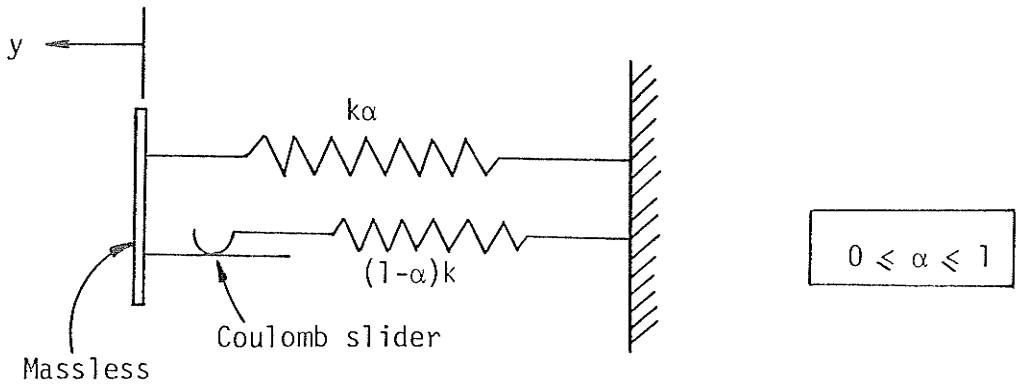

(a) Idealized Model

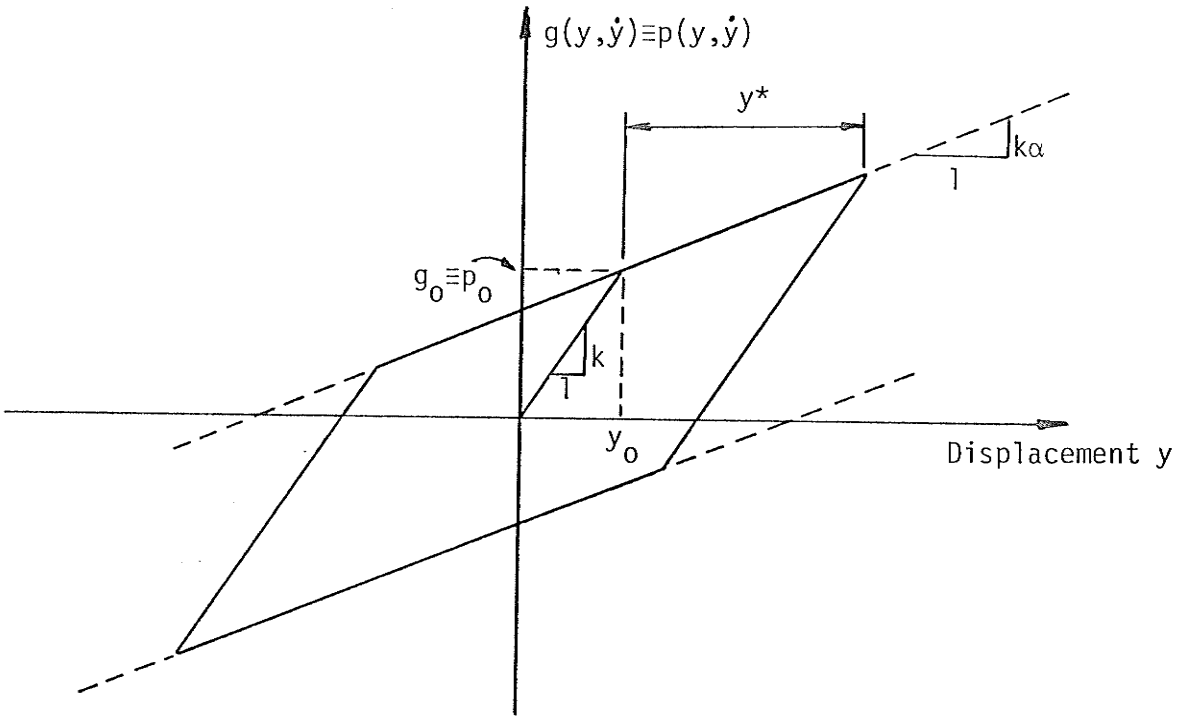

(b) Restoring Force Versus Displacement

Figure 4.1 Bilinear Hysteretic Element

An expression for E[pp] can be readily obtained once the probability density function of the restoring force, pr(p), is known. pr(p) is obtained as follows.

Consider the input process y whose probability density function pr(y) is given mathematically as

$$pr(y) = \frac{1}{\sqrt{2\pi}\,\sigma_y} e^{\frac{-y^2}{2\sigma_y^2}} , \qquad (4.1)$$

where σ_y is the standard deviation or root-mean-square (rms) value of the displacement [12]. The process y is assumed to have zero mean. pr(y) is sketched as shown in Figure 4.2. Let y_o be the yield displacement of the hysteretic element and let y^* be the mean of the peak values of y which are beyond the yield level y_o (see Appendix E for the derivation of y^* for a Gaussian process). The random process for y may be represented by an equivalent process (dissipating the same amount of energy as the original process) which has a mean yield peak value of y^* and a mean frequency of yielding, f^*. This mean frequency is equal to the frequency of positive slope crossing at the level y_o, and is given by [41]

$$f^* = \frac{1}{2\pi}\frac{\sigma_{\dot{y}}}{\sigma_y} e^{\frac{-y_o^2}{2\sigma_y^2}} , \qquad (4.2)$$

where $\sigma_{\dot{y}}$ is the standard deviation of the velocity. Accordingly, the restoring force may be plotted against y by assuming that y^* is the mean yield peak value, see Figure 4.1(b), and that the mean frequency of the hysteretic loop is f^*. The area enclosed by the loop is then the amount of

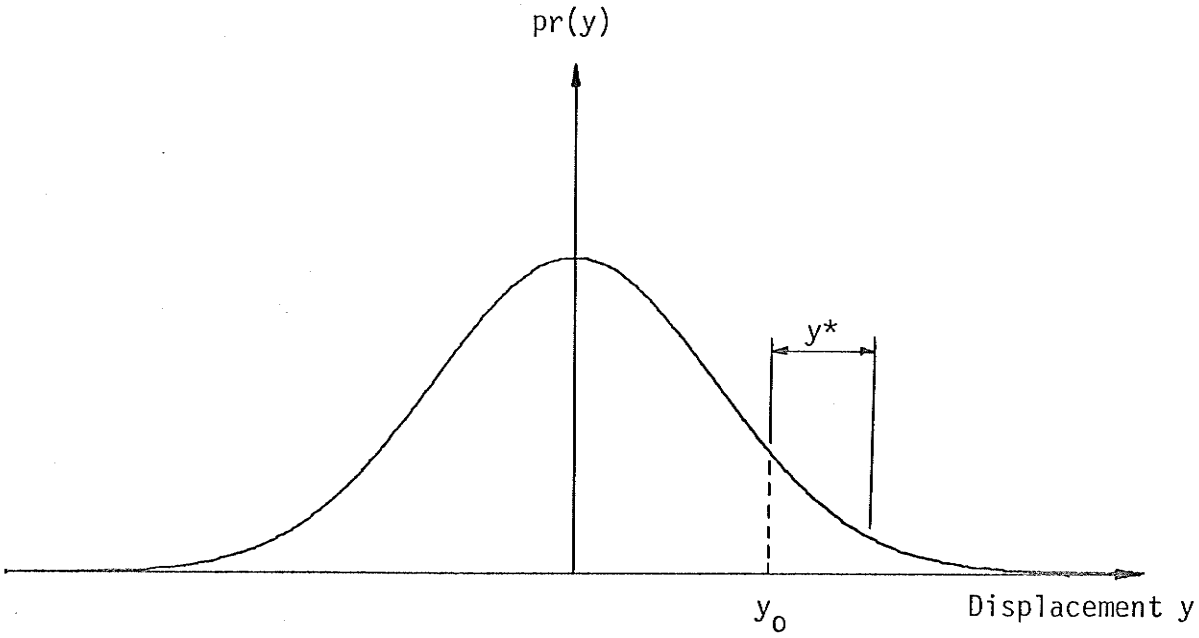

Figure 4.2 Probability Density Function of Displacement

energy dissipation per cycle.

With this representation of y, the probability density functions of the restoring force are obtained for the following cases in Appendix F:

$\underline{p_o - k\alpha y^* > 0}$

$$pr(p) = \begin{cases} \frac{A}{2}\left[e^{I_1} + e^{I_2}\right], & |p| < p_o - k\alpha y^* \\ \frac{A}{2}\left[\frac{1}{\alpha} e^{I_3/\alpha^2} + e^{I_2}\right], & p_o + k\alpha y^* > |p| > p_o - k\alpha y^* \end{cases} . \qquad (4.3)$$

$\underline{p_o - k\alpha y^* = 0}$

$$pr(p) = \frac{A}{2}\left[\frac{1}{\alpha} e^{I_3/\alpha^2} + e^{I_2}\right], \quad |p| < p_o + k\alpha y^* . \qquad (4.4)$$

$\underline{p_o - k\alpha y^* < 0}$

$$pr(p) = \begin{cases} \frac{A}{2\alpha}\left[e^{I_3/\alpha^2} + e^{I_4/\alpha^2}\right], & |p| < -p_o + k\alpha y^* \\ \frac{A}{2}\left[\frac{1}{\alpha} e^{I_3/\alpha^2} + e^{I_2}\right], & p_o + k\alpha y^* > |p| > p_o + k\alpha y^* \end{cases} . \qquad (4.5)$$

Elasto-plastic case ($\alpha = 0$)

$$pr(p) = \begin{cases} \frac{A}{2}\left[e^{I_1} + e^{I_2}\right], & |p| < p_o \\ \frac{1}{4}\left[\operatorname{erfc}\left(\frac{y_o - y^*}{\sqrt{2}\,\sigma_y}\right) - \operatorname{erfc}\left(\frac{y_o - y^*}{\sqrt{2}\,\sigma_y}\right)\right], & p = \pm p_o \end{cases} . \qquad (4.6)$$

In equation (4.3) through (4.6), I_1, I_2, I_3, I_4 and A are given the following meanings:

$$I_1 = - [p/k - y^*(1-\alpha)]^2/2\sigma_y^2 \ , \ I_2 = - [p/k + y^*(1-\alpha)]^2/2\sigma_y^2 \ ,$$

$$I_3 = - [p/k - y_o(1-\alpha)]^2/2\sigma_y^2 \ , \ I_4 = - [p/k + y_o(1-\alpha)]^2/2\sigma_y^2 \ ,$$

and

$$A = \frac{1}{\sqrt{2\pi}\ k\sigma_y} \ .$$

The mean square value of p can be obtained by taking the second moment of pr(p), thus

$$E[pp] = \int_{\text{limit}} p^2 pr(p)dp \ . \tag{4.7}$$

where the integration limits of p are shown in equations (4.3) through (4.6) for different cases.

The term $E[p\dot{y}]$ means the average power dissipation and is equal to the area of the loop of Figure 4.1(b) multiplied by the mean yield frequency, hence,

$$E[p\dot{y}] = 4\ ky_o(1-\alpha)y^* \cdot \frac{1}{2\pi} \frac{\sigma_{\dot{y}}}{\sigma_y} e^{\frac{-y_o^2}{2\sigma_y^2}} \ . \tag{4.8}$$

The term $E[\dot{y}\dot{y}]$ is simply the mean square velocity, thus,

$$E[\dot{y}\dot{y}] = \sigma_{\dot{y}}^2 \ . \tag{4.9}$$

The power ratio of the hysteretic element for Gaussian displacement input may be formed by using equations (4.7) through (4.9) and solving numerically.

4.3 NUMERICAL RESULTS AND DISCUSSIONS

The power ratio as derived in the last section for the bilinear hysteretic element was validated by means of both a physical-analog model and a digital simulation model. The physical-analog model is described in Appendix G and the digital simulation program is described in Appendix H. The derivations in the last section are referred to as the computational model.

The elasto-plastic case (α=0) was chosen to compare the results of the three models because it is a highly nonlinear case. In line with this thinking, the displacement was chosen as a low-pass Gaussian process (ratio of cut-off frequencies infinite). In the physical-analog model, it was found that an averaging time of 40 seconds (sampling rate 0.2 second) yielded repeatedly close results for the evaluation of averages. Hence, this averaging time was employed for the evaluation of $\overline{p\dot{y}}$, $\overline{pp}$ and $\overline{\dot{y}\dot{y}}$. Whereas in the digital simulation model, a total of 256 data was found to give statistical regularity to within 10 percent, although the results presented here used a total of 1280 data. In the computational model, Simpson's one-third rule [45] was employed to numerically integrate equations (4.7) and (E.7). An integration interval was subdivided into 20 integration strips and was found to give steady results.

The power ratio obtained from the three models is shown plotted against different values of a non-dimensional quantity, y_o/σ_y, in Figure 4.3. In general, the results from the three models agree closely. The digital simulation results are consistently lower than the results from the computation model, whereas the results from the physical-analog model are between those of the other two models. The difference between the computation and simulation results is most likely due to different form factors of input displacement waveform of the two models. Results beyond y_o/σ_y = 1.6

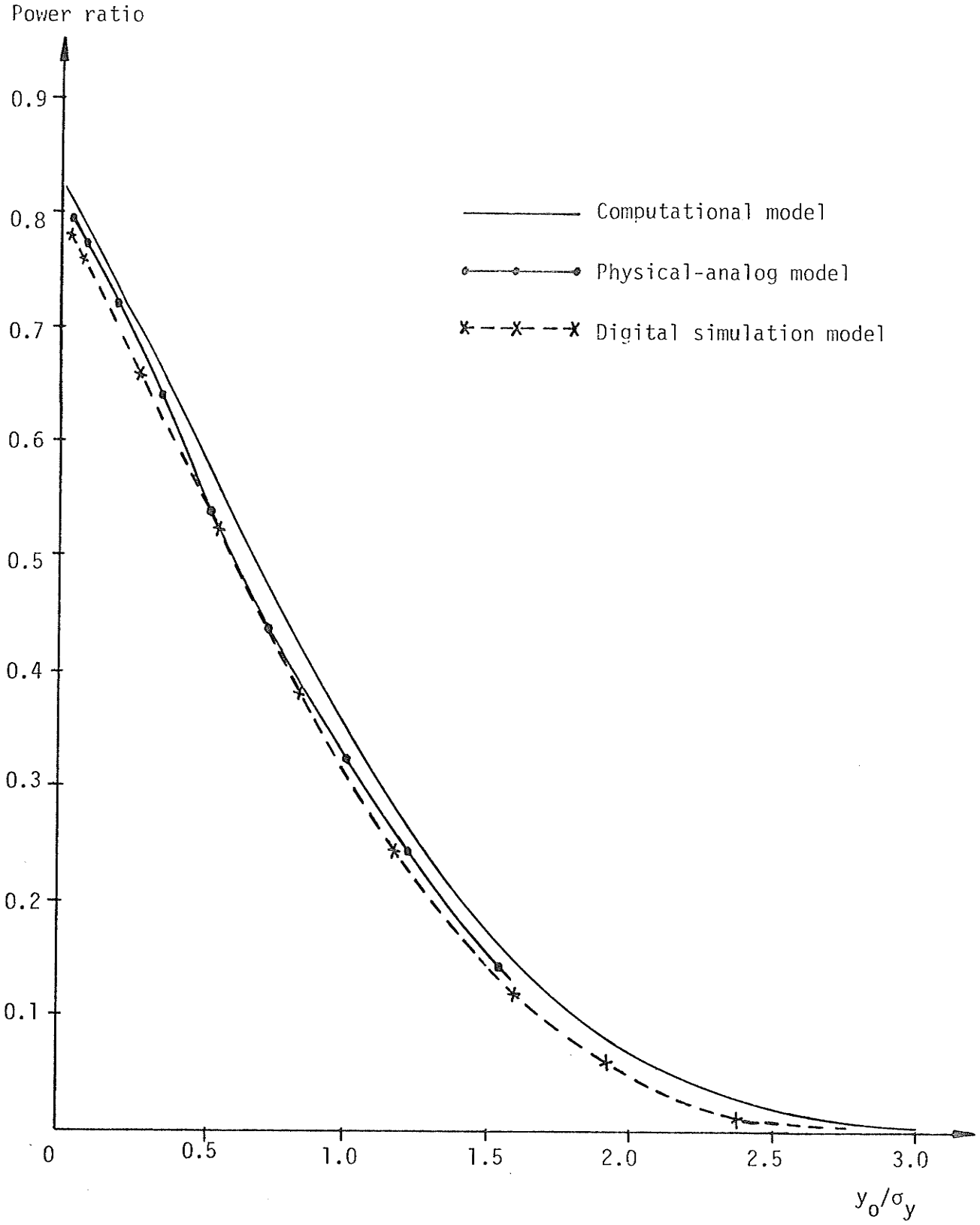

Figure 4.3 Comparison of Power Ratio

cannot be obtained from the physical-analog model because of the limitations of the amplifiers used. For high values of y_o/σ_y, the power ratio tends to zero. This is what one would expect because for large value of y_o/σ_y, there is essentially no yielding (linear system), hence no power dissipation and the power ratio is zero. At the lower scale of y_o/σ_y, the power ratio is around 0.8. At first sight, this result is quite surprising. The power ratio might be expected to tend to unity as y_o/σ_y becomes smaller and smaller, for the element is yielding and, hence, dissipating energy virtually all of the time. To investigate this discrepancy between the expected outcome and the performance of the models, digital simulation using deterministic waveforms was performed. The three input displacement waveforms and the resultant steady state velocity and force waveforms are as shown in Figure 4.4. The simulation range was limited to small values of y_o/σ_y and 2 cycles (256 data points) were used in all cases.

In the case of the triangular input waveform, the force and velocity waveforms are almost in phase and proportional to each other, and the calculated power ratio is 0.992. Theoretically, as the value of y_o/σ_y approaches zero, the force and velocity will be exactly in phase and a power ratio of one may be expected. With a sinusoidal input waveform, the force and velocity are almost in phase, but not proportional to each other, and the power ratio in this case is 0.905. Finally, a square input waveform yields a velocity which is zero (except at the points immediately before and after the zero crossing of displacement), hence the power ratio is identically zero.

From the above, it is found that the power ratio of an hysteretic

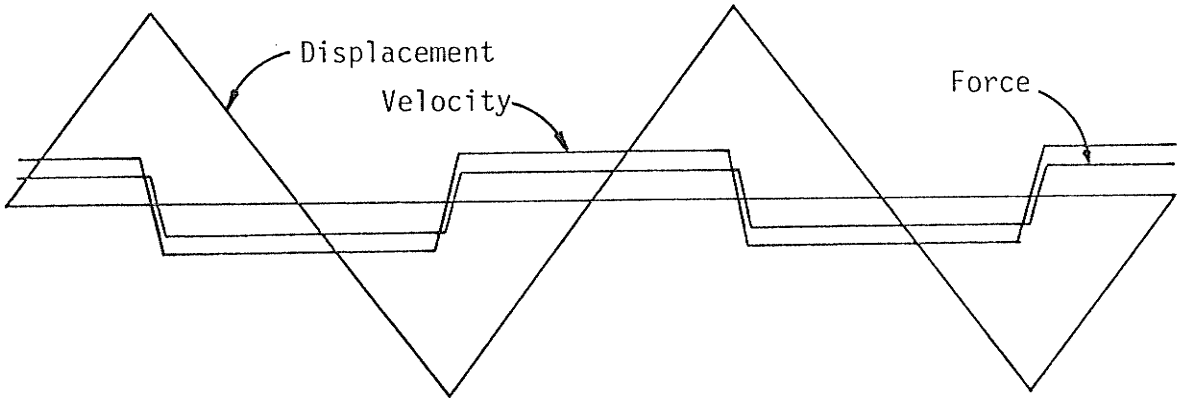

(a) Triangular Waveform

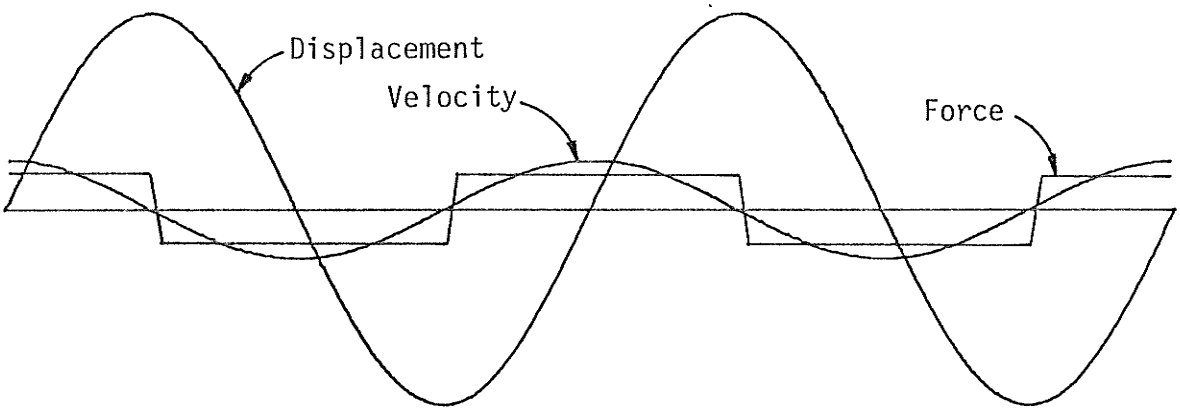

(b) Sinusoidal Waveform

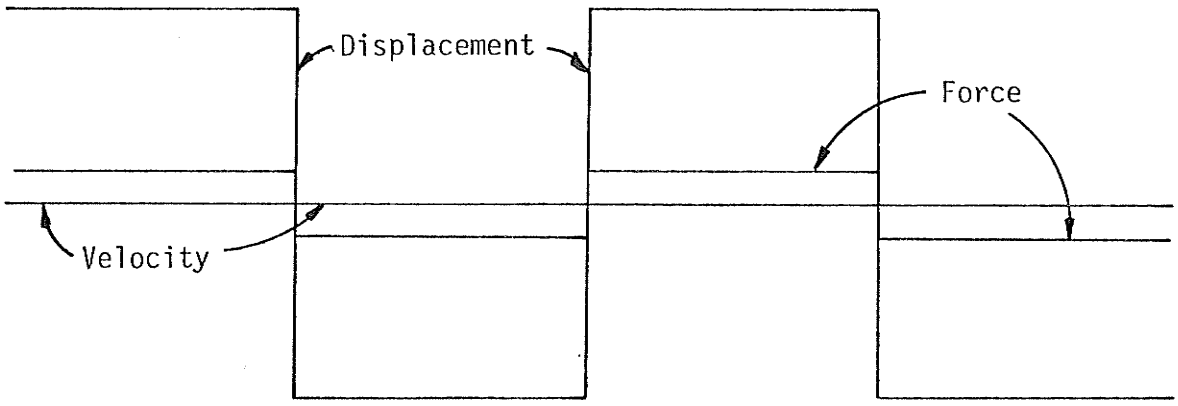

(c) Square Waveform

Figure 4.4 Illustrations of Different Waveform Effects (not drawn to scale)

element is waveform dependent. It may be noted that the power ratio is unity only when the force is proportional to the velocity, as is the case of a viscous damper. A clearer insight into the loss behavior of the bilinear hysteretic element can be obtained by remembering that the power ratio is simply the zero-lag correlation coefficient between force and velocity. Thus, taking the case of a sinusoidal input waveform (Figure 4.4(b)), it may be noted that harmonics higher than the first in the the force waveform have no correlative equivalent in the velocity waveform. From this, it is clear that the power ratio of the hysteretic element alone is a measure of its efficiency in converting input motion to loss and that this efficiency depends upon the form factor of the input displacement waveform, as well as upon y_o/σ_y. This is, of course, an excellent property of the power ratio, for, as expected, it will always give the true power ratio for any system containing an hysteretic element no matter how the system is forced.

Figures 4.5 and 4.6 are plots of power ratio for the triangular and sinusoidal input waveforms, respectively, as computed by the simulation model. Results for different values of y_o/σ_y and α are given. Figure 4.7 contains the corresponding plots of power ratio for a Gaussian low-pass input waveform (0-1 Hertz), as obtained from the computational model. The use of simulation model requires processing of over 256 random input data for each value of power ratio; consequently, the computational model, the accuracy of which has been demonstrated, was used here for computational efficiency. In all these plots, when either the value of α or y_o/σ_y increases (except when y_o/σ_y is small), the element becomes more linear, hence the power ratio drops. It is interesting to note that

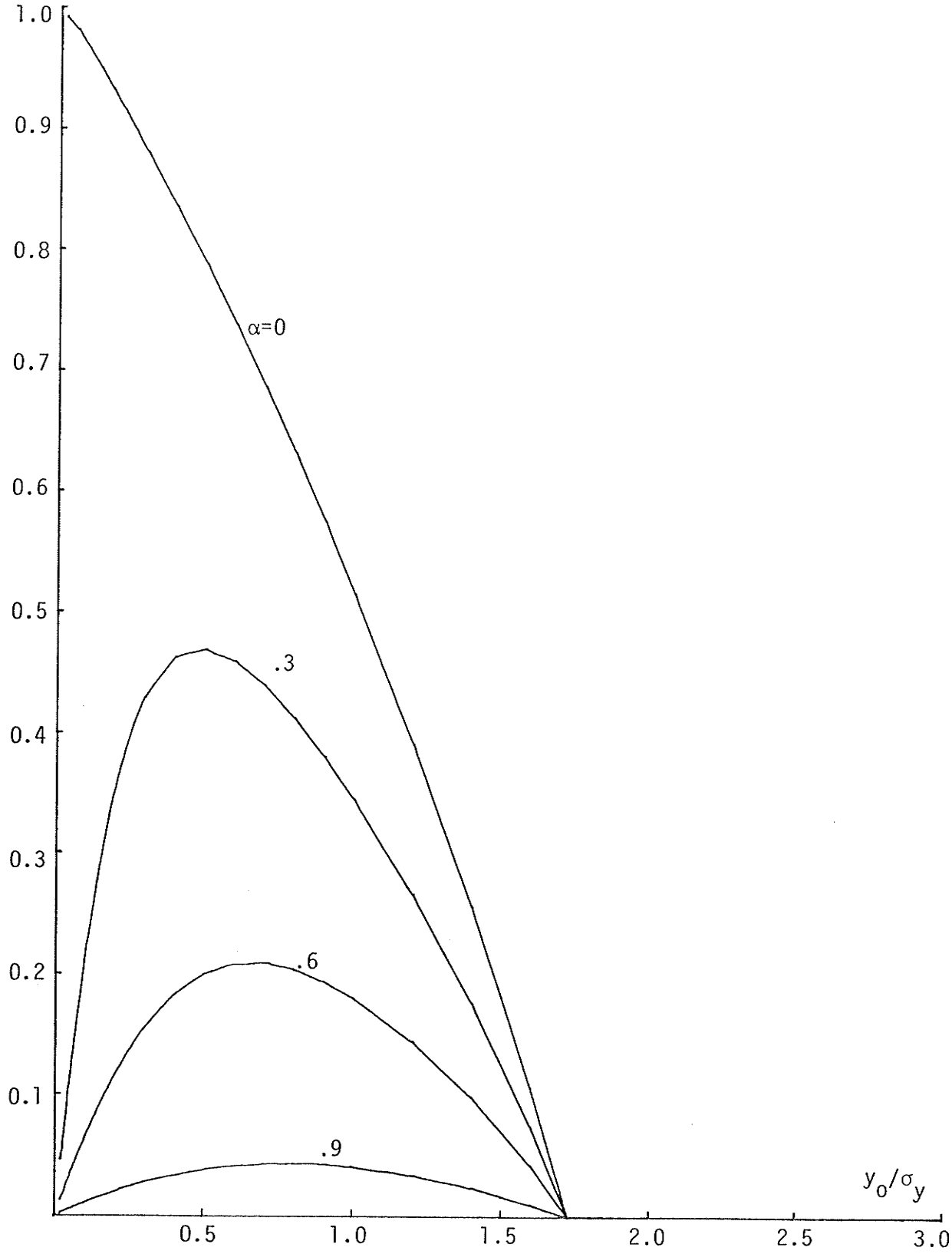

Figure 4.5 Plots of Power Ratio--Triangular Input Waveform

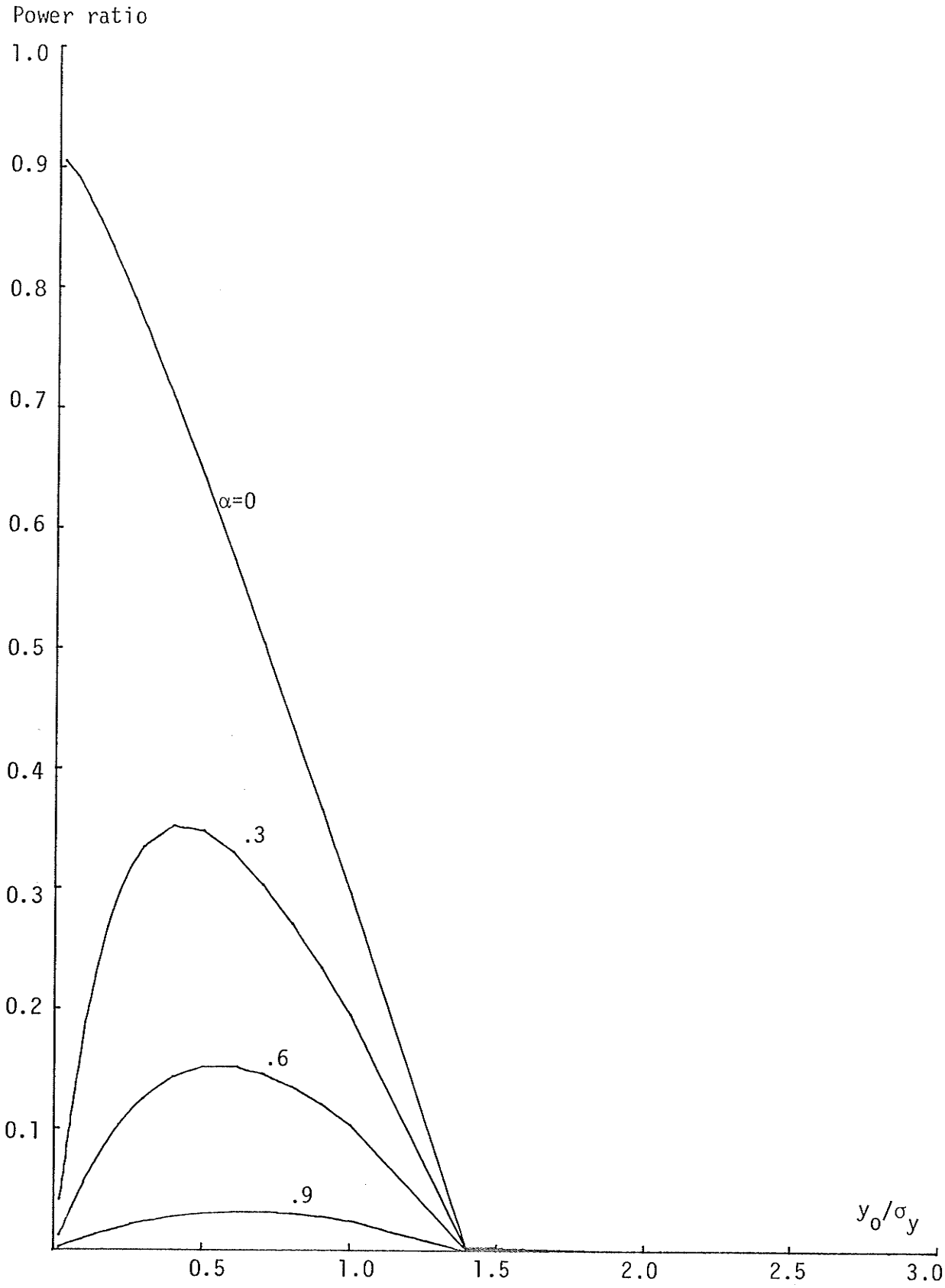

Figure 4.6 Plots of Power Ratio--Sinusoidal Input Waveform

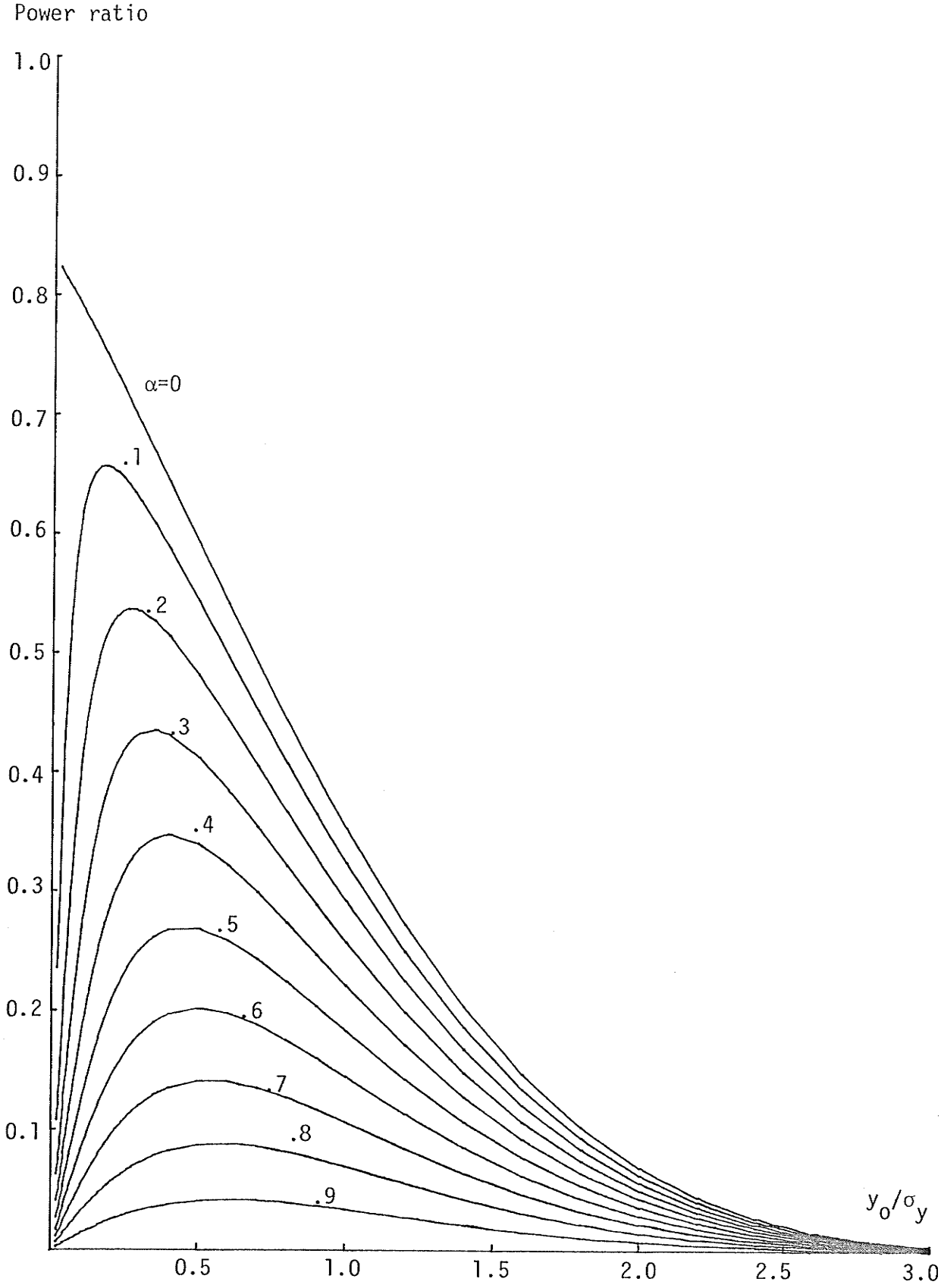

Figure 4.7 Plots of Power Ratio--Gaussian Low-Pass Waveform (0-1 Hz)

the values of power ratio are sharply truncated for the triangular and sinusoidal cases, whereas for the Gaussian case, the power ratio drops asymptotically to zero.

With reference to Figure 4.7, some interesting features can be noted in the region where y_o/σ_y is small. These may be best illustrated with the aid of Figure 4.8(a), which shows the energy storage and dissipation of the bilinear hysteretic model of Figure 4.1(a) in a quarter cycle of oscillation. The first spring $k\alpha$ is linear, and hence only stores energy. The second spring $(1-\alpha)k$ is linear for displacement amplitude less than y_o, hence stores energy in this region. Beyond y_o, this spring becomes plastic and therefore, only dissipates energy, the amount of which is equal to the shaded area ($\hat{y}$ is the maximum displacement amplitude). Now, consider the case when α equals 0, i.e. when the first spring does not exist. For small values of y_o/σ_y, as in Figure 4.8(b), there is little build-up in stored energy, and almost all energy is dissipated, hence, the power ratio has a maximum value, see Figure 4.7. Physically, for an elasto-plastic element, there is a lack of energy storage which gives rise to central tendency, i.e. there is no tendency for the element to return to its original configuration. When the values of α increases, substantially more energy stored is brought about by the first spring, and if y_o/σ_y is small, as in Figure 4.8(b), the amount of dissipation is negligible when compared to the huge amount of storage, hence, the value of power ratio is small. In fact, with the exception for α equals 0, all curves tend to zero power ratio as y_o/σ_y tends to zero, see Figure 4.7. The large amount of energy storage indicates that there is a strong tendency for the element to return to its

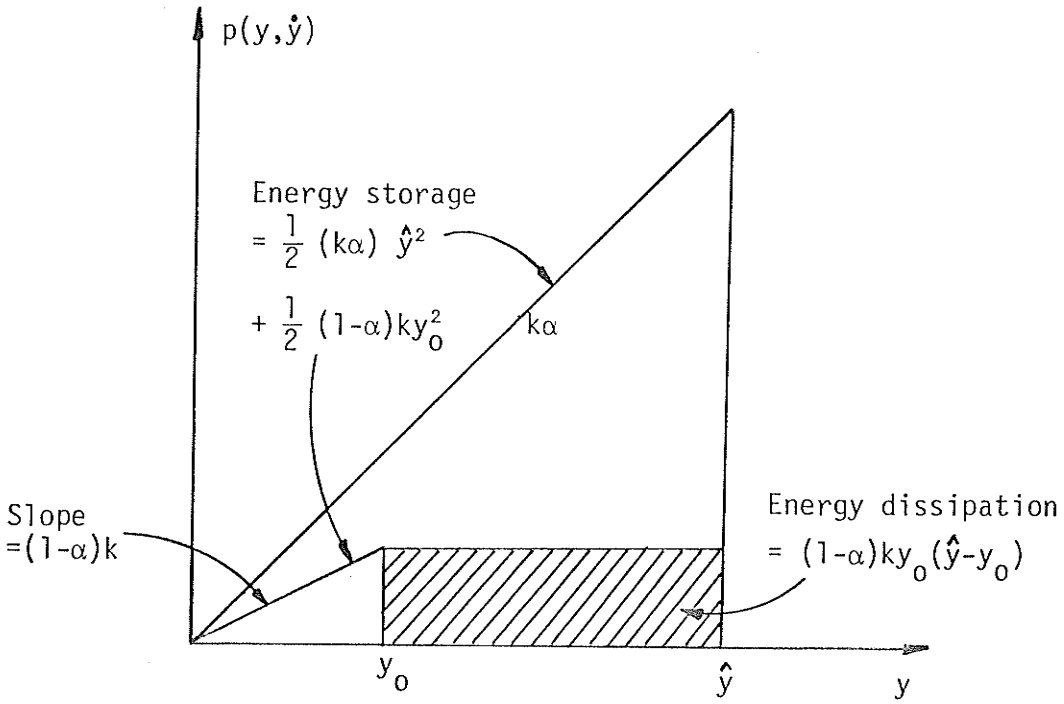

(a) Moderate y_o

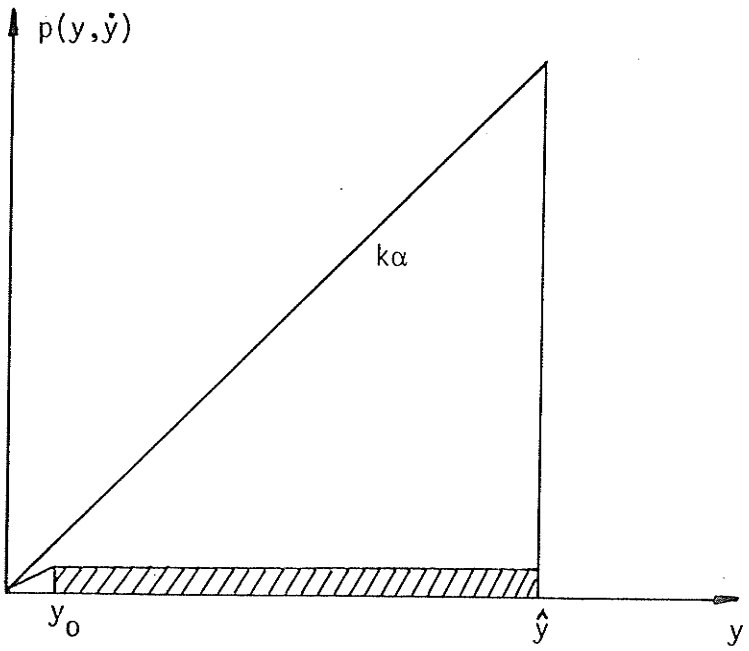

(b) Small y_o

Figure 4.8 Energy Storage and Dissipation of a Bilinear Hysteretic Element in 1/4 Cycle

original position, and there is virtually no dissipation relative to storage of energy.

In addition to the waveform dependency just described, the power ratio indicates that the hysteretic element is also bandwidth dependent. In Figure 4.7, where the cut-off frequency ($f_1 = 0$ Hz, $f_2 = 1$ Hz) ratio is infinite, the power ratio has a maximum value of 0.82 when α equals 0. In Figure 4.9, in which the cut-off frequency ($f_1 = 1$ Hz, $f_2 = 2$ Hz) ratio is 2, the maximum power ratio increases to 0.87. Finally, for a narrow-band input process, as in Figure 4.10, in which the cut-off frequency ratio approaches 1, the maximum power ratio is nearly 0.9, close to the result of the sinusoidal case (Figure 4.6).

Work was then carried out to study the frequency dependent nature of the hysteretic element using the computational model with an input displacement having a Gaussian distribution. The results are graphed in Figure 4.11 for the case of α equals 0 and y_o/σ_y equals 0.08. It is found that the calculated power ratio depends on the ratio of, rather than the difference in, the cut-off frequencies f_1 and f_2 of the input displacement process. Thus, an input process having cut-off frequencies 1 and 10 Hz and another process having cut-off frequencies 10 and 100 Hz will have the same effect on the hysteretic element as far as the value of power ratio is concerned. Shown in Figure 4.11 is the power ratio plotted against the number of octaves between f_1 and f_2, which is referred to as the bandwidth ratio F_{12} and is mathematically defined as $\log(f_2/f_1)/\log 2$. When F_{12} tends to zero, the input becomes a narrow-band process, the power ratio has a value of 0.85, which, for α equals 0 and y_o/σ_y equals 0.08, agrees with the value given in Figure 4.10.

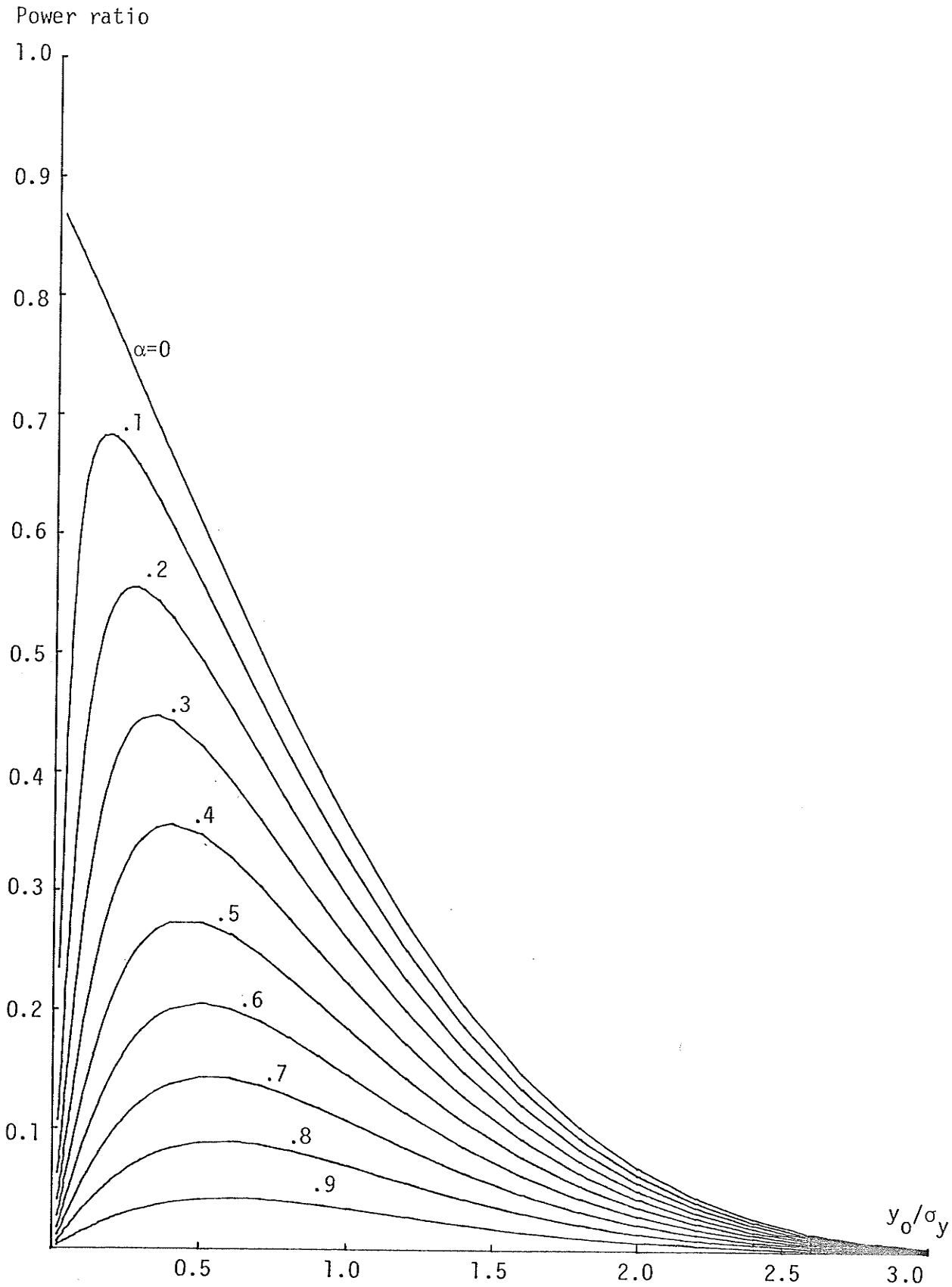

Figure 4.9 Plots of Power Ratio--Gaussian Waveform (1-2 Hz)

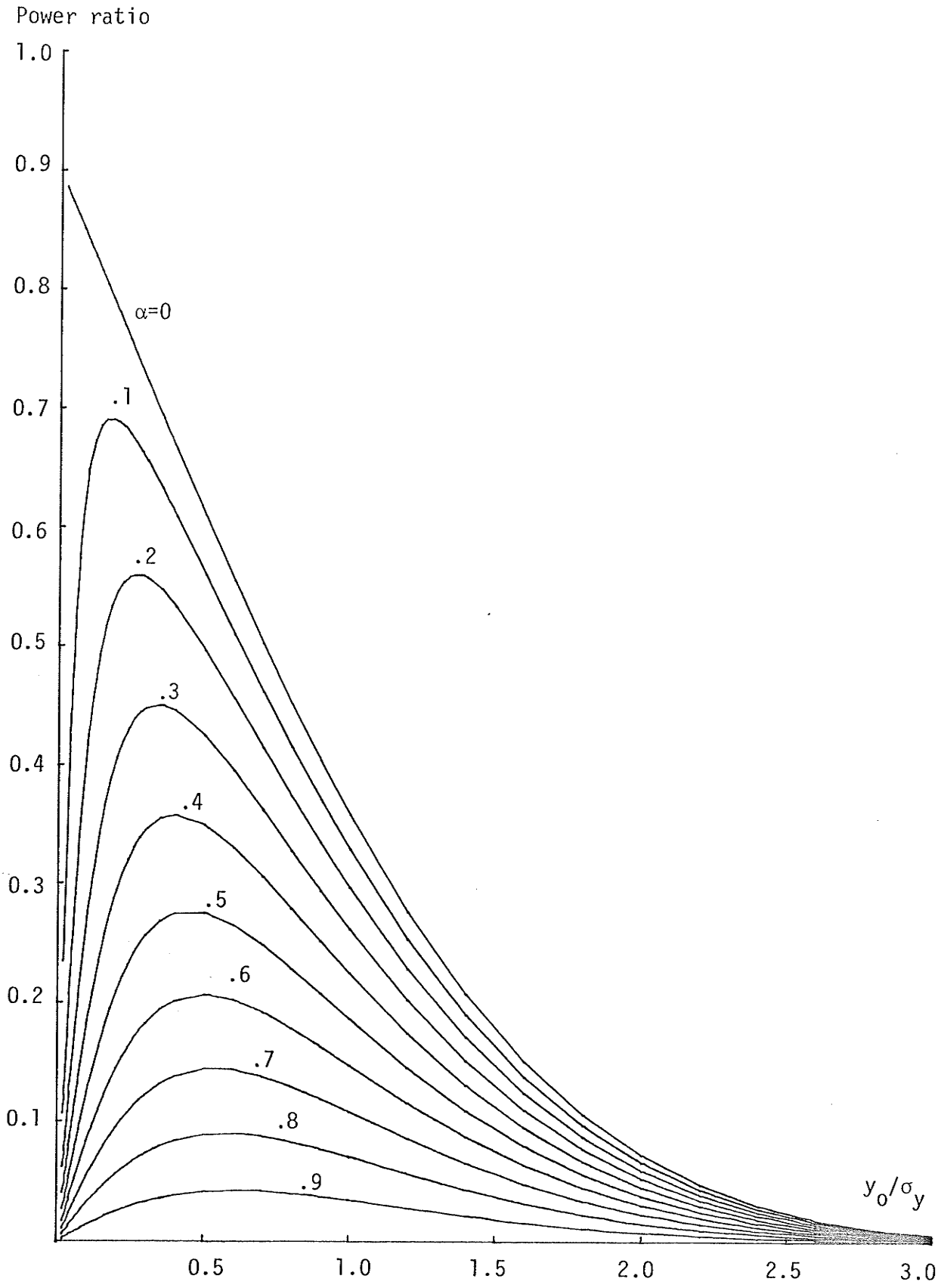

Figure 4.10 Plots of Power Ratio--Gaussian Narrow-Band Waveform

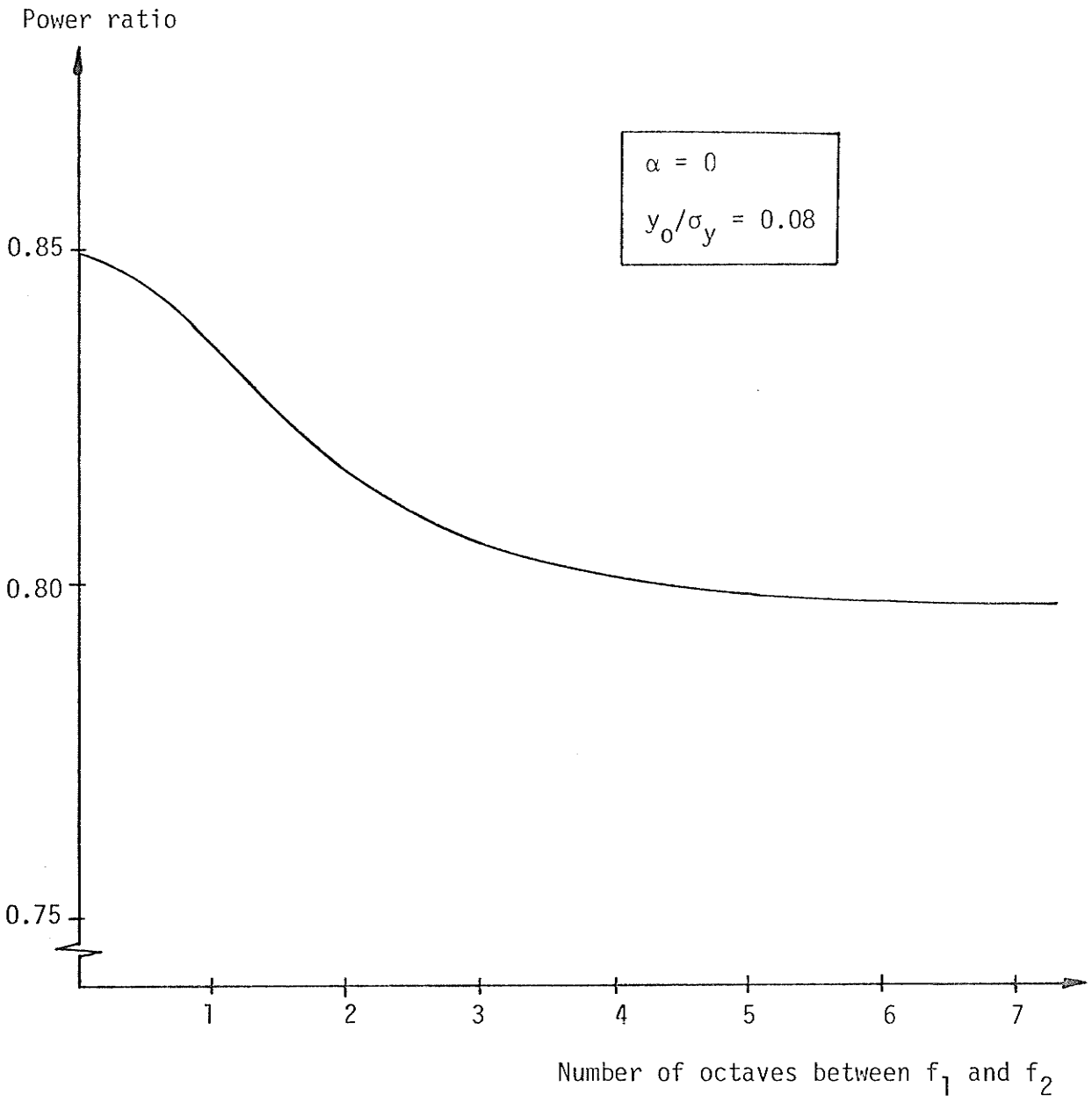

Figure 4.11 Effect of Bandwidth Ratio in a Bilinear Hysteretic Element

When F_{12} increases, the power ratio drops more or less in a semi bell-shape fashion. For large values of F_{12}, the power ratio drops asymptotically: When F_{12} equals 7, the power ratio is 0.7966; and for a low-pass process (F_{12} infinite), the power ratio is 0.7961. This bandwidth ratio dependency of the bilinear hysteretic element demonstrates once again, the dependency of the element upon the form factor of the input displacement waveform. This is because, in practice, the bandwidth ratio affects the form factor (peak amplitude/r.m.s. amplitude) of a random process. It is expected that the effect of bandwidth ratio for other values of α and y_o/σ_y will be similar to that shown in Figure 4.11. The extensive computations involved in exploring a wide range of these values, together with the need to explore other features of the hysteretic element caused deferral of further investigation of bandwidth ratio effects.

Interesting characteristics of a bilinear hysteretic element such as its waveform and bandwidth ratio dependencies have been investigated. The study of this nonlinear element is crucial to the understanding of hysteresis in general and gives ways to the study of a 1-DOF hysteretic system.

CHAPTER V

POWER RATIO IN BILINEAR HYSTERETIC SYSTEMS

5.1 INTRODUCTION

In the investigation of the isolated, bilinear hysteretic element the form factor of the displacement waveform was clearly an independent controlled variable. Thus, the behavior of the element with different form factors could be investigated. When the element forms part of a vibrating system, however, displacement will, in general, be a dependent variable. The loss in the system will depend upon the amplitude and form factor of the displacement across the hysteretic element and, in turn, the amplitude response to a given forcing will depend upon the effective loss in the system. This interdependence between the loss mechanism, forcing and response is the essential problem in studying the nonlinear structures that are of interest in the present context. To pursue this study with minimum additional complexities a single mass was added to the bilinear hysteretic element and the mass subjected to a known force, p(t).

5.2 1-DOF SYSTEMS

In the system of Figure 5.1, m, k, α are as previously defined and their values are assumed to be known. Thus, everything is known except the displacement, velocity and acceleration responses of the mass. The Coulomb slider moves at a force level of $\pm (1-\alpha)ky_o$, where y_o is the yield displacement of the system. The total restoring force $g(y,\dot{y})$ of the hysteretic element is, as before, shown in Figure 4.1(b). The equation

of motion of this system is

$$m\ddot{y} + g(y,\dot{y}) = p \ , \qquad (5.1)$$

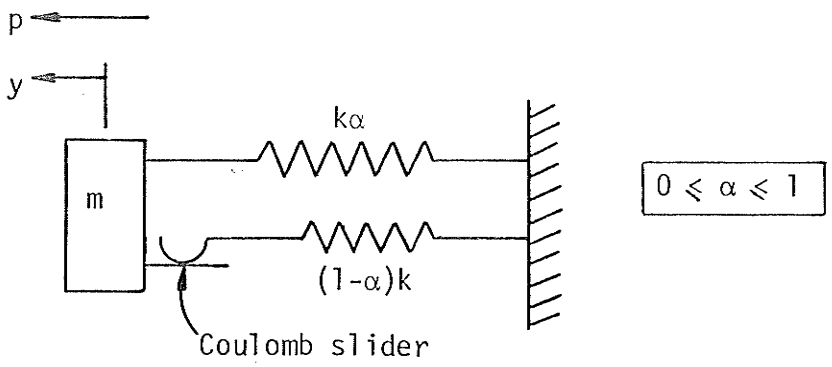

Figure 5.1 Model of a 1-DOF Bilinear Hysteretic System

As before, only average measures of the responses will be discussed and it is important to note that the probability distributions of the responses will not in general have the same form as that of the input force.

5.2(i) Theoretical Model

A complete theoretical model of the 1-DOF hysteretic system which yields a closed form solution is not realizable. To help to further the investigation, however, a preliminary theoretical model has been produced on the basis of weak nonlinearity and known hysteretic properties. The assumption of weak nonlinearity severely limits the applicability of the model, and the model is presented not as a tool to validate results from other models, but to offer some insight to the problem and possibly, to give a basis for further investigation.

It is assumed that the displacement response of the bilinear

hysteretic system to a Guassianly distributed forcing function is also Gaussian. This assumption is satisfactory in cases where the root-mean-square value of the displacement response is small compared with the yield displacement. Using this assumption, y^*, the mean of the peak values of y which are greater than the yield level y_o, can be calculated using the procedure given in Appendix E. The average power dissipation $\overline{p\dot{y}}$, again, can be approximated by equation (4.8) as

$$\overline{p\dot{y}} = 4\, ky_o(1-\alpha)y^*, \frac{1}{2\pi}\frac{\sigma_{\dot{y}}}{\sigma_y} e^{\frac{-y_o^2}{2\sigma_y^2}} . \qquad (5.2)$$

Using equation (5.2), the power ratio W of the bilinear hysteretic system is given by

$$W = \frac{4\, ky_o(1-\alpha)y^*.\frac{1}{2\pi}\frac{\sigma_{\dot{y}}}{\sigma_y} e^{\frac{-y_o^2}{2\sigma_y^2}}}{\sigma_p \cdot \sigma_{\dot{y}}} ,$$

where σ_p is the r.m.s. value of the forcing function.

By letting g_o equal ky_0, the power ratio becomes

$$W = \frac{2}{\pi}\frac{g_o}{\sigma_p}(1-\alpha)\frac{y^*}{\sigma_y} e^{\frac{-y_o^2}{2\sigma_y^2}} . \qquad (5.3)$$

The power ratio, then, depends upon three dimensionless parameters, α, $\frac{g_o}{\sigma_p}$ and $\frac{y_o}{\sigma_y}$ †. α is a system parameter, $\frac{g_o}{\sigma_p}$ is a system and forcing parameter, and $\frac{y_o}{\sigma_y}$ is a system and response parameter. Unfortunately, these parameters are not independent. $\frac{y_o}{\sigma_y}$, being an output parameter, will depend on the other two input parameters. Equation (5.3) will be of more

† $\frac{y^*}{\sigma_y}$ in equation (5.3) is a function of $\frac{y_o}{\sigma_y}$

value if $\frac{y_o}{\sigma_y}$ can be expressed in terms of α and $\frac{g_o}{\sigma_p}$.

Relationships of an approximate nature between $\frac{y_o}{\sigma_y}$ and $\frac{g_o}{\sigma_p}$ and α have been obtained for weakly nonlinear systems [5,24,27]. Unfortunately, similar relationships for highly nonlinear hysteretic systems were not available. To obtain such relationships, the probability distributions and the frequency spectrum of the responses need to be more exactly derived. This is a major undertaking and contributions from many sources will be required. For this reason, further study on the theoretical model was deferred and the simulation of the system of Figure 5.1 was performed on a digital computer so that exploration over a wide range of system and input parameters could be investigated.

5.2(ii) Simulation Model

A number of advantages were seen in developing a simulation model. Firstly, it takes relatively less time to develop than a satisfactory physical model, which is complicated to design and requires extremely fine workmanship to build. Secondly, the simulation model is an "ideal" system. And thirdly, with the simulation model, a wide range of parameters can be explored. The difficulties inherent in a satisfactory validation of such a model, however, make the subsequent testing of a physical model highly desirable.

In the simulation model, the system responses (velocity, displacement and restoring force) are computed using step-by-step numerical integration [6]. The model is assumed to consist of a sequence of successively changing linear systems, each existing for an equal time step. The nonlinearity of the model is accounted for by using new properties corresponding to the current deformed state at the beginning of each time

step. Dynamic equilibrium is established at the beginning of the time step and the motion of the model during the time step is evaluated on the basis of a linear acceleration mechanism. The responses computed at the end of a time step are used as initial conditions for the next step, thus the process can be continued step-by-step for any desired time. A time step of about one-tenth of the small amplitude vibration period of the model was used to give stable results [6]. To account for the change of state in the hysteretic element, a special subdivided time step, found by trial and error, is introduced to treat this effect accurately. Further details of this program appear in Appendix I.

Mean values of $\overline{\dot{y}\dot{y}}$ and $\overline{p\dot{y}}$ (or $\overline{g\dot{y}}$) may be evaluated once the system responses are known. Values of power ratio can then be found for various values of the model and forcing parameters. These parameters may be grouped into three dimensionless variables, namely, α, $\frac{g_o}{\sigma_p}$ and a frequency parameter. In this case force is the controlled input variable and, hence, $\frac{g_o}{\sigma_p}$ replaced $\frac{y_o}{\sigma_y}$ used in the hysteretic element investigation. The frequency parameter includes the forcing frequency parameters (e.g. cut-off frequencies) and the small amplitude natural frequency of the model.

5.3 SIMULATION RESULTS AND DISCUSSIONS

Preliminary investigations were performed using both periodic (sinusoidal, triangular and square) and random excitation. In all cases, 256 input data points were used. Increasing this number by a factor of eight in a number of test runs produced less than eight percent difference in the results. Hence, a sample size of 256 was considered adequate

to explore the form of the response of the 1-DOF hysteretic model.

In the periodic excitation cases, an excitation frequency of 0.078 Hz (8 cycles over 256 input data, sampling rate 0.4 second) was first selected. A small amplitude natural frequency f_o of 0.113 Hz ($k = 0.5$ N/metre, $m = 1$ kg) was selected for the model such that it is just higher than the forcing frequency and at the same time, gives a vibration period at least ten times [6] greater than the integration time step. An integration time step of 0.4 second was chosen equal to the sampling time for computational efficiency. In the random excitation cases, the frequency range of the forcing spectrum was from 0.09 to 0.23 Hz. The small amplitude natural frequency of the model was first chosen to be 0.2 Hz (close to the upper cut-off frequency of the forcing). Again, the integration time step was 0.4 second. Figures 5.2, 5.3, 5.4 and 5.5 are plots of power ratio versus g_o/σ_p, for a range of values of α, for sinusoidal, triangular, square and random forcing excitation respectively.

From Figures 5.2, 5.3 and 5.4, it may be seen that the results for the three periodic input waveforms are very similar. This is in sharp contrast with the results obtained from the pure hysteretic element. This difference is due to the "smoothing" effect of the mass in converting force to velocity and displacement. Thus, to a first approximation, velocity and displacement are sinusoidal in waveform for each of the three periodic force waveforms used. Consequently, the form factor of the displacement waveform of the hysteretic element is not much affected by the changes in forcing waveform. It will be remembered that displacement form factor is significant in determining the loss effectiveness of

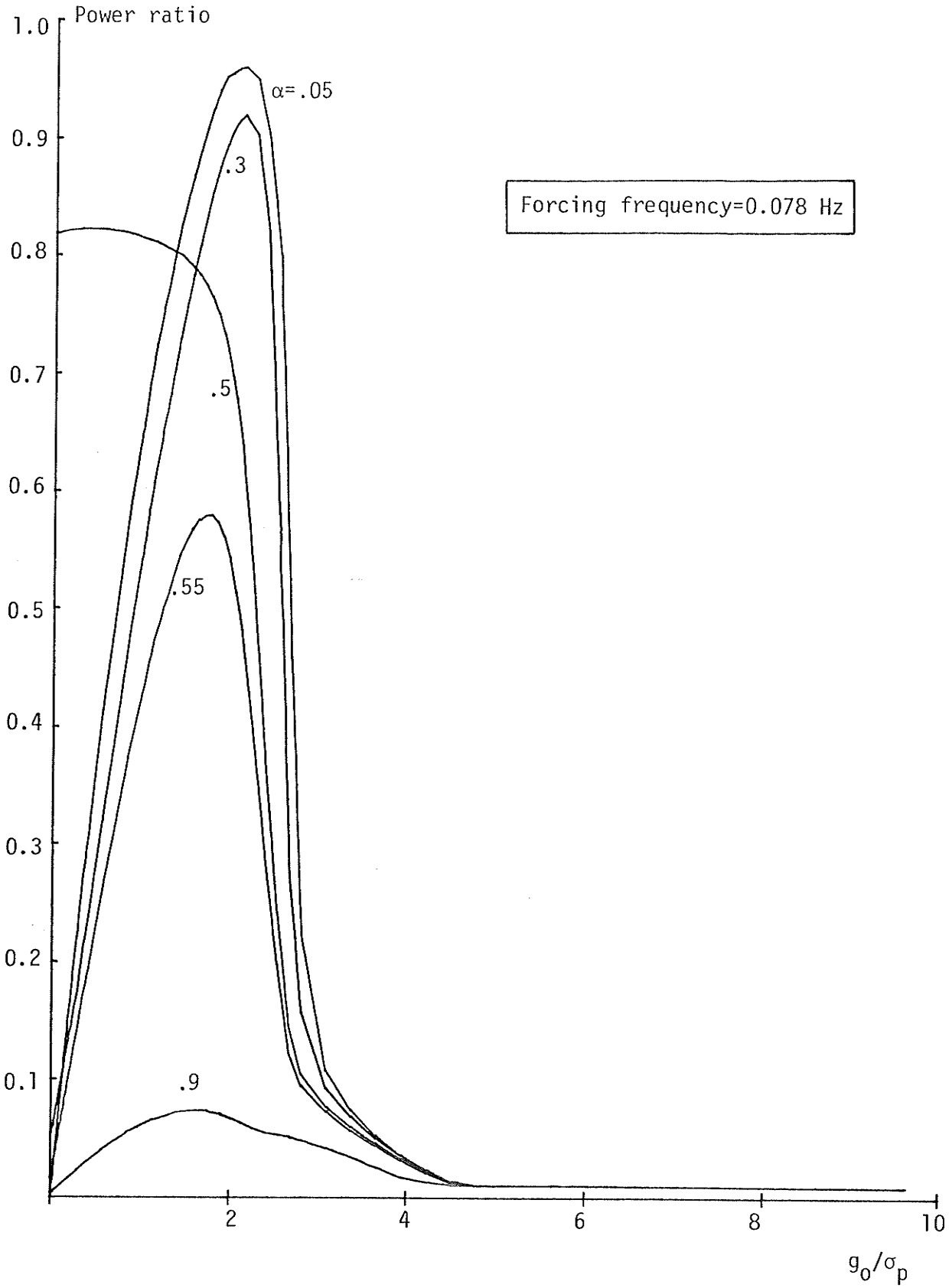

Figure 5.2 Plots of Power Ratio--Sinusoidal Input Waveform, f_o=0.113 Hz

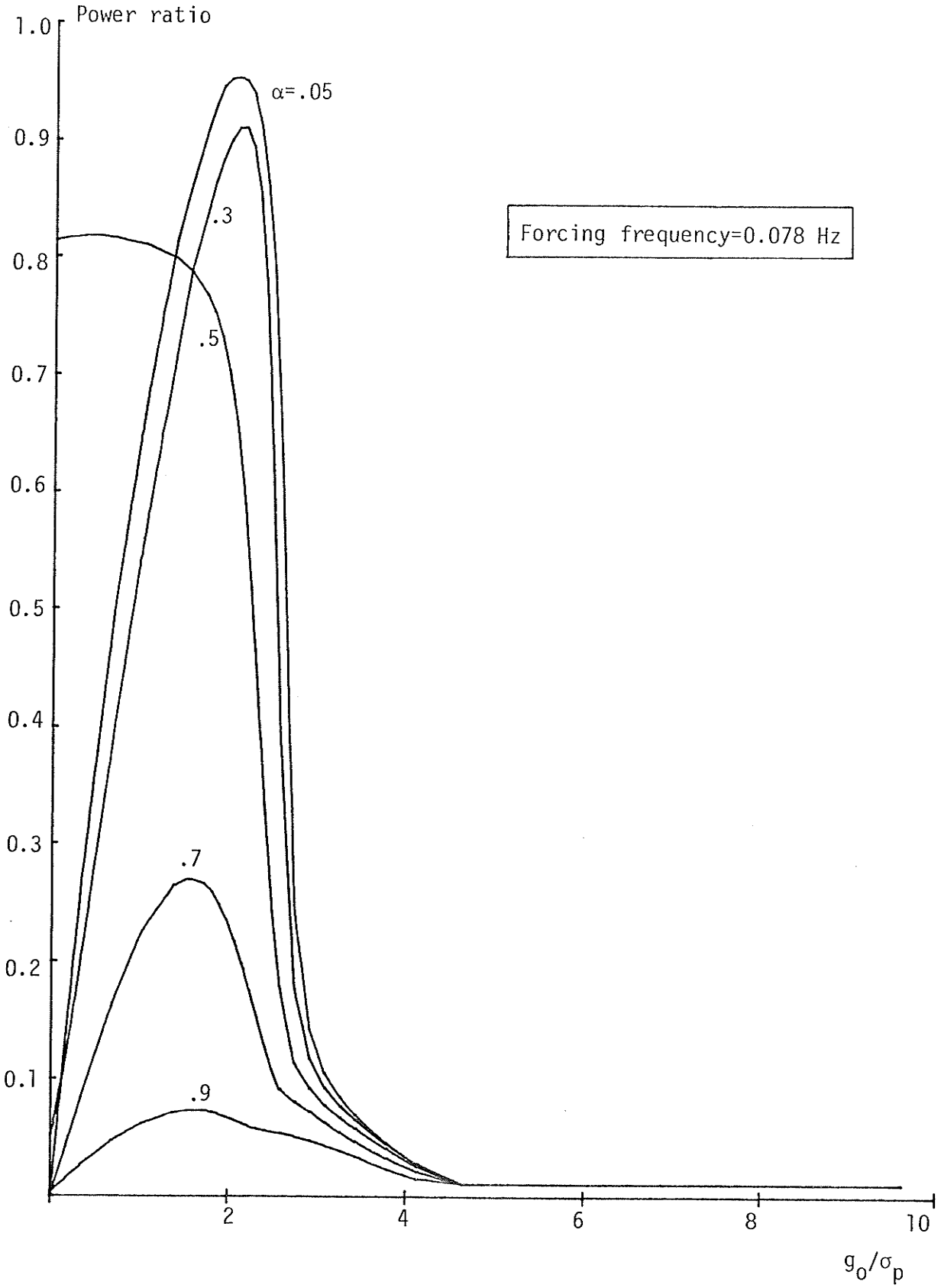

Figure 5.3 Plots of Power Ratio--Triangular Input Waveform, f_o=0.113 Hz

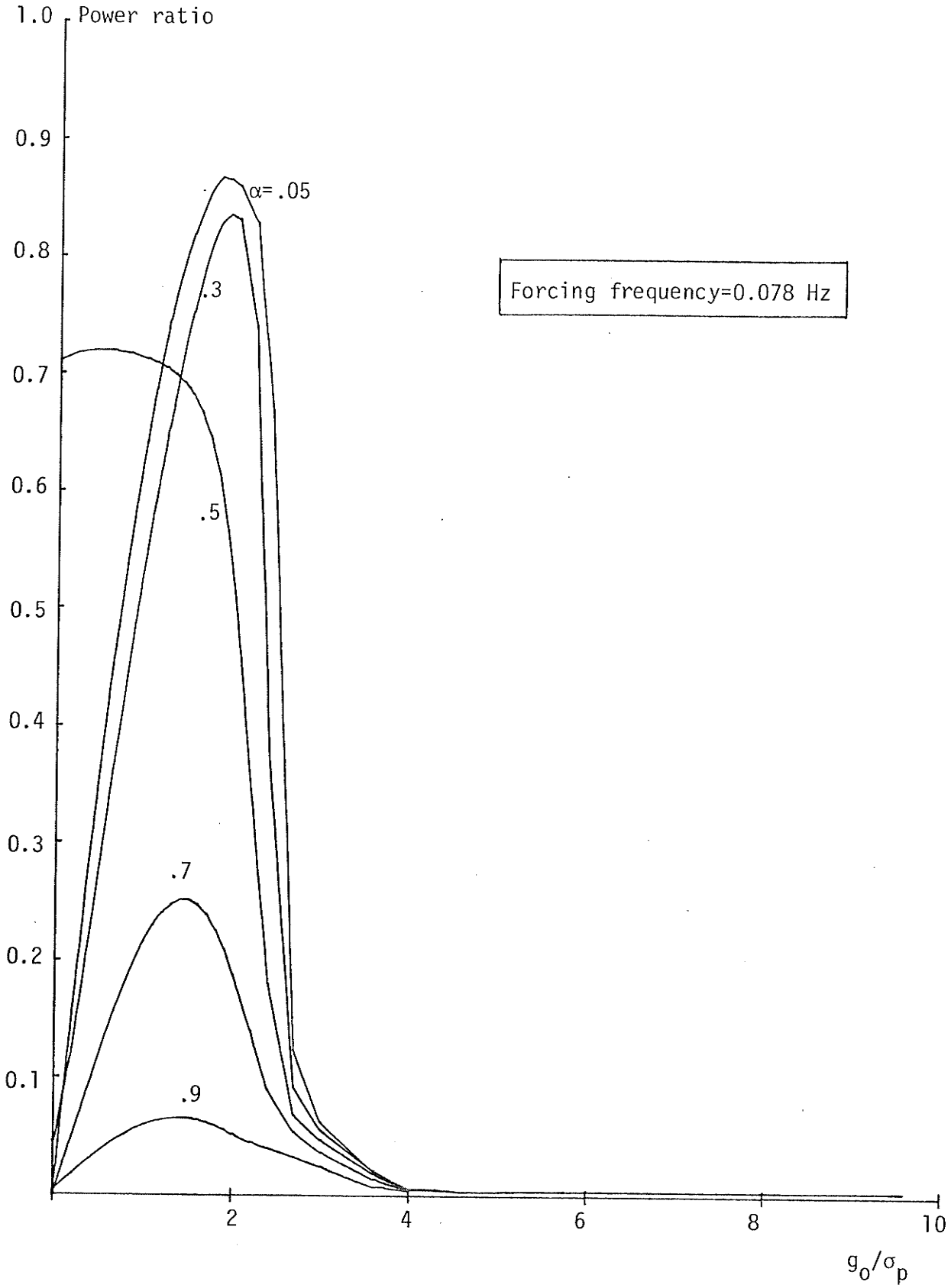

Figure 5.4 Plots of Power Ratio--Square Input Waveform, f_o=0.113 Hz

an hysteretic element.

Another interesting feature of the response of the hysteretic system to periodic excitations is indicated by the peaks in the power ratio for certain combinations of α and $\frac{g_o}{\sigma_p}$. This is due to the fact that the addition of a mass produces a system which will store energy in both kinetic and potential forms. The resonant frequency of the system is governed not by k directly but by the effective stiffness which depends upon α and the extent of yielding induced by the applied force. If the forcing frequency is less than the small amplitude natural frequency and α less than 0.5, a value of g_o/σ_p can be found that will "tune" the resonant frequency of the system to coincide with that of the forcing. Thus a peak in the power ratio curve is produced at this value of g_o/σ_p by the offsetting effect of two forms of energy storage. The case of α equals 0.5 is interesting. When the excitation σ_p is large compared with g_o, the system always yields. Hence, the effective stiffness of the system is $k\alpha$ and the resonant frequency ($\sqrt{k\alpha/m}/2\pi$) is found to be 0.079, which is approximately equal to the forcing frequency. Consequently, with α equals 0.5 the system is virtually at resonance and the power ratio is maximum for all values of σ_p that are comparable with, or greater than the yield force g_o (see Figures 5.2 through 5.4).

For other values of α, it is found that as g_o/σ_p approaches zero, the power ratio does not necessary tend to zero. This is again contrary to the results obtained from an hysteretic element in which the power ratio tends to zero as y_o/σ_y approaches zero for all values of α except zero. In the case of a pure hysteretic element, the potential energy will

dominate as σ_y become large ($y_o/\sigma_y \to 0$) for α non-zero, hence the power ratio will tend to zero. In the case of an hysteretic system, under similar circumstances both the potential energy and kinetic energy levels may be large depending upon the relationship between the forcing and the "resonant" frequencies. As a result of the offsetting effect of the two forms of energy, the total storage energy may not be large. Hence, the power ratio does not necessarily tend to zero. The results for α equals zero are not stable in the present case because of the lack of central tendency.

For α greater than 0.5, the effective resonant frequency of the system is always less than the forcing frequency. Hence, a peak in the power ratio is not a result of simple resonance, but corresponds to a circumstance when the total storage energy is minimum.

Similar curves to those just discussed but for the random forcing function are shown in Figure 5.5, from which it may be seen that the peaks of the curves are less sharp. This is because forcing energy is more evenly distributed among the various frequencies of forcing, hence, the effective resonance is spread out. As before, the values of power ratio do not necessarily tend to zero as g_o/σ_p approaches zero. It is of interest to note that the power ratio does not seem to be asymptotic with zero as g_o/σ_p tends to infinity, e.g. Figure 5.5. It was thought that this might be caused by the fact that at large values of g_o/σ_p the system becomes nearly linear and is very lightly damped. Thus, if a peak in the input spectrum is close in frequency to the resonant frequency of the system a non-zero power ratio might be expected. To investigate this effect, a series of simulation runs were performed with the 1-DOF system

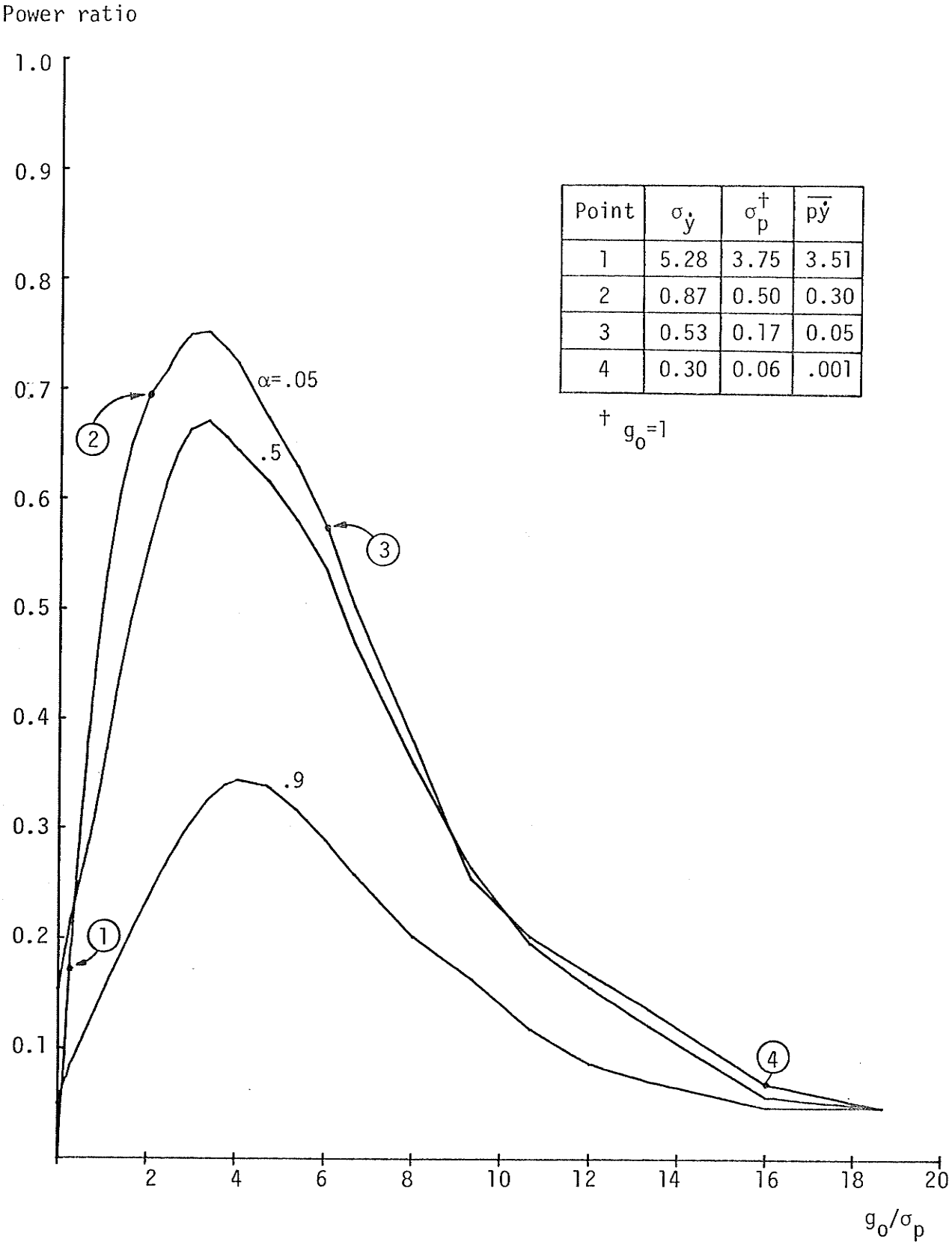

Point	$\sigma_{\dot{y}}$	$\sigma_p^{\dagger}$	$\overline{p\dot{y}}$
1	5.28	3.75	3.51
2	0.87	0.50	0.30
3	0.53	0.17	0.05
4	0.30	0.06	.001

† $g_o=1$

Figure 5.5 Plots of Power Ratio--Narrow-Band Excitation, f_o=0.2 Hz

set to α equals 0.99. In this way, a virtually linear, very lightly damped system is simulated.

In the first exploratory experiment the small amplitude natural frequency of the system was incremented in small steps from 0.02 Hz to 0.6 Hz and the power ratio determined at each frequency. The results are shown plotted in Figure 5.6 and, as expected, the system when measured under these conditions is, in effect, a spectrum analyser. This is confirmed by reference to Figure 5.7 which shows the spectrum of the narrow-band forcing as obtained by digital Fourier transformation.

From Figure 5.6 it is clear that with the particular narrow-band random forcing used, power ratio of approximately zero to 0.4 are to be expected at high values of g_o/σ_p. The actual value to be expected will depend upon the position of the small amplitude natural frequency of the 1-DOF system. To confirm this, plots similar to that shown in Figure 5.5 were made with the small amplitude natural frequency set to 0.123 Hz and then to 0.113 Hz. These plots are presented in Figures 5.8 and 5.9 respectively. The plot of Figure 5.5 for which the small amplitude natural frequency is 0.2 Hz may also be included in this discussion. In each of the three cases there is good agreement between the power ratio indicated at the small amplitude natural frequency (Figure 5.6) and at large values of g_o/σ_p (Figures 5.5, 5.8 and 5.9).

Although the power ratio may have a significant value at large values of g_o/σ_p, this effect may not have a significant impact on the general performance of the system because in such cases, the excitation level is extremely small. In Figures 5.5 and 5.8, some values of the excitation level σ_p, velocity $\sigma_{\dot{y}}$ and actual power dissipation $\overline{p\dot{y}}$ are given

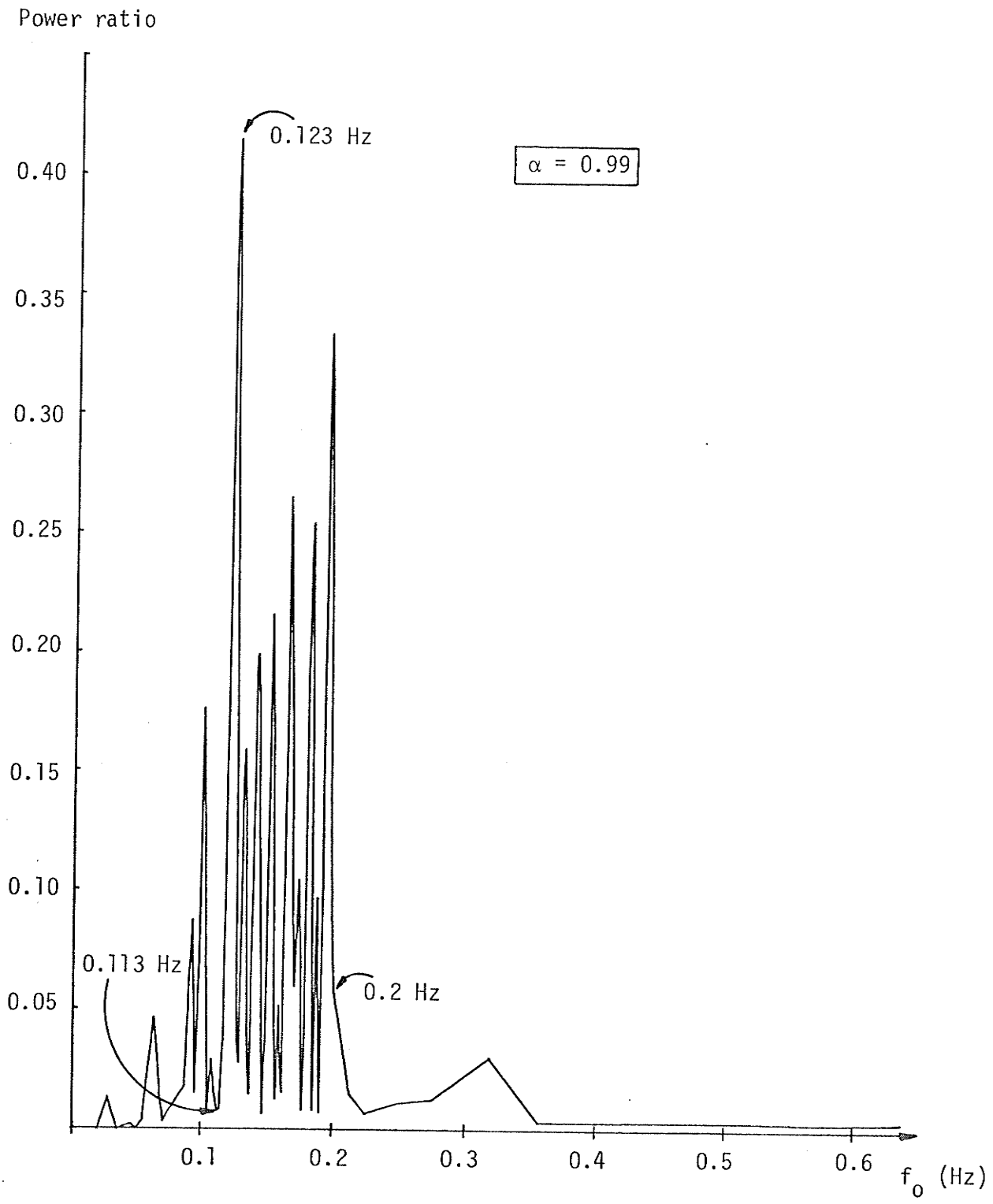

Figure 5.6 Power Ratio Versus Small Amplitude Natural Frequencies f_o -- Narrow-Band Excitation

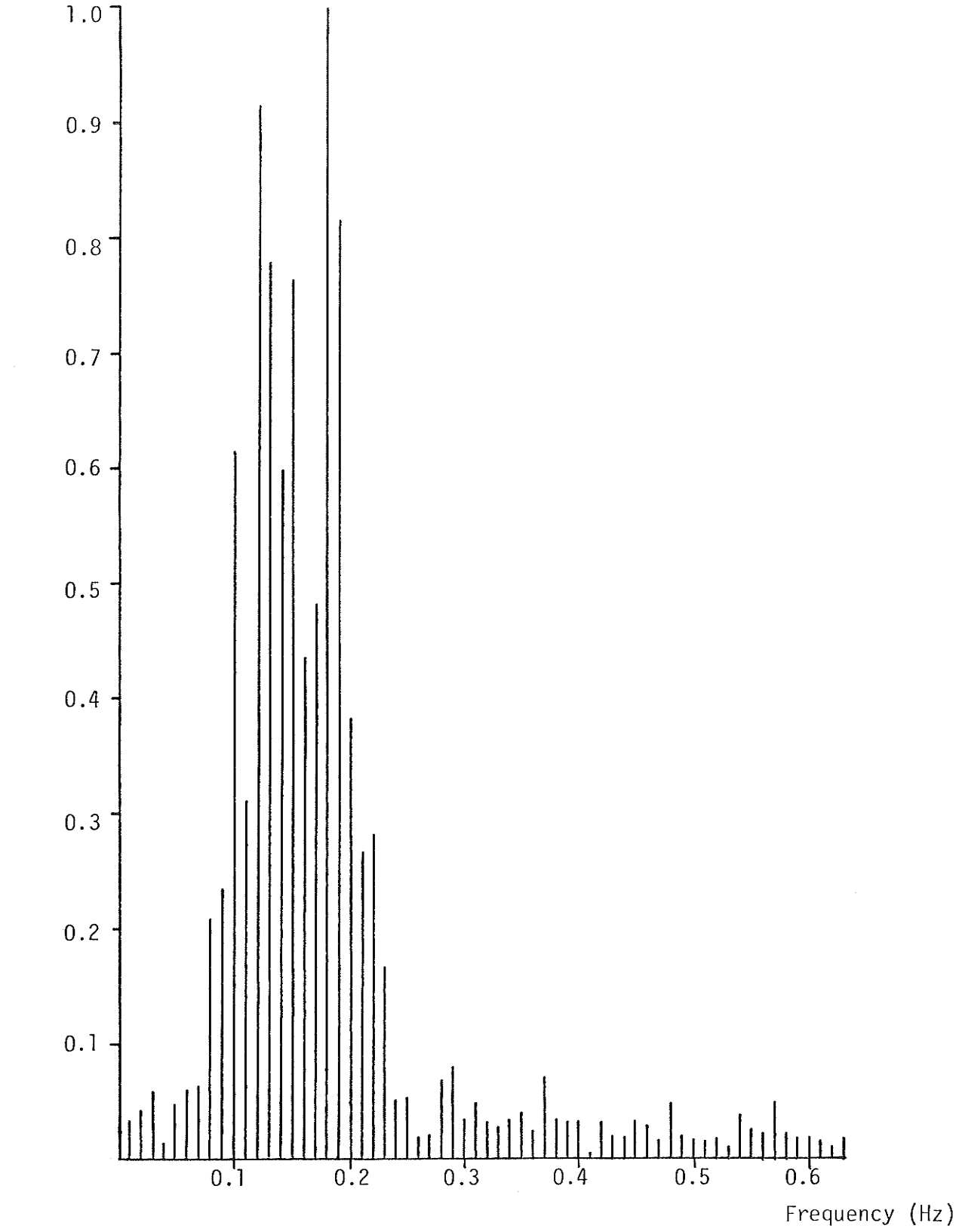

Figure 5.7 Amplitude Spectrum of Narrow-Band Random Forcing

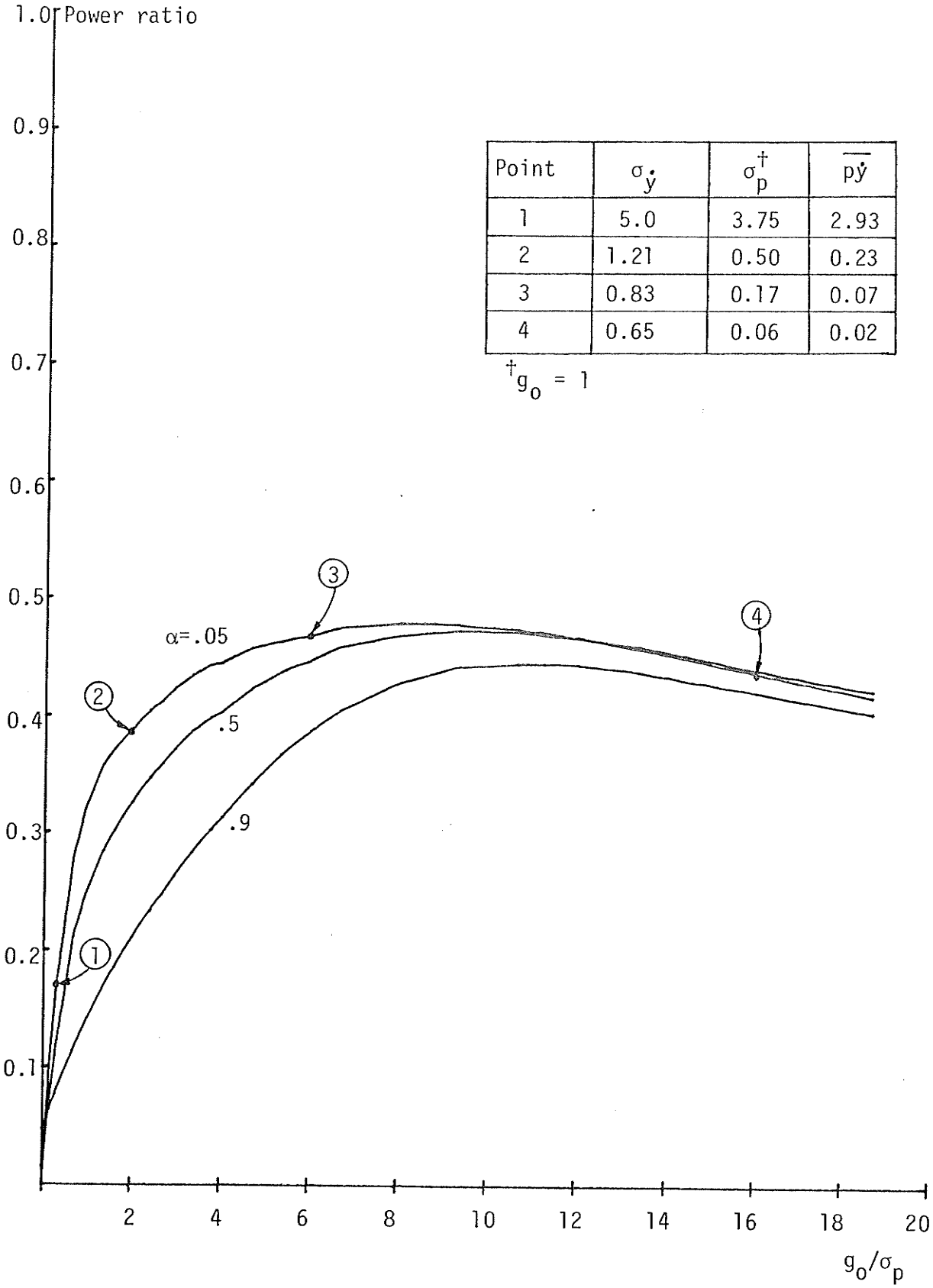

Point	$\sigma_{\dot{y}}$	$\sigma_p^{\dagger}$	$\overline{p\dot{y}}$
1	5.0	3.75	2.93
2	1.21	0.50	0.23
3	0.83	0.17	0.07
4	0.65	0.06	0.02

$^{\dagger}g_o = 1$

Figure 5.8 Plots of Power Ratio--Narrow-Band Excitation, f_o=0.123 Hz

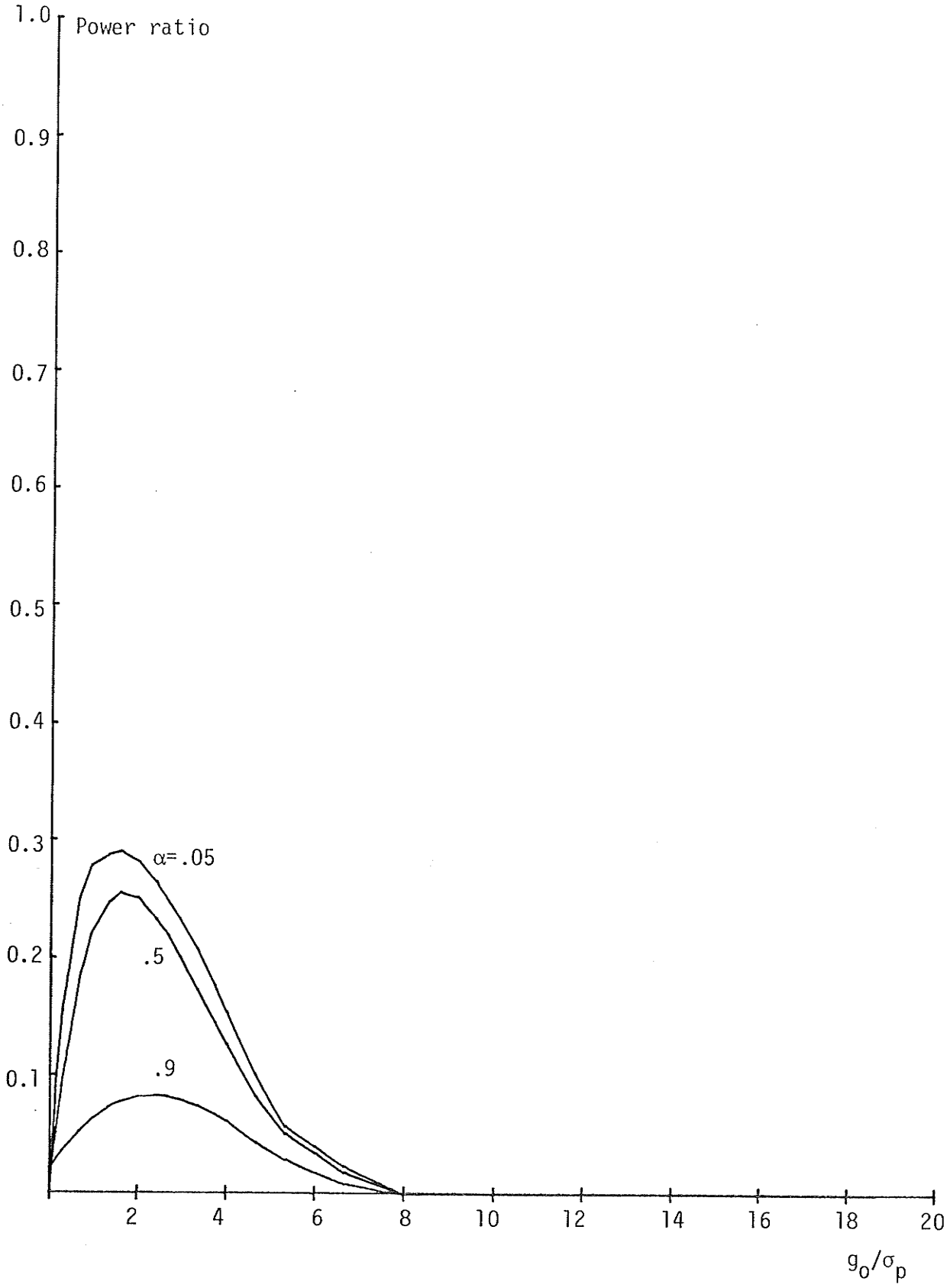

Figure 5.9 Plots of Power Ratio--Narrow-Band Excitation, f_o=0.113 Hz

at selected values of g_o/σ_p. In both figures, it is noted that at point 4 (corresponds to large g_o/σ_p), the values of $\sigma_{\dot{y}}$, σ_p and $\overline{p\dot{y}}$ are small compared to those at smaller values of g_o/σ_p (points 1,2 and 3). Hence, what proportion of power input is being dissipated at large values of g_o/σ_p is really immaterial. What is important is that the power ratio always give the true proportion of power dissipation for any system no matter how the system is forced.

A last observation on Figures 5.5 and 5.9 is that the values of power ratio of the latter are consistently lower than those of the former figure. This may be explained by referring to Figure 5.6. The small amplitude natural frequency employed in the case of Figure 5.9 is 0.113. As g_o/σ_p becomes small the system becomes nonlinear, and the effective resonant frequency will shift to the left into a low energy content part of the forcing spectrum so that the system has small kinetic energy. The case of Figure 5.5 has a small amplitude natural frequency of 0.2 Hz and increasing non-linearity will drive the effective resonant frequency into a region of high energy content. For a certain excitation level of g_o/σ_p or y_o/σ_y, the potential energy in each case will, in general, stay constant. Hence the case of Figure 5.9 will have more storage energy and a lower power ratio than the case of Figure 5.5.

The work presented so far deals with periodic excitation and narrow-band random excitation. To deal with more general random excitation, a broad-band random excitation is used in the simulation model. The forcing spectrum as obtained by digital Fourier transformation is shown in Figure 5.10. As in the case of narrow-band excitation, a quasi-linear study is performed on the model to determine the small amplitude natural frequency

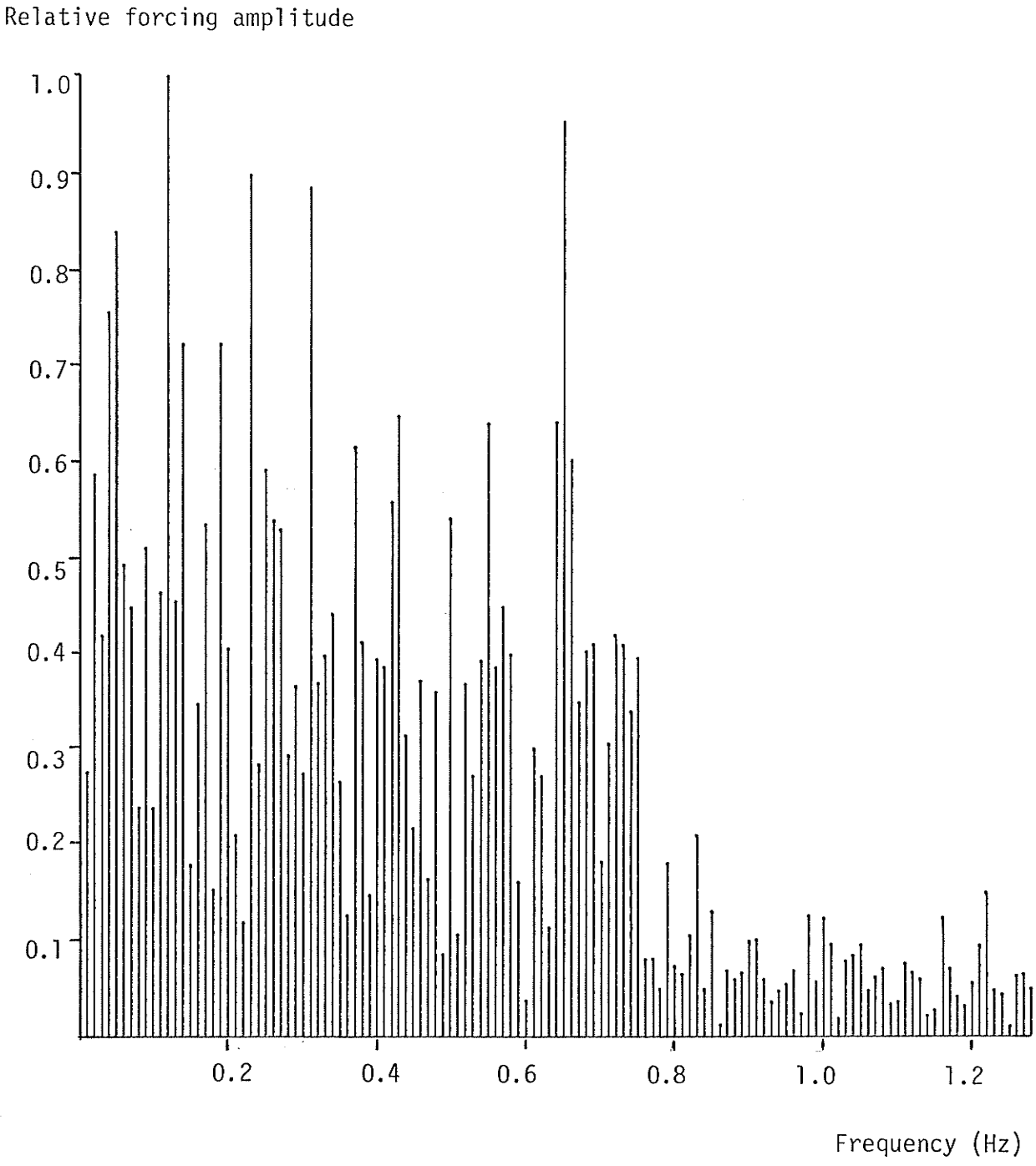

Figure 5.10 Amplitude Spectrum of Broad-Band Random Forcing

which will give rise to a peak power ratio or a relatively small power ratio. It is found in this quasi-linear study that a small amplitude natural frequency of 0.276 gives rise to a power ratio of 0.015 whereas a small amplitude natural frequency of 0.366 gives rise to a peak power ratio of 0.191. Hence, plots of power ratio are drawn using these two small amplitude natural frequencies, the former case is shown in Figure 5.11 and the latter case shown in Figure 5.12. In Figure 5.11, the power ratio drops to a small value as $\frac{g_o}{\sigma_p}$ becomes large. And in Figure 5.13, the power ratio drops to a higher power ratio, as expected. For value of $\frac{g_o}{\sigma_p}$ below 4, the plots in both figure look similar to each other, except that the values of the former plots are consistently a bit lower than the latter. The similarity is certainly due to similar forcing frequency coverage in both cases. It is noted that in Figure 5.13, for large values of $\frac{g_o}{\sigma_p}$, the curves cross each other for different values of α. This result is surprising but it is not impossible because as the value of $\frac{g_o}{\sigma_p}$ increases, the effective resonant frequency shifts to the right and is approaching the small amplitude natural frequency. In the shifting process, if there happens to be a high energy content region in the neighborhood of the effective natural frequency, as is in the present case, then the power ratio will increase. Hence, the higher the value of α, (more linear system), the more significant the increase in power ratio is.

As mentioned earlier, the portion where g_o/σ_p is large in the power ratio plots does not have much importance as far as the performance of the system is concerned. The region of high level of excitation (g_o/σ_p small) is relatively more important when dealing with structural overload. For these reasons, Figures 5.5 and 5.11 are replotted versus

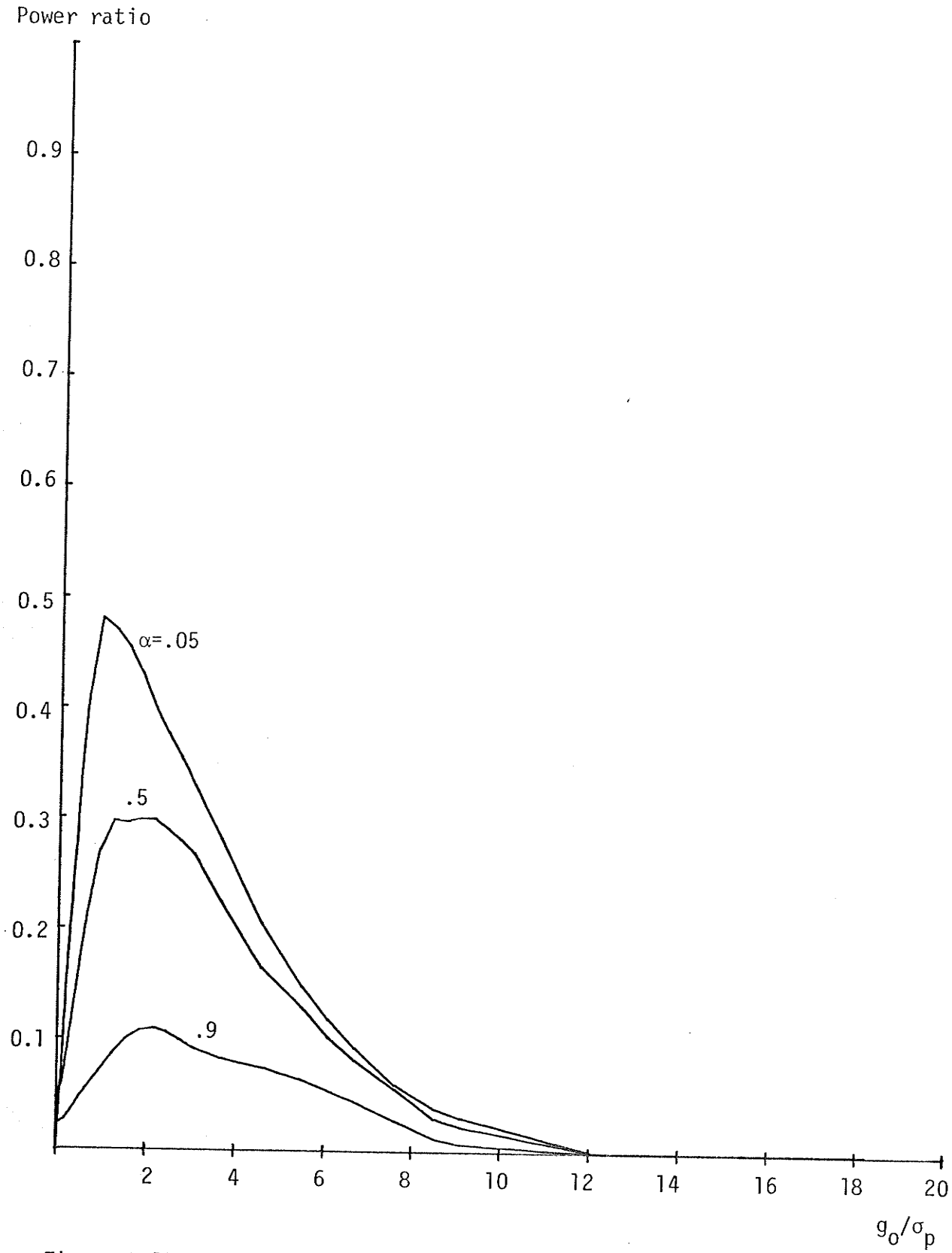

Figure 5.11 Plots of Power Ratio--Broad-Band Excitation, f_o=0.276 Hz

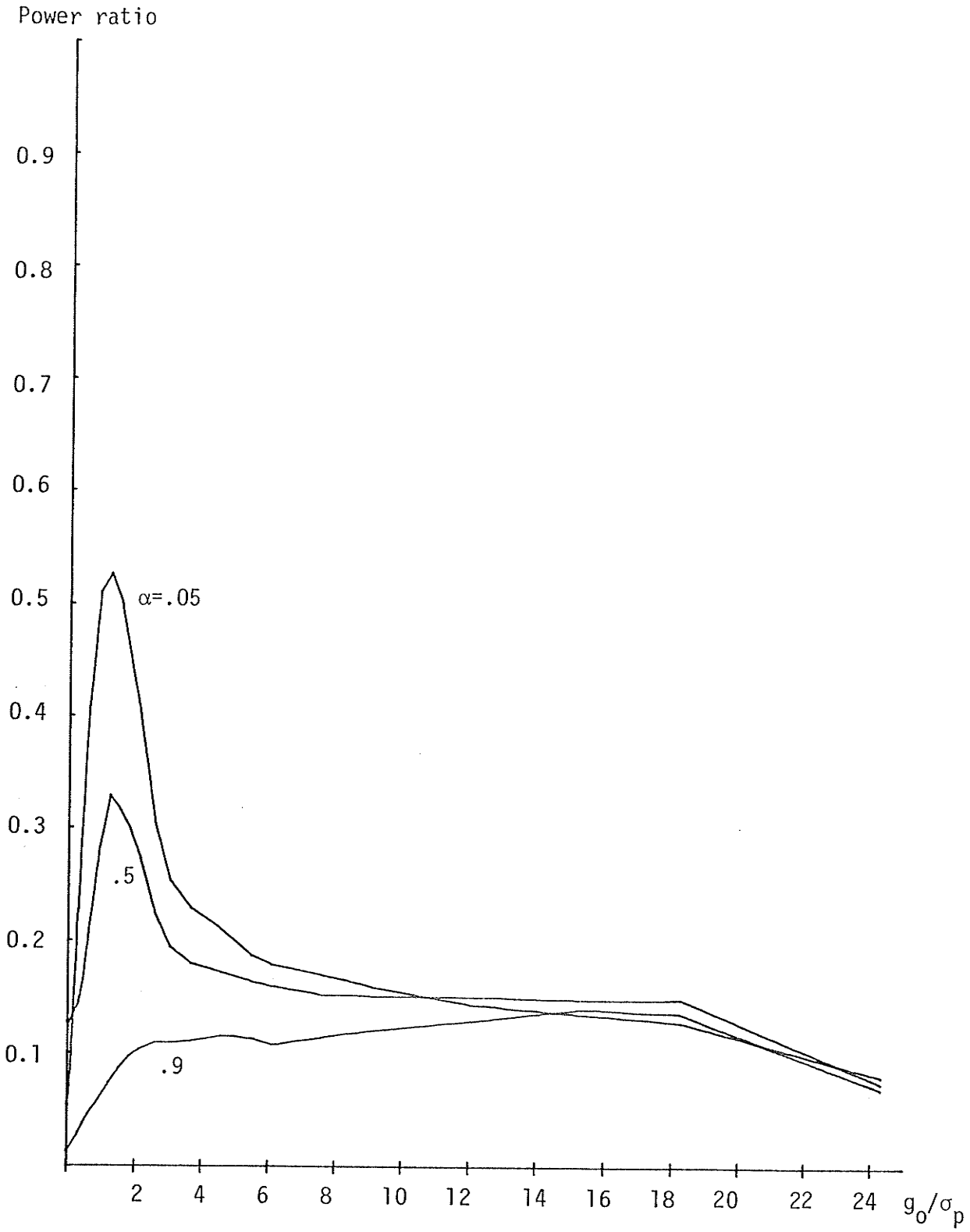

Figure 5.12 Plots of Power Ratio--Broad-Band Excitation, f_o=0.366 Hz

σ_p/g_o so that the region corresponds to large excitation level can be more clearly seen. These plots are shown in Figures 5.13 and 5.14 respectively.

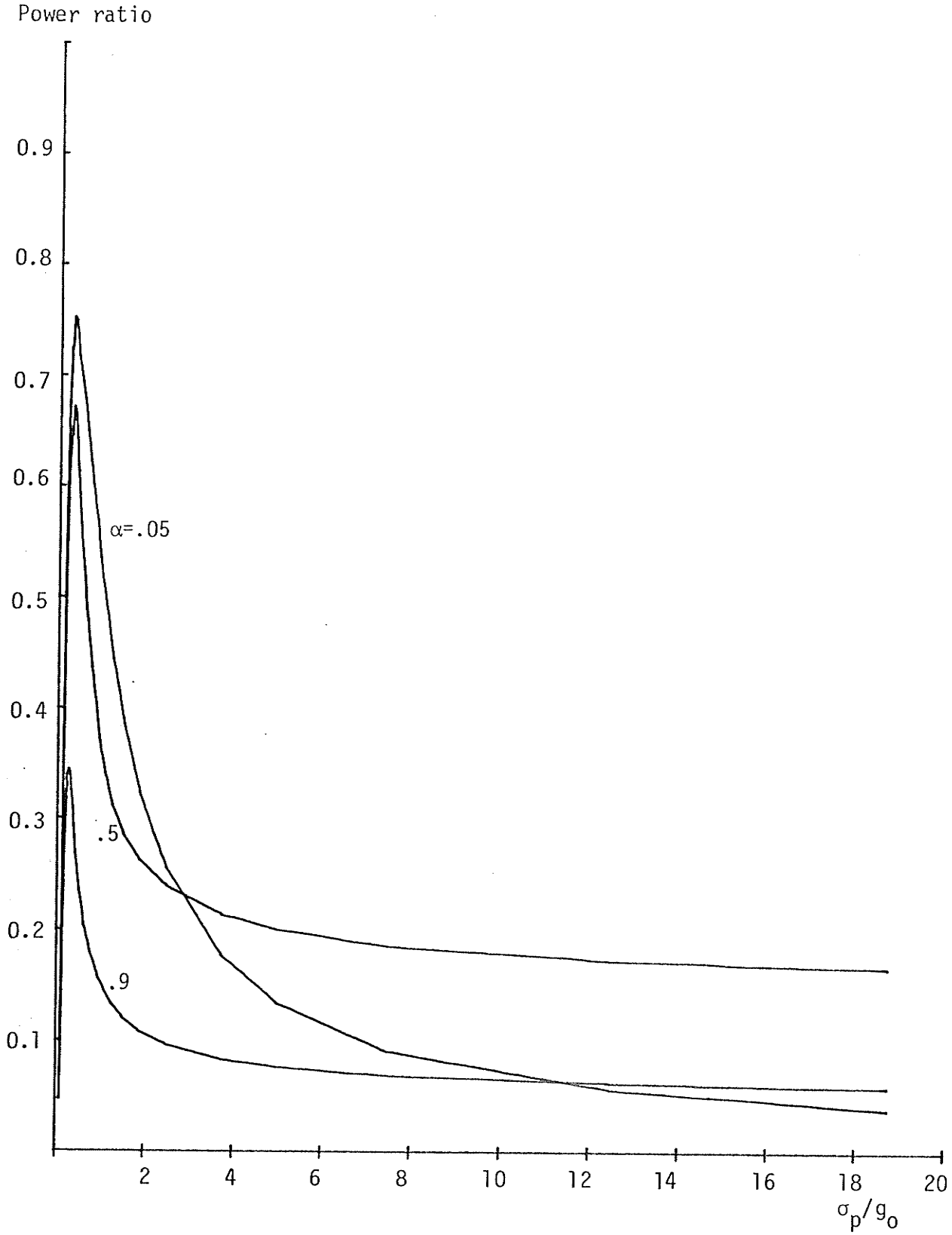

Figure 5.13 Power Ratio Versus σ_p/g_o--Narrow-Band Excitation, f_o=0.2 Hz

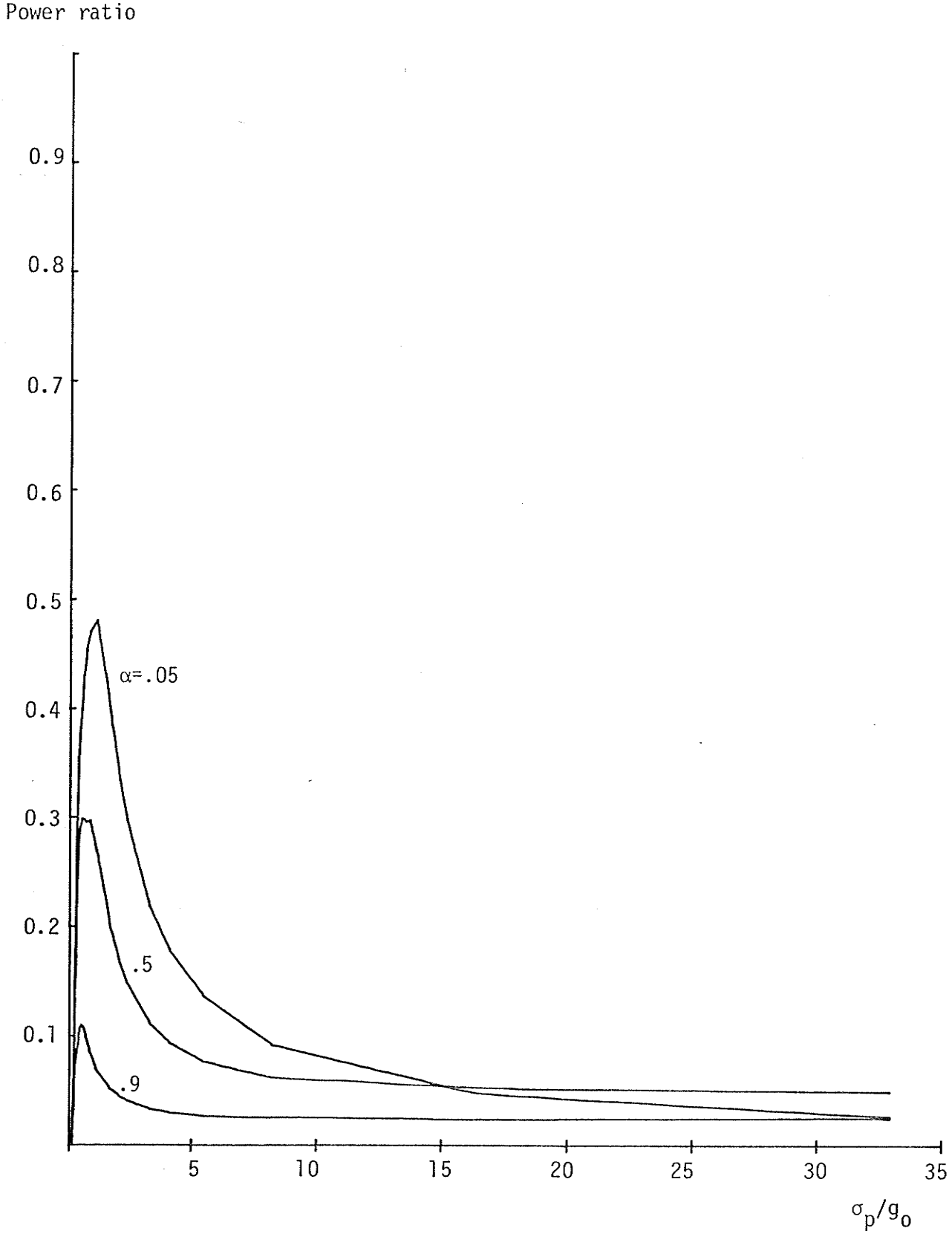

Figure 5.14 Power Ratio Versus σ_p/g_o--Broad-Band Excitation, f_o=0.276 Hz

5.4 CONCLUSIONS AND RECOMMENDATIONS

From the work which forms the basis of this thesis it may be concluded that the bilinear hysteretic element can usefully be characterized by power measurements and in particular that the power ratio is useful in describing the loss effectiveness of such an element. Loss effectiveness is given simply by the ratio of power dissipated to apparent power supplied to the element. It is shown that, for any given bilinear hysteretic element, a high degree of loss effectiveness is obtained at root-mean-square amplitudes that are in the region of twice the yield displacement. Thus, it is concluded that any bilinear hysteretic element that might be included in a structure will similarly be most effective as a loss mechanism over a limited range of root-mean-square displacement values. The theoretical model permits of the calculation of power ratio for a bilinear hysteretic element of given properties and for which the displacement is random, Gaussianly distributed, of known root-mean-square value.

Although much further investigation of the hysteretic element is needed this was deferred in favor of persuing the problem of single degree of freedom hysteretic system. Here the real problems of dealing with a strongly nonlinear system emerge from the response dependent nature of the system parameters. A generally applicable theoretical model has not been found but a digital computer simulation of the system has enabled exploration of the performance of the system over a wide range of variables. These results show that the hysteretic single degree of freedom system has, of course, a forcing frequency dependency in addition to the other characteristics exhibited by the hysteretic element alone. This leaves no doubt that effectiveness of a bilinear hysteretic element in a struc-

ture will depend upon the relationship between the spectrum of the forcing and the frequency response of the structure as well as the forcing amplitude.

Much work remains to be done on the hysteretic element coupled to linear systems. Nevertheless, the start made here is encouraging in the view that such structures may well be most suited to conditions where occasional, severe overload must be allowed for. The bilinear element can provide the two important properties of self-healing and peak force limiting. Thus, the design of a structure for severe overload might proceed on the basis of linear elements calculated to withstand the maximum peak force delivered to them through their adjacent bilinear elements. The power dissipating properties of the bilinear elements would of course be most important in limiting the power flow into the linear elements.

Further work proposed to move towards this design goal includes extension of the work reported here. For example, a systematic exploration of the single degree of freedom simulation model with confirmation from results from the physical model to find optimum performance is required. Extension of this model to a linear multidegree of freedom system driven through a bilinear element will also be required. Finally, several such linear systems coupled through hysteretic elements will be investigated. Throughout, a search for better mathematical modelling will be continued.

As an important adjunct to these conceptual and theoretical developments much work needs to be carried out to establish the adequacy of the bilinear hysteretic element as a model for practical

elements such as sliding steel on concrete surfaces. The techniques expressed in this thesis will play an important part in the laboratory investigations of such frictional fuses.

LIST OF REFERENCES

1. B.J. LAZAN 1968 Damping of Materials and Members in Structural Mechanics. Oxford: Pergamon Press, first edition.

2. S.H. CRANDALL 1970 Journal of Sound and Vibration 11, 3-18. The role of damping in vibration theory.

3. G.C. HART and R. VASUDEVAN 1975 Journal of the Structural Division, ASCE 101, 11-30. Earthquake design of buildings: damping.

4. T.K. CAUGHEY 1960 Journal of Applied Mechanics 27, 649-652. Random excitation of a system with bilinear hysteresis.

5. T.K. CAUGHEY 1963 Journal of the Acoustical Society of America 35, 1706-1711. Equivalent linearization techniques.

6. R.W. CLOUGH and J. PENZIEN 1975 Dynamics of Structures. New York: McGraw-Hill Book Company.

7. N.M. NEWMARK and E. ROSENBLUETH 1971 Fundamentals of Earthquake Engineering. Englewood Cliffs: Prentice-Hall, Inc.

8. W.T. THOMSON 1964 Vibration Theory and Applications. Englewood Cliffs: Prentice-Hall, Inc.

9. E. SKUDRZYK 1968 Simple and Complex Vibratory Systems. University Park: The Pennsylvania State University Press.

10. S.H. CRANDALL and W.D. MARK 1963 Random Vibration in Mechanical Systems. New York: Academic Press.

11. J.D. ROBSON 1963 An Introduction to Random Vibration. Edinburgh: Edinburgh University Press.

12. A. PAPOULIS 1965 Probability, Random Variables, and Stochastic Process. New York: McGraw-Hill Book Company.

13. Y.K. LIN 1967 Probabilistic Theory of Structural Dynamics. New York: McGraw-Hill Book Company.

14. D.E. NEWLAND 1975 An Introduction to Random Vibrations and Spectral Analysis. London: Longman Group Limited.

15. G.C. HART and J.T.P. YAO 1977 Journal of the Engineering Mechanics Division, ASCE 103, 1089-1104. System identification in structural dynamics.

16. W.T. THOMSON, G.C. HART and M.L. WATSON 1977 ASCE Fall Convention and Exhibit, San Francisco, Oct. 17-21. System identification methods in earthquake engineering.

17. P. CARAVANI and W.T. THOMSON 1974 Journal of Applied Mechanics, ASME 96, 379-382. Identification of damping coefficients in multidimensional linear systems.

18. J.G. BELIVEAU 1976 Journal of Applied Mechanics, ASME 98, 335-339. Identification of viscous damping in structures from modal information.

19. J.D. COLLINS, G.C. HART, T.K. HASSELMAN and B. KENNEDY 1974 Journal of the American Institute of Aeronautics and Astronautics 12, 185-190. Statistical identification of structures.

20. P. CARAVANI, M.L. WATSON and W.T. THOMSON 1977 Journal of Applied Mechanics, ASME 99, 135-139. Recursive least-squares time domain identification of structural parameters.

21. W. GERSCH, N.N. NIELSEN and H. AKAIKE 1973 Journal of Sound and Vibration 31, 295-308. Maximum likelihood estimation of structural parameters from random vibration data.

22. J.J. STOKER 1950 Nonlinear Vibrations in Mechanical and Electrical Systems. New York: Interscience Publishers, Inc.

23. T.K. CAUGHEY 1963 Journal of the Acoustical Society of America 35, 1683-1692. Derivation and application of the Fokker-Planck equation to discrete nonlinear dynamic systems subjected to white random excitation.

24. S.H. CRANDALL 1963 Journal of the Acoustical Society of America 35, 1700-1705. Perturbation techniques for random vibration of nonlinear systems.

25. R.H. LYON 1960 Journal of the Acoustical Society of America 32, 953-960. Response of a nonlinear string to random excitation.

26. D. KARNOFF 1967 Journal of Applied Mechanics 34, 212-214. Power balance method for nonlinear random vibration.

27. D. KARNOFF and R.H. BROWN 1967 Journal of the Acoustical Society of America 42, 54-59. Random vibration of multidegree-of-freedom hysteretic structures.

28. L.D. LUTES and H. TAKEMIYA 1974 Journal of the Engineering Mechanics Division, ASCE 100, 343-358. Random vibration of yielding oscillator.

29. L.D. LUTES 1970 Journal of the Engineering Mechanics Division, ASCE 96, 227-242. Equivalent linearization for random vibration.

30. W.D. IWAN and I-M YANG 1972 Journal of Applied Mechanics 545-550. Application of statistical linearization techniques to nonlinear multidegree-of-freedom systems.

31. W.D. IWAN and L.D. LUTES 1968 Journal of the Acoustical Society of America 43, 545-552. Response of the bilinear hysteretic system to stationary random excitation.

32. Y.K. WEN 1980 Journal of Applied Mechanics 47, 150-154. Equivalent linearization for hysteretic systems under random excitation.

33. R.H. LYON and G. MAIDANIK 1962 Journal of the Acoustical Society of America 34, 623-639. Power flow between linearly coupled oscillators.

34. D.E. NEWLAND 1966 Journal of Sound and Vibration 3, 262-276. Calculation of power flow between coupled oscillators.

35. T.D. SCHARTON and R.H. LYON 1967 Journal of the Acoustical Society of America 43, 1332-1343. Power flow and energy sharing in random vibration.

36. J.L. ZEMAN and J.L. BOGDANOFF 1969 Journal of the American Institute of Aeronautics and Astronautics 7, 1225-1231. A comment on complex structural response to random vibrations.

37. W. GERSCH 1969 Journal of the Acoustical Society of America 46, 1180-1185. Average power and power exchange in oscillators.

38. W. GERSCH 1970 Journal of the Acoustical society of America 48, 403-413. Mean-square responses in structural systems.

39. P. MA, K. MCLACHLAN and A. SHAH 1980 Proceedings of Canadian Society for Civil Engineering Annual Conference, Winnipeg. On the provision of viscous damping in structural models.

40. R.H. LYON 1975 Statistical Energy Analysis of Dynamical Systems: Theory and Applications. Cambridge: The MIT Press.

41. S.O. RICE 1944 Bell System Technical Journal 23, 282-332; 24, 46-156 (1945). Mathematical analysis of random noise. Reprint in N. WAX(ed), Selected Papers on Noise and Stochastic Processes, New York: Dover Publications, Inc. 1954.

42. E.L. WILSON, J.P. HOLLINGS and H.H. DOVEY 1975 Report No. EERC 75-13, University of California, Berkely. Three-dimensional analysis of building systems (extended version).

43. N. MINORSKY 1947 Nonlinear Mechanics. Ann Arbor: J.W. Edwards.

44. A. JOSEPH, K. POLMERANZ, J. PRINCE and D. SACHER 1978 Physics for Engineering Technology. New York: John Wiley & Sons.

45. M.L. JAMES, G.M. SMITH, J.C. WOLFORD 1977 Applied Numerical Methods for Digital Computation with Fortran and CSMP. New York: IEP-A Dun-Donnelley Publisher. 2nd Edition.

A P P E N D I X A

3-DOF LINEAR MODEL AND THE CORRESPONDING MEASURING SYSTEM

APPENDIX A

3-DOF LINEAR MODEL AND THE CORRESPONDING MEASURING SYSTEM

A 3-DOF structural model was constructed as shown in Figure A.1. There are three masses m_1, m_2 and m_3 which are supported by vertical ligaments. A pair of hard brass strips, one above the mass and one below, are attached to the mass on one end and to a rod on the other end. The other end of the rod, in turn, is attached to an adjacent mass. The strips, together with the connecting rods, constitute the spring connections having stiffness k_1, k_2 and k_3, between the masses.

The viscous damping is provided electromagnetically. Consider coil 1, which is fixed to the frame, the left part of which is inserted into the air gap between a pair of light-weight magnets. These magnets also form a significant part of mass m_1. In previous work [39] it was shown that such an arrangement provides pure viscous damping of the motion of the mass m_1. The damping constant is given by $c = (BL)^2/R$ where B is the magnetic flux density, L is the total length of wire of the coil in the magnetic field, and R is the value of the resistance of the coil circuit (not shown). Similar damping is provided between masses m_1 and m_2 and between m_2 and m_3. Thus, by varying the value of resistance in the coil circuit, different values of damping can be achieved throughout the system. To achieve high levels of damping a negative electrical resistance must be added to the inherent coil resistance and, hence, an active circuit (amplifier) is needed [39].

The physical model of Figure A.1 is idealized in the top part of

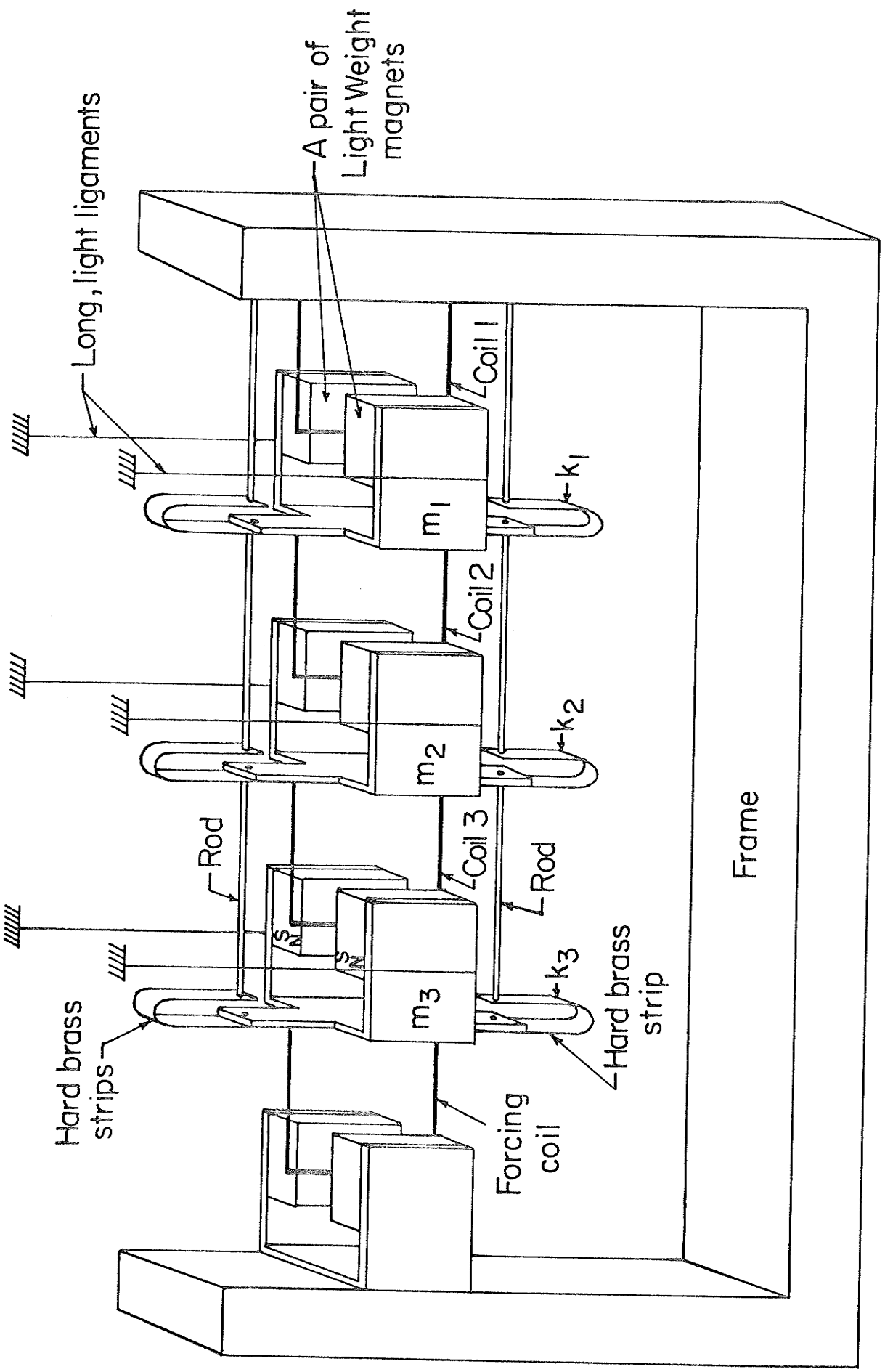

Figure A.1 3-DOF Linear Structural Model

Figure A.2 which is a block diagram of the entire measuring system. The three coils are connected to coil amplifiers A_1, A_2 and A_3, respectively. Each amplifier has a control switch, SW, with which a wide range of values of damping may be selected†. A stationary random signal is passed through an adjustable filter and then through the amplifier, A_p, which generates a current proportional to input voltage. The resulting current in the forcing coil interacts with the magnetic field and thus creates an excitation force on m_3. The accelerometers a_1, a_2 and a_3 together with their associated charge amplifiers give voltage outputs ($v_{\ddot{y}}$) proportional to the instantaneous acceleration of the masses. Each charge amplifier also contains an integrator so that output voltages ($v_{\dot{y}}$) proportional to the velocity of the masses are also produced. These voltages are further amplified to suit the requirements of a multiplier. Similar amplification is also given to the voltage (v_p) which is proportional to the current in the forcing coil.

A simple switching system allows any pair of voltages to be simultaneously applied to the multiplier inputs. In addition, the multiplier has internal switching so that the squaring of a single input may be performed. Finally, the output of the multiplier is averaged over time and hence all elements of the matrices $\overline{[\ddot{y}\ddot{y}^T]}$, $\overline{[\dot{y}\dot{y}^T]}$, and $\overline{[p\dot{y}^T]}$ can be be switch-selected and evaluated.

In this model, the fundamental measurement of motion is the acceleration of each mass with the appropriate velocity and displacement being derived by single and double integration of the acceleration signal with

---

† switch position 0,1,2 or 3 may be selected which results in an increasing damping value

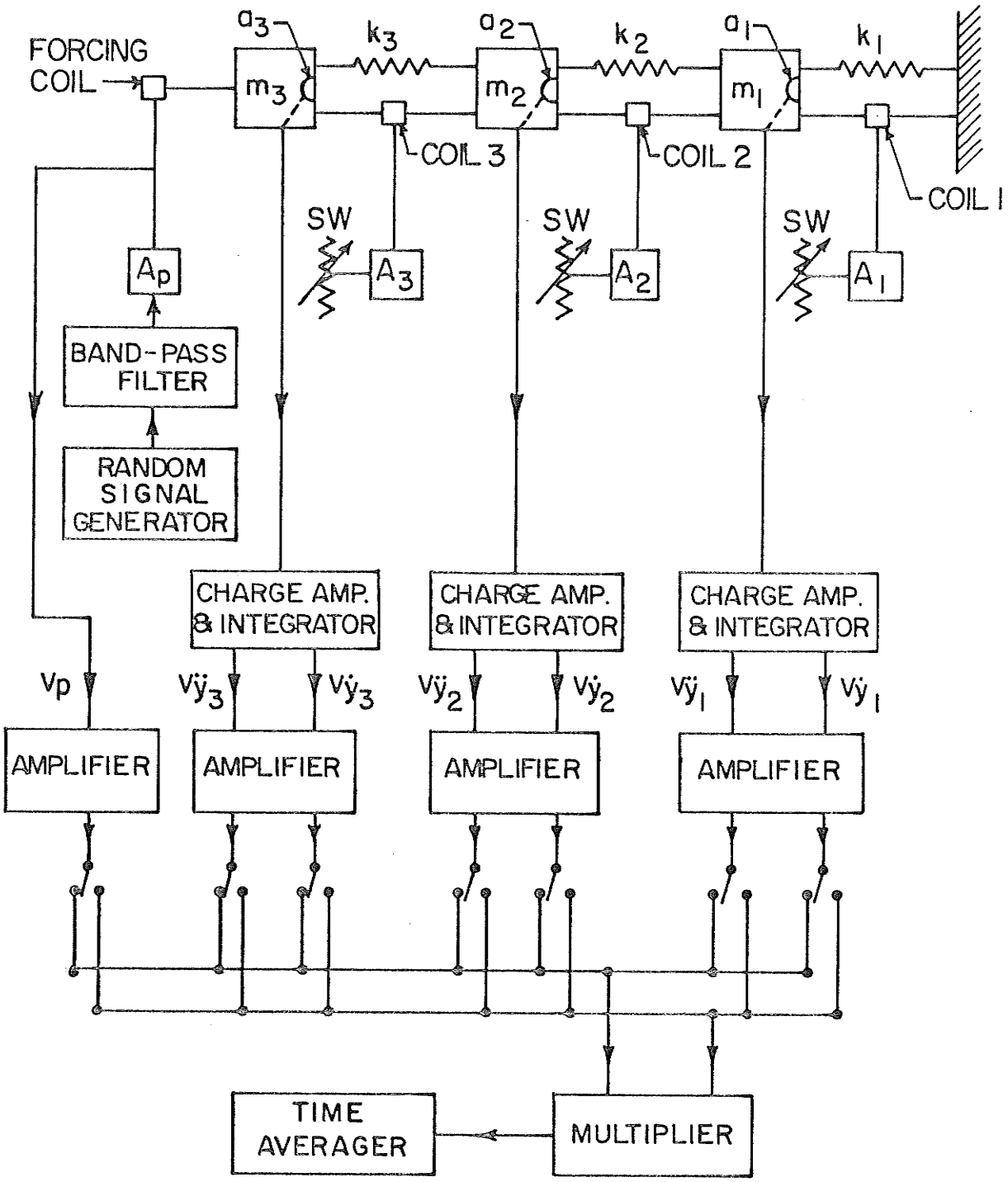

Figure A.2 Block Diagram of the Measuring System

respect to time. Though in a small model such as that used here, direct measurement of displacement is not difficult, in full scale structure such direct measurement is very impracticable. Thus it is felt that dependence upon the measurement of displacement should be avoided. It should also be mentioned that the analogue integrators used with the physical model (Figure A.2) have small relative phase errors between 0.2 Hz and 1 Hz. These phase discrepancies produced unacceptable errors in the evaluation of $\overline{[\ddot{y}\dot{y}^T]}$ and $\overline{[y\dot{y}^T]}$. For these reasons, the validation of the equations (2.3) and (2.4) was performed by means of computer simulation (Appendix B).

Using this model, force, velocity and acceleration were measured as voltages generated by or derived from tranducers. It was necessary therefore, to convert these measurements into their appropriate units by employing appropriate sensitivity factors. First, the sensitivity of the accelerometer in each mass was noted (say, s_1 pC/ms^{-2}), and the sensitivity of each charge amplifier was found to be s_2 mV/pC. Each final stage amplifier has a voltage gain s_3. Then the sensitivity of the acceleration is given by $1/s_1s_2s_3$ ms^{-2}/mV or $1000/s_1s_2s_3$ ms^{-2}/V.

To calibrate the velocities, the model was excited by a sinusoidally varying force having radian frequency ω. At the steady state, the peak acceleration and velocity voltage of each mass were noted. Thus using the known calibration of each accelerometer, the actual peak acceleration of each mass was found. The actual peak velocities were then obtained by dividing the corresponding actual peak acceleration by ω. The sensitivity of velocity was obtained by dividing each actual velocity by the corresponding peak velocity voltage, having an unit of ms^{-1}/V.

To calibrate the force, the model was driven by a relatively high frequency sinusoidal excitation, say 50 Hz, to ensure that the force and acceleration were in phase. The peak acceleration and force voltages were measured for the mass at which the force was acting. The actual acceleration was obtained by multiplying the peak acceleration voltage by the sensitivity of acceleration. The actual force was then the product of the mass and the actual acceleration. The sensitivity of force was obtained by dividing the actual forcing by the peak force voltage, giving the sensitivity in N/V.

During the course of the experiments, caution was exercised to ensure that no part of the system was overloaded. This was accomplished by occasionally checking the waveforms of the force, velocity and acceleration on the oscilloscope, to make sure that there was no distortion.

The multiplier, being an analogue device, was checked periodically for calibration accuracy and before each run the zero settings were checked and adjusted.

It was noted that the input signal band-pass filter of Figure A.2 does not have an infinite rate of cut-off beyond the cut-off frequencies as in the case of an ideal filter. In fact, the cut-off rate of the filter used was 24 dB/octave beyond each cut-off frequency f_1 and f_2, as shown in Figure A.3. In this study, it was then assumed that the signal was completely cut-off an octave from the cut-off frequencies, and this assumption was found to give satisfactory results in later work. Let $\overline{\Delta f}$ be the filter bandwidth and f_c be its central frequency, the filter signal extends beyond both sides of the bandwidth $\overline{\Delta F}$, the amount of extension is shown in Figure A.3. An effective bandwidth Δf is

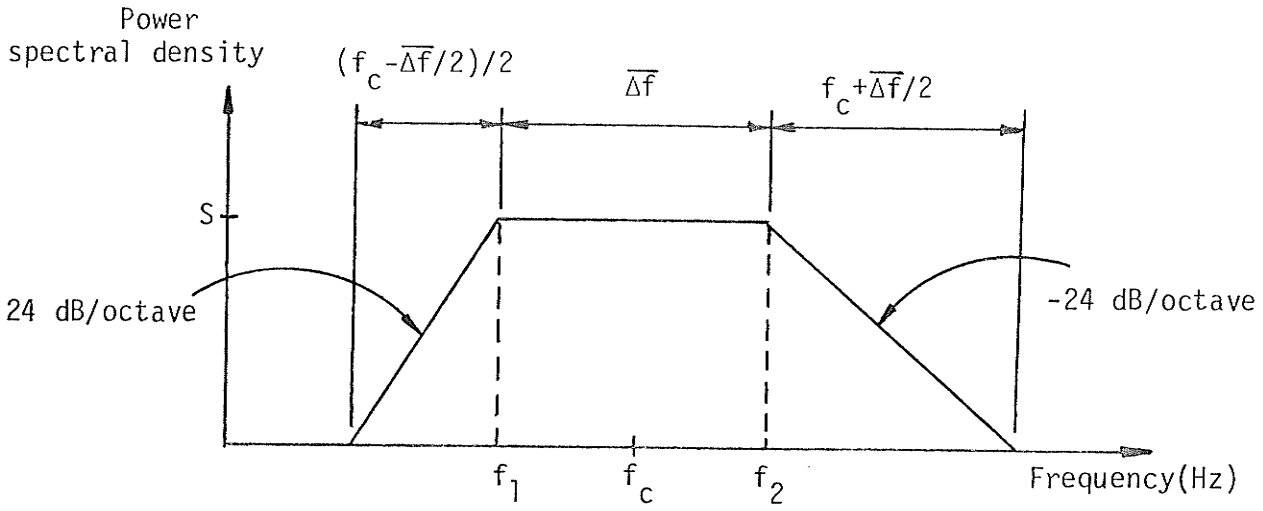

Figure A.3 Filter Characteristics

defined as one which will give the same mean square value of signal as the original filter. If S is the constant spectral density of the signal, then, Δf is given by

$$S\,\Delta f = \frac{S}{2}\,\frac{1}{2}\,(f_c - \overline{\Delta f}/2) + S\,\overline{\Delta f} + \frac{S}{2}\,(f_c + \overline{\Delta f}/2)\ ,$$

solving the above equation,

$$\Delta f = \frac{9}{8}\,\overline{\Delta f} + \frac{3}{4}\,f_c\ .$$

The physical properties of the model are:-

$$\left.\begin{aligned} [m] &= \begin{bmatrix} 0.097 & 0 & 0 \\ 0 & 0.098 & 0 \\ 0 & 0 & 0.090 \end{bmatrix} \text{ Kg}\ , \\ [k] &= \begin{bmatrix} 553 & -258 & 0 \\ -258 & 550 & -292 \\ 0 & -292 & 292 \end{bmatrix} \text{ N/m}\ , \\ \{f\}^T &= \langle 3.88 \quad 10.9 \quad 15.3 \rangle \text{ Hz}\ , \end{aligned}\right\} \qquad (A.1)$$

and $$[\phi] = \begin{bmatrix} 1.022 & 2.467 & 1.783 \\ 1.963 & 0.891 & -2.357 \\ 2.403 & -1.919 & 1.276 \end{bmatrix}$$

where {f} is the resonant frequency vector and $[\phi]$ is the undamped free vibration mode shape matrix.

As an example of how the model was used to compare conventional methods with the power methods of Chapter II, the results shown in Table A.1 are included. Here comparison is made between the modal damping values of the model as determined by the half-power method and by the modal power equation under broad-band random excitation (Section 2.3(i)). In this example, all damping control switches were set to position 1. The modal damping C_1, C_2 and C_3 as obtained by both method are shown in Table A.1. Results by both methods agreed generally to within ten percent.

METHOD	C_1	C_2	C_3
Half-power method (sinusoidal forcing)	0.32	1.66	4.13
Modal power equation (Broad-band random forcing)	0.29	1.69	4.47

TABLE A.1 Modal Dampings (N-s/m) of the Linear Model Obtained by Sinusoidal and Random Excitation

A P P E N D I X B

DYNAMIC RESPONSE ANALYSIS AND DAMPING IDENTIFICATION PROGRAM FOR LINEAR SYSTEMS

APPENDIX B

DYNAMIC RESPONSE ANALYSIS AND DAMPING IDENTIFICATION PROGRAM FOR LINEAR SYSTEMS

A FORTRAN coded program was compiled for the dynamic response analysis and damping identification of multi-degree of freedom linear systems. The response analysis part of the program was extracted from the extended TABS program [42]. The remaining part of this program was written for the solution of viscous damping matrix using equations (2.3) and (2.4). No limit was imposed on the number of degrees of freedom of the system, although it mainly depends on the capacity of each computing installation. External excitations may be in the form of forces acting on the masses or ground motion in the form of acceleration. The organization chart of the program is shown in Figure B.1 and the following is a brief description of each subprogram.

In the MAIN program, control data are read and storage areas are created for the arrays in the subprograms. It also serves as a link between the various program segments.

The EARTH subprogram accepts input data for the mass matrix and the stiffness matrix. It then calls the subprogram EIGEN in which the modal frequency vector and the free vibration undamped mode shape matrix are calculated. Control is returned to the EARTH subprogram and damping values are input either as modal damping ratio or as a damping matrix. In the latter case, it is assumed that the damping matrix can be uncoupled by the mode shape matrix, so that uncoupled modal equations can be obtained.

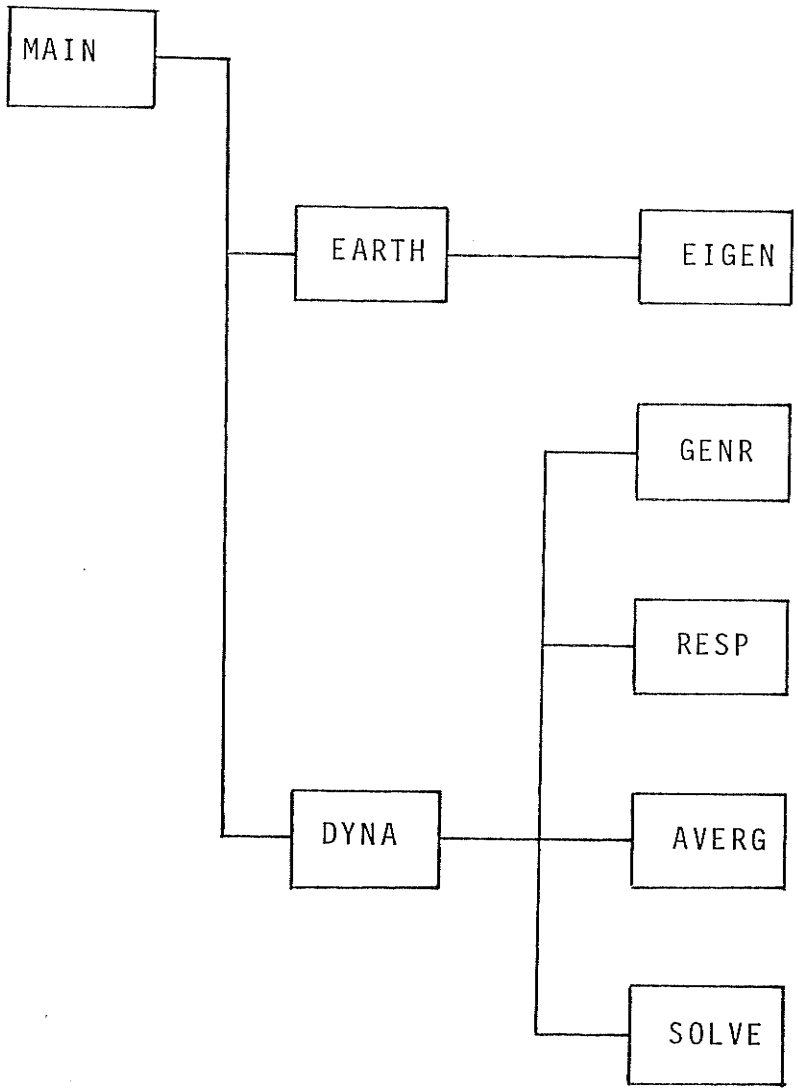

Figure B.1 Linear Systems Program Organization Chart

The subprogram DYNA first calls the GENR subprogram for the provision of excitation data. Data may be supplied either by the user as a time series, or it may be generated as a sinusoidal, or normal random time function (GGNMP subprogram of IMSL is called to generate the random data). If the excitations are in the form of ground acceleration, the effective forcing takes the form of $\{p\} = -[m]\{1\}\ \ddot{y}_G(t)$, where $\{1\}$ is a unit vector and $\ddot{y}_G(t)$ is the ground acceleration. Control is returned to DYNA, and modal response analysis is performed by calling the subprogram RESP, in which the modal displacement $\{Y(t)\}$, velocity $\{\dot{Y}(t)\}$ and acceleration $\{\ddot{Y}(t)\}$ responses are evaluated for each equal time step using explicit integration of the Duhamel integral. Control is then transferred to DYNA and the displacement $\{y(t)\}$, velocity $\{\dot{y}(t)\}$ and acceleration $\{\ddot{y}(t)\}$ responses are calculated by superimposing the corresponding responses from all modes.

The AVERG subprogram is called by DYNA to form the time average quantities of $\overline{[\ddot{y}\dot{y}^T]}$, $\overline{[\dot{y}\dot{y}^T]}$, $\overline{[y\dot{y}^T]}$ and $\overline{[p\dot{y}^T]}$. Each element of these matrices is obtained by forming the products of the corresponding functions for all time points and dividing the sum of these products by the number of time points. Control is transferred back to DYNA where the damping matrix is evaluated using equation (2.3), which is rearranged as follows.

$$[c] = (\overline{[p\dot{y}^T]} - [m]\overline{[\ddot{y}\dot{y}^T]} - [k]\overline{[y\dot{y}^T]})(\overline{[\dot{y}\dot{y}^T]})^{-1} \ . \qquad (B.1)$$

The quantities on the right hand side of equation (B.1) are known quantities, hence, standard subprograms for the manipulation of matrices are called to evaluate the right hand side of this equation.

To evaluate the damping matrix using equation (2.4), it is rewritten as

$$[k]^{-1}[c]\overline{[\dot{y}\dot{y}^T]} + \overline{[\dot{y}\dot{y}^T]}[c][k]^{-1} = [d] \ , \qquad (B.2)$$

where [d] is the resultant matrix of the known right hand side of equation (2.4). [d] is symmetrical. In order to solve for [c], equation (B.2) is rearranged as a set of n(n+1)/2 simultaneous linear equations, thus

$$[Z] \begin{Bmatrix} c_{11} \\ c_{12} \\ \cdot \\ \cdot \\ \cdot \\ c_{nn} \end{Bmatrix} = \begin{Bmatrix} d_{11} \\ d_{12} \\ \cdot \\ \cdot \\ \cdot \\ d_{nn} \end{Bmatrix} \ , \qquad (B.3)$$

where $<C_{11}, C_{12}, \ldots C_{nn}>^T$ are the n(n+1)/2 elements of the symmetrical [c] matrix. [Z] is a square matrix whose elements are linear combinations of the elements of $[k]^{-1}$ and $\overline{[\dot{y}\dot{y}^T]}$. $<d_{11}, d_{12}, \ldots, d_{nn}>^T$ is the n(n+1)/2 elements of the matrix [d]. A SOLVE subprogram is called by DYNA to solve the simultaneous equations of equation (B.3).

APPENDIX C

INTERPRETATIONS OF $\overline{p\dot{y}}$ AND $\sqrt{\overline{pp}} \cdot \sqrt{\overline{\dot{y}\dot{y}}}$

APPENDIX C

INTERPRETATIONS OF $\overline{p\dot{y}}$ AND $\sqrt{\overline{pp}} \cdot \sqrt{\overline{\dot{y}\dot{y}}}$

Consider first a 1-DOF linear system subjected to sinusoidal excitation p(t). The equation of motion is

$$m\ddot{y} + c\dot{y} + ky = p \ . \tag{C.1}$$

Multiplying equation (C.1) throughout by $\dot{y}$ and taking time average on each term, one obtains $\overline{p\dot{y}} = c\ \overline{\dot{y}\dot{y}}$ after noting that $\overline{\ddot{y}\dot{y}} = \overline{y\dot{y}} = 0$. $\overline{p\dot{y}}$ represents the "true" power supplied to the system and is equal to the actual power dissipation $c\ \overline{\dot{y}\dot{y}}$.

By taking the square on both sides of equation (C.1), one obtains, after taking time averages on each resulting term,

$$\overline{pp} = m^2\ \overline{\ddot{y}\ddot{y}} + c^2\ \overline{\dot{y}\dot{y}} + 2mk\ \overline{\ddot{y}y} + k^2\ \overline{yy} \ . \tag{C.2}$$

From the harmonic nature of the response, one has $\ddot{y} = \omega_p\dot{y} = \omega_p^2 y$, where ω_p is the forcing radian frequency. Making use of this result, equation (C.2) becomes

$$\overline{pp} = c^2\ \overline{\dot{y}\dot{y}} + (m\ \omega_p^2 - k)^2\ \overline{yy} \ . \tag{C.3}$$

Multiplying both sides of equation (C.3) by $\overline{\dot{y}\dot{y}}$, the equation becomes

$$\overline{pp} \cdot \overline{\dot{y}\dot{y}} = (c\ \overline{\dot{y}\dot{y}})^2 + (m\ \overline{\dot{y}\dot{y}}\ \omega_p - k\ \overline{yy}\ \omega_p)^2 \ . \tag{C.4}$$

Equation (C.4) shows that the square of the apparent power is equal to the sum of the square of power dissipation and the square of the power storage. The power storage is a combination of power due to kinetic and potential energy.

Now consider a nonlinear system subjected to stationary random excitation p(t). The equation of motion is in the form of

$$m\ddot{y} + c\dot{y} + k\, g(y,\dot{y}) = p \ , \qquad (C.5)$$

where $g(y,\dot{y})$ is a bilinear restoring force.

Multiplying equation (C.5) by $\dot{y}$ and taking time averages on each resulting term, we have

$$\overline{p\dot{y}} = c\ \overline{\dot{y}\dot{y}} + \overline{k\ g(y,\dot{y})\dot{y}} \ . \qquad (C.6)$$

The first term on the right hand side of equation (C.6) is the power dissipation due to viscous damping, whereas the remaining term represents power loss due to hysteresis. Hence, $\overline{p\dot{y}}$ is the sum of both sources of power dissipation.

The term $\sqrt{\overline{pp}} \cdot \sqrt{\overline{\dot{y}\dot{y}}}$ has the same meaning in nonlinear systems. It is the total average apparent power supplied to the system.

A P P E N D I X D

RELATIONSHIPS BETWEEN POWER RATIO AND VISCOUS DAMPING COEFFICIENT IN LINEAR SYSTEMS

APPENDIX D

RELATIONSHIPS BETWEEN POWER RATIO AND VISCOUS DAMPING COEFFICIENT IN LINEAR SYSTEMS

D.1 1-DOF SYSTEM

With the system and forcing properties as shown in Figure 3.1, the mean square forcing can be expressed as

$$\overline{pp} = R_{pp}(0) = S_{pp} \frac{\Delta\omega}{2\pi} , \tag{D.1}$$

where $R_{pp}(0)$ is the zero-lag autocorrelation of the input forcing. R_{pp} and S_{pp} are a Fourier transform pair.

The mean square velocity of the system is given by [10]

$$\overline{\dot{y}\dot{y}} = R_{\dot{y}\dot{y}}(0) \simeq \frac{S_{pp}}{2\pi} \int_0^\infty |H(j\omega)|^2 \, d\omega , \tag{D.2}$$

where $R_{\dot{y}\dot{y}}(0)$ is the zero-lag autocorrelation of the velocity and the system function $H(j\omega)$ is given by

$$H(j\omega) = \frac{1}{\omega_o \eta m - j(\omega m - \frac{k}{\omega})} . \tag{D.3}$$

In equation (D.3), $j = \sqrt{-1}$, $\omega_o = (k/m)^{1/2}$ is the natural frequency of the system, $\eta = 2\xi$ is the loss factor and $\xi = C/(2\omega_o m)$ is the damping ratio. $|H(j\omega)|^2$ is sketched in Figure 3.1(c). Using equation (D.3), equation (D.2) leads to

$$\overline{\dot{y}\dot{y}} = \frac{1}{2\pi} \frac{S_{pp}}{\omega_o^2 \eta^2 m^2} \int_0^\infty \frac{d\omega}{1+(\omega^2-\omega_o^2)/\eta^2\omega^2\omega_o^2} . \tag{D.4}$$

If the system curve of $|H(j\omega)|^2$ is sharply peaked, then the integrand of equation (D.4) can be simplified by noting that $\omega + \omega_o \doteq 2\omega$ [40]. After performing the integration, equation (D.4) leads to

$$\overline{\dot{y}\dot{y}} = \frac{S_{pp}}{4\omega_o \eta m^2} \quad . \tag{D.5}$$

The zero-lag correlation between the input force and the response velocity is

$$\overline{p\dot{y}} = R_{p\dot{y}}(0) = \frac{S_{pp}}{2\pi} \int_o^\infty H(j\omega)\, d\omega \quad . \tag{D.6}$$

Complex integration of equation (D.6) yields

$$\overline{p\dot{y}} = \frac{S_{pp}}{4m} \quad . \tag{D.7}$$

From equations (D.1),(D.5) and (D.7), and noting that $\Delta f = \Delta\omega/2\pi$, the square of the power ratio is given by

$$W^2 = \frac{(\overline{p\dot{y}})^2}{\overline{pp} \cdot \overline{\dot{y}\dot{y}}} = \frac{\omega_o \xi}{2\Delta f} = \frac{c}{4m \cdot \Delta f} \quad . \tag{D.8}$$

D.2 BAND-LIMITED EXCITATION OF n-DOF SYSTEM

For the system as shown in Figure 3.2, the equations of motion in the generalized coordinates {Y} are given as

$$\ddot{Y}_j + C_j \dot{Y}_j + K_j Y_j = P_j \ , \ (j = 1,n) \ , \tag{D.9}$$

where {Y} is related to the physical displacement coordinates {y} by the mode shape matrix $[\phi]$ as $\{y\} = [\phi]\{Y\}$. $[C] = [\phi]^T[c][\phi]$ and $[K] = [\phi]^T [k][\phi]$ are the generalized diagonal damping and stiffness matrices, respectively; $\{P\} = [\phi]^T\{p\}$ is the generalized load vector, and [M], the generalized mass matrix, is normalized as an identity matrix.

For the particular forcing as described in Section 3.2, it is basically an i-th mode excitation. Then the system behaves like a 1-DOF system in the modal sense. Equation (D.8) may then be applied to such a system:

$$\frac{\overline{P_i \dot{Y}_i}^2}{\overline{P_i P_i} \cdot \overline{\dot{Y}_i \dot{Y}_i}} = \frac{C_i}{4\ \Delta f_i} \quad , \tag{D.10}$$

where $P_i = \phi_{ri}\ p_r$ and $\dot{y}_r = \phi_{ri}\ \dot{Y}_i$.

By transforming the left hand side of equation (D.10) back to the physical coordinates, the square of the power ratio measured at the forcing point, the r-th mass, is related to the modal damping as

$$W^2 = \frac{(\overline{P_r \dot{y}_r})^2}{\overline{P_r P_r} \cdot \overline{\dot{y}_r \dot{y}_r}} = \frac{C_i}{4\ \Delta f_i} \quad . \tag{D.11}$$

D.3 BROAD-BAND EXCITATION OF n-DOF SYSTEM

The velocities $\{\dot{y}\}$ and loading $\{p\}$ in the physical coordinates are related to those in the generalized coordinates by the mode shape in the form

$$\dot{y}_r = \sum_{j=1}^{n} \phi_{rj}\ \dot{Y}_j \quad (j=1,n) \ , \tag{D.12}$$

and

$$P_j = \phi_{rj}\ p_r \quad (j=1,n) \ . \tag{D.13}$$

From equations (D.12) and (D.13),

$$\overline{p_r \dot{y}_r} = \left(\frac{P_1}{\phi_{r1}} \text{ or } \frac{P_2}{\phi_{r2}} \text{ or } \ldots \frac{P_n}{\phi_{rn}}\right) (\phi_{r1}\ \dot{Y}_1 + \ldots + \phi_{rn}\ \dot{Y}_n)$$

$$= \overline{P_1 \dot{Y}_1} + \overline{P_2 \dot{Y}_2} + \ldots + \overline{P_n \dot{Y}_n} \ . \tag{D.14}$$

Equations (D.1) and (D.7) when written in the generalized coordinates, become

$$S_j = \overline{P_j P_j}/\Delta f \quad , \quad \text{and}$$

$$\overline{P_j \dot{Y}_j} = S_j/4 \quad , \quad (j=1,n) \; , \tag{D.15}$$

where S_j is the power spectral density of the loading P_j.

Equation (D.15) becomes, after making use of equation (D.13)

$$\overline{P_j \dot{Y}_j} = \frac{\overline{P_j P_j}}{4\ \Delta f} = \phi_{rj}^2 \frac{\overline{p_r p_r}}{4\ \Delta f} \quad , \; (j=1,n) \; . \tag{D.16}$$

Backsubstitution of equation (D.16) into equation (D.14) leads to

$$\overline{p_r \dot{y}_r} = \frac{\overline{p_r p_r}}{4\ \Delta f} L_r^2 \; , \tag{D.17}$$

where $L_r^2 = \sum_{j=1}^{n} \phi_{rj}^2$.

Next consider the formation of $\overline{\dot{y}_r \dot{y}_r}$. From equation (D.12), after noting $\overline{\dot{Y}_j \dot{Y}_k} = 0$ for $j \neq k$, $\overline{\dot{y}_r \dot{y}_r}$ is given by

$$\overline{\dot{y}_r \dot{y}_r} = \sum_{j=1}^{n} \phi_{rj}^2 \; \overline{\dot{Y}_j \dot{Y}_j} \; . \tag{D.18}$$

By applying equation (D.5) in the modal sense and making use of equation (D.15), equation (D.5) becomes

$$\overline{\dot{Y}_j \dot{Y}_j} = \frac{S_j}{4\ \omega_j \eta_j} = \frac{\overline{P_j P_j}}{4\ \Delta f \omega_j \eta_j} \quad , \; (j=1,n) \; , \tag{D.19}$$

where ω_j and η_j are the modal frequency and loss factor respectively of the j-th mode. By making use of equation (D.13) and noting that $C_j = \omega_j \eta_j$, equation (D.19) leads to

$$\overline{\dot{Y}_j \dot{Y}_j} = \phi_{rj}^2 \frac{\overline{p_r p_r}}{4\ \Delta f C_j} \quad , (j=1,n) \ . \tag{D.20}$$

Substituting equation (D.20) into equation (D.18), the mean square velocity is expressed as

$$\overline{\dot{y}_r \dot{y}_r} = \frac{\overline{p_r p_r}}{4\ \Delta f} \sum_{j=1}^{n} \frac{\phi_{rj}^4}{C_j} \ . \tag{D.21}$$

From equations (D.17) and (D.21), the square of power ratio at the location of forcing is given by

$$W^2 = \frac{\overline{p_r \dot{y}_r}^2}{\overline{p_r p_r}\ \overline{\dot{y}_r \dot{y}_r}} = \frac{C_o}{4\ \Delta f} \ , \tag{D.22}$$

where $C_o = \dfrac{1}{\sum_{j=1}^{n} \dfrac{1}{C_j^*}}$,

and $C_j^* = \dfrac{L_r^4 C_j}{\phi_{rj}^4}$.

Equation (D.22) reduces to the form of equation (D.11) when the excitation is limited to within the vicinity of the i-th mode. Also, it reduces to the form of equation (D.8) in the case of a 1-DOF system. The power ratio thus presented enables one to describe energy loss versus energy supplied for a system with any given bandwidth of excitation.

A P P E N D I X E

DERIVATION OF MEAN PEAK VALUES BEYOND A LEVEL OF y_o FOR A GAUSSIAN PROCESS

APPENDIX E

DERIVATION OF MEAN PEAK VALUES BEYOND A LEVEL OF y_o FOR A GAUSSIAN PROCESS

If y is a Gaussian process with zero mean, then the expected number of peaks (or maxima) per second lying in the interval y, $y + dy$, denoted by E[pk], is given by Rice [41]:

$$E[pk]dy = \frac{(2\pi)^{-3/2}}{G_{33}} \left[|G|^{1/2} e^{\frac{-G_{11} y^2}{2|G|}} + G_{13} y \left(\frac{\pi}{2G_{33}}\right)^{1/2} e^{\frac{-y^2}{2\sigma_y^2}} \left(1 + \text{erf} \frac{G_{13} y}{[2|G|G_{33}]^{1/2}}\right)\right] dy \quad . \quad (E.1)$$

where $G = \begin{bmatrix} \sigma_y^2 & 0 & -\sigma_{\dot{y}}^2 \\ 0 & \sigma_{\dot{y}}^2 & 0 \\ -\sigma_{\dot{y}}^2 & 0 & \sigma_{\ddot{y}}^2 \end{bmatrix}$, $|G| = \sigma_{\dot{y}}^2 (\sigma_y^2 \sigma_{\ddot{y}}^2 - \sigma_{\dot{y}}^4)$,

$G_{11} = \sigma_{\dot{y}}^2 \sigma_{\ddot{y}}^2$, $G_{13} = \sigma_{\dot{y}}^4$, $G_{33} = \sigma_{\dot{y}}^2 \sigma_y^2$ and erf is the error function.

For a band-pass filter having cut-off frequencies f_1 and f_2, the following relationships hold:

$$\frac{\sigma_{\ddot{y}}^2}{\sigma_{\dot{y}}^2} = (2\pi)^2 \frac{\int_{f_1}^{f_2} f^4 \, S \, df}{\int_{f_1}^{f_2} f^2 \, S \, df} = (2\pi)^2 \left[\frac{3}{5} \frac{f_2^5 - f_1^5}{f_2^3 - f_1^3}\right] \equiv F_5 \quad , \quad (E.2)$$

$$\frac{\sigma_{\dot{y}}^2}{\sigma_y^2} = (2\pi)^2 \left[\frac{1}{3} \frac{f_2^3 - f_1^3}{f_2 - f_1}\right] \equiv F_3 \quad , \quad (E.3)$$

where S is the uniform power spectral density of y.

Using equations (E.2) and (E.3), equation (E.1), after simplifying, becomes

$$E[pk]dy = \frac{(2\pi)^{-3/2}}{\sigma_y}\left[\sqrt{F_5-F_3}\; e^{\frac{-F_5 y^2}{2\sigma_y^2[f_5-F_3]}} + \left(\frac{\pi F_3}{2\sigma_y^2}\right)^{1/2} y\, e^{\frac{-y^2}{2\sigma_y^2}}\left(1+\text{erf}\,\frac{y(F_3)^{1/2}}{\sigma_y[2(F_5-F_3)]^{1/2}}\right)\right]dy \quad . \qquad (E.4)$$

Equation (E.4) is the expected number of peaks per second lying in the interval y, y + dy. To obtain the probability density function of peaks, equation (E.4) must be normalized. This is achieved by dividing E[pk] by the expected number of peaks per second over the entire domain of y. This latter quantity may be obtained by integrating the expression of equation (E.4) from $y = -\infty$ to ∞ and the result is found to be $\frac{1}{2\pi}\frac{\sigma_{\ddot{y}}}{\sigma_{\dot{y}}}$, and from equation (E.2), it is equal to $(F_5)^{1/2}/2\pi$. Hence, the probability density function of peaks, for a band-pass process, is

$$pr(pk) = \frac{2\pi\, E[pk]}{(F_5)^{1/2}} \quad , \qquad (E.5)$$

where E[pk] is given by equation (E.4).

Equation (E.5) applies to any frequency range of y. In particular, if f_1 is zero in equations (E.2) and (E.3), equation (E.5) then gives the result for a low-pass process.

For a Raleigh process,

$$F_5 = (2\pi)^2\frac{\int f^4 S\, df}{\int f^2 S\, df} = (2\pi)^2 \lim_{\Delta f\to 0}\frac{f_y^4 S\,\Delta f}{f_y^2 S\,\Delta f}$$

$$F_5 = (2\pi)^2 f_y^2 = F_3$$

where f_y is the frequency of the narrow-band process. By substituting these values of F_5 and F_3 into equation (E.5), equation (E.5) is reduced to

$$pr(pk) = \frac{y}{\sigma_y^2} e^{\frac{-y^2}{2\sigma_y^2}}, \qquad (E.6)$$

which is the familiar expression for the distribution of peaks in a Rayleigh process.

The mean yield peak value may readily be obtained from the probability density function of peaks, which is as shown in Figure E.1. The

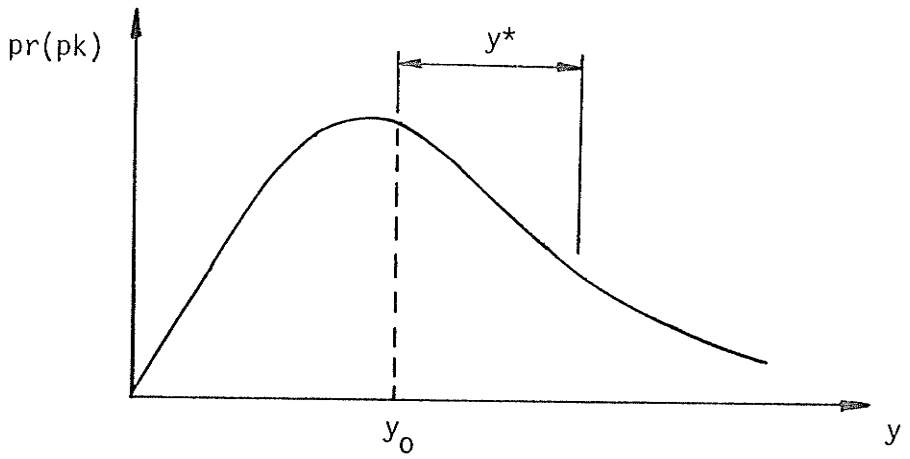

Figure E.1 Probability Density Function of Peaks

mean yield peak value y^* is given by

$$y^* = \frac{\int_{y_o}^{\infty} y\,pr(pk)\,dy}{\int_{y_o}^{\infty} pr(y)\,dy} - y_o \,. \qquad (E.7)$$

The first term of the right hand side of equation (E.7) is the mean yield peak value referred to $y = o$, hence y_o is subtracted from it to give y^*.

The integration of equation (E.7) was numerically performed.

A P P E N D I X F

PROBABILITY DENSITY FUNCTION OF BILINEAR HYSTERETIC RESTORING FORCE

APPENDIX F

PROBABILITY DENSITY FUNCTION OF BILINEAR HYSTERETIC RESTORING FORCE

The bilinear restoring force is sketched against y as depicted in Figure F.1. The coordinates of all four vertices, together with the equations of the four sides of the loop, are labeled as shown. Three cases arise according to whether $p_o - k\alpha y^*$ is greater than, equal to, or less than zero, where p_o is the yield force. Figure F.1 belongs to the first case.

CASE 1 ($p_o - k\alpha y^* > 0$)

Consider a strip of width dp, where the absolute value of p is less than $(p_o - k\alpha y^*)$. The probability of p lying in the region p to $p + dp$ is equal to the probability of y lying in the two regions of dy, as shown in Figure F.1. Mathematically,

$$pr(p)dp = pr(y_1)dy_1 + pr(y_2)dy_2 \ . \qquad (F.1)$$

By substituting equation (4.1), the expression for pr(y), into equation (F.1), the latter equation becomes

$$pr(p)dp = \frac{1}{\sqrt{2\pi}\,\sigma_y}\left[e^{\frac{-y_1^2}{2\sigma_y^2}}\,dy_1 + e^{\frac{-y_2^2}{2\sigma_y^2}}\,dy_2\right].$$

The values of y_1 and y_2 can be obtained by solving the equations of the sides of the loop. By noting that $dp/dy_1 = dp/dy_2 = k$ and $\sigma_{p_o} = k\sigma_y$, the above equation becomes

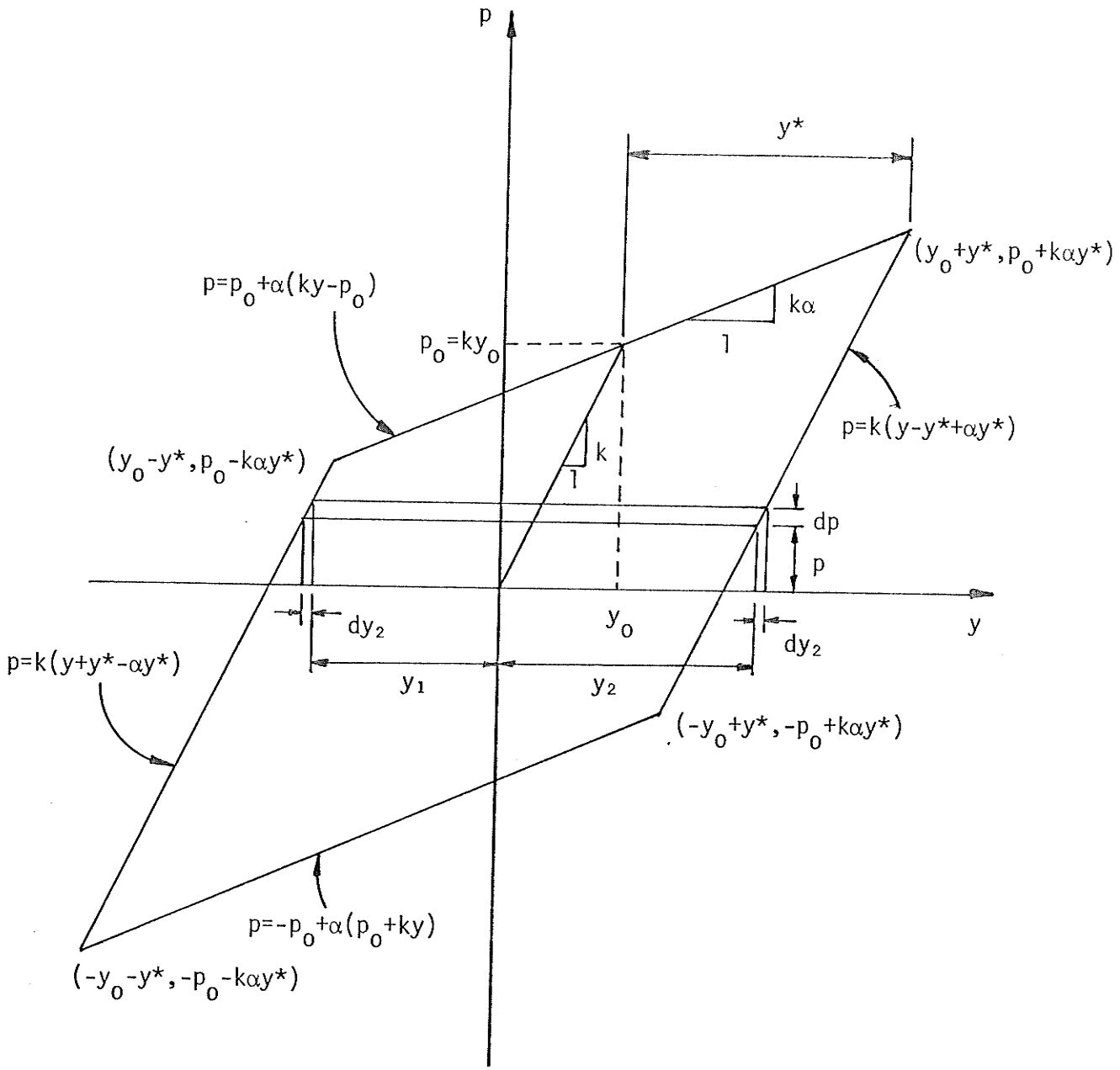

Figure F.1 Restoring Force Versus Displacement
($p_o-k\alpha y^*>0$)

$$pr(p) = \frac{1}{\sqrt{2\pi}\,\sigma_{p_o}}\left[e^{\frac{-[p/k-y^*(1-\alpha)]^2}{2\sigma_y^2}} + e^{\frac{-[p/k+y^*(1-\alpha)]^2}{2\sigma_y^2}}\right] \qquad (F.2)$$

$$|p|<p_o - k\alpha y^* \ .$$

By considering a strip dp (not shown in Figure F.1), where the absolute value of p is greater than $(p_o - k\alpha y^*)$, and using the same procedure as before, pr(p) in this region becomes

$$pr(p) = \frac{1}{\sqrt{2\pi}\,\sigma_{p_o}}\left[\frac{1}{\alpha}\, e^{\frac{-[p/k-y_o(1-\alpha)]^2}{2\alpha^2\ \sigma_y^2}} + e^{\frac{-[p/k+y^*(1-\alpha)]^2}{2\sigma_y^2}}\right] \qquad (F.3)$$

$$p_o + k\alpha y^* > |p| > p_o - k\alpha y^* \ .$$

It is interesting to note that an entire loop is prescribed for a complete cycle, each value of y is traversed twice, hence the total probability of the restoring force

$$\int_{-p_o + k\alpha y^*}^{p_o - k\alpha y^*} pr(p)dp + 2\int_{p_o - k\alpha y^*}^{\infty} pr(p)dp$$

is equal to 2. For this reason, pr(p) needs to be normalized. This is achieved by dividing all expressions of pr(p) by 2. By defining

$$\left.\begin{aligned} I_1 &= \frac{-[p/k-y^*(1-\alpha)]^2}{2\sigma_y^2}\ , \\ I_2 &= \frac{-[p/k+y^*(1-\alpha)]^2}{2\sigma_y^2}\ , \\ I_3 &= \frac{-[p/k-y_o(1-\alpha)]^2}{2\sigma_y^2}\ , \\ I_4 &= \frac{-[p/k+y_o(1-\alpha)]^2}{2\sigma_y^2}\ , \\ \text{and} \quad A &= \frac{1}{\sqrt{2\pi}\,\sigma_{p_o}}\ , \end{aligned}\right\} \qquad (F.4)$$

equations (F.2) and (F.3) become

$$pr(p) = \begin{cases} \frac{A}{2}\left[e^{I_1} + e^{I_2}\right] , & |p|<p_o - k\alpha y^* \\ \frac{A}{2}\left[\frac{1}{\alpha} e^{I_3/\alpha^2} + e^{I_2}\right] , & p_o + k\alpha y^* > |p| > p_o - k\alpha y^* \end{cases} . \qquad (F.5)$$

CASE 2 ($p_o - k\alpha y^* = 0$)

Figure F.2(a) illustrates the second case. By using the procedures described in Case 1, the probability density function of p is

$$pr(p) = \frac{A}{2}\left[\frac{1}{\alpha} e^{I_3/\alpha^2} + e^{I_2}\right] , \quad |p|<p_o + k\alpha y^* . \qquad (F.6)$$

CASE 3 ($p_o - k\alpha y^*<0$)

Similarly from Figure F.2(b), the probability density function of p is

$$pr(p) = \begin{cases} \frac{A}{2\alpha}\left[e^{I_3/\alpha^2} + e^{I_4/\alpha^2}\right] , & |p|< - p_o + k\alpha y^* \\ \frac{A}{2}\left[\frac{1}{\alpha} e^{I_3/\alpha^2} + e^{I_2}\right] , & p_o + k\alpha y^* > |p| > - p_o + k\alpha y^* \end{cases} . \qquad (F.7)$$

CASE 4 (Elasto-plastic case, $\alpha = 0$)

The above cases deal with all combinations of system parameters except for $\alpha = 0$. In this case, a separate evaluation of pr(p) is required.

Lets consider Figure F.3. Within the region $|p|<p_o$, pr(p) can be obtained by a procedure similar to that of case 1, thus

$$pr(p) = \frac{A}{2}\left[e^{I_1} + e^{I_2}\right] , \quad |p|<p_o . \qquad (F.8)$$

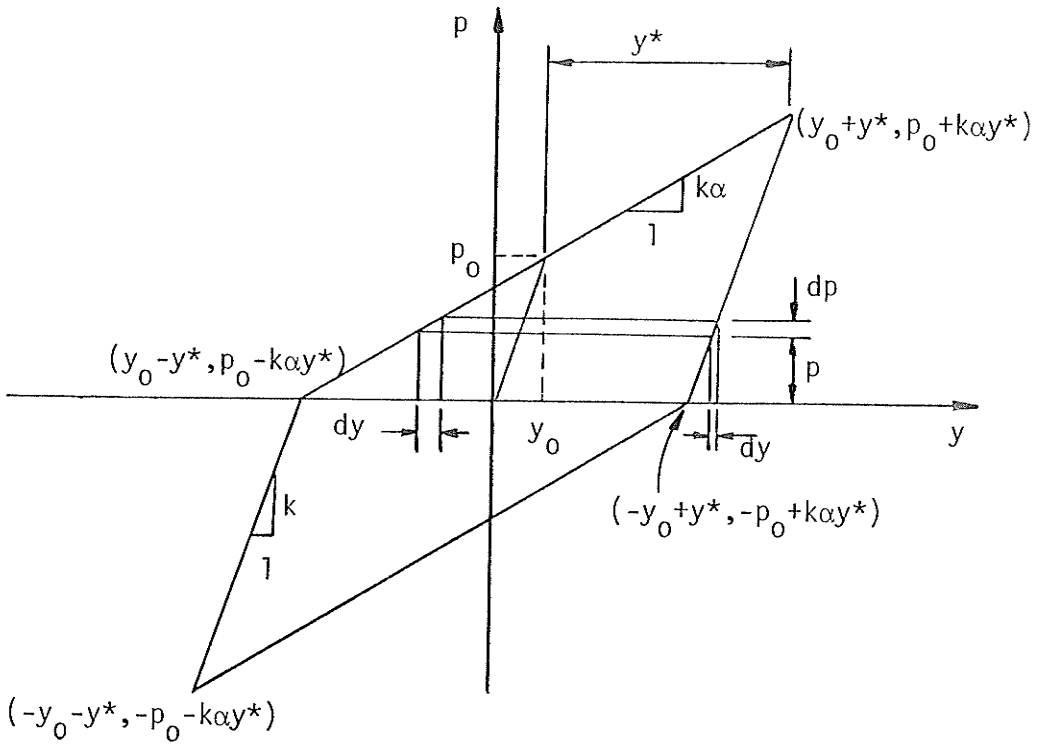

(a) $p_o - k\alpha y^* = 0$

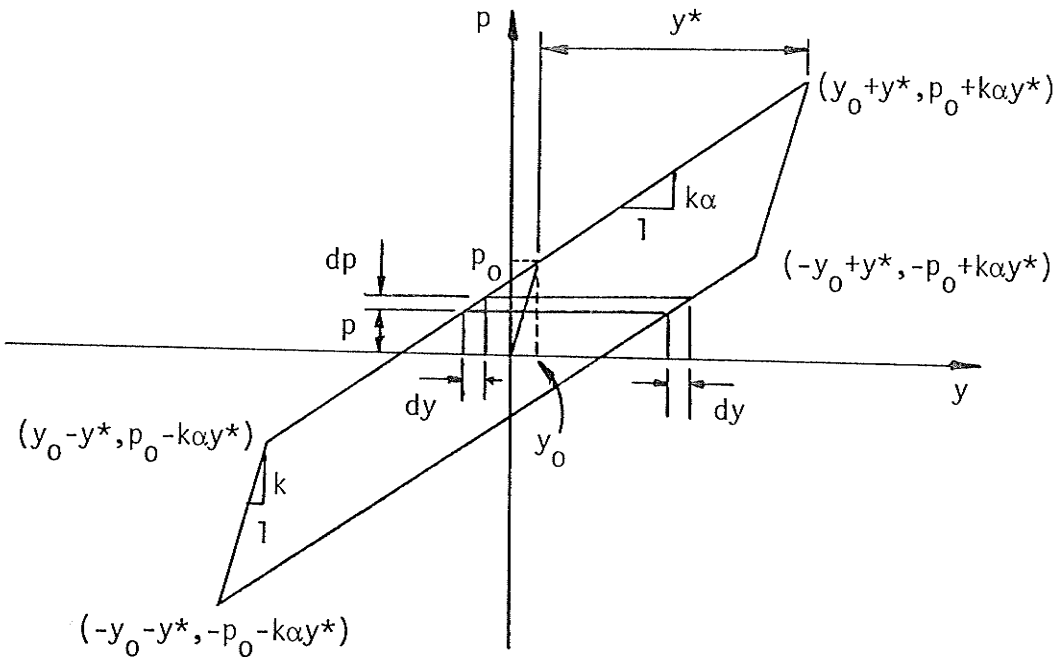

(b) $p_o - k\alpha y^* < 0$

Figure F.2 Restoring Force Versus Displacement
($p_o - k\alpha y^* \leq 0$)

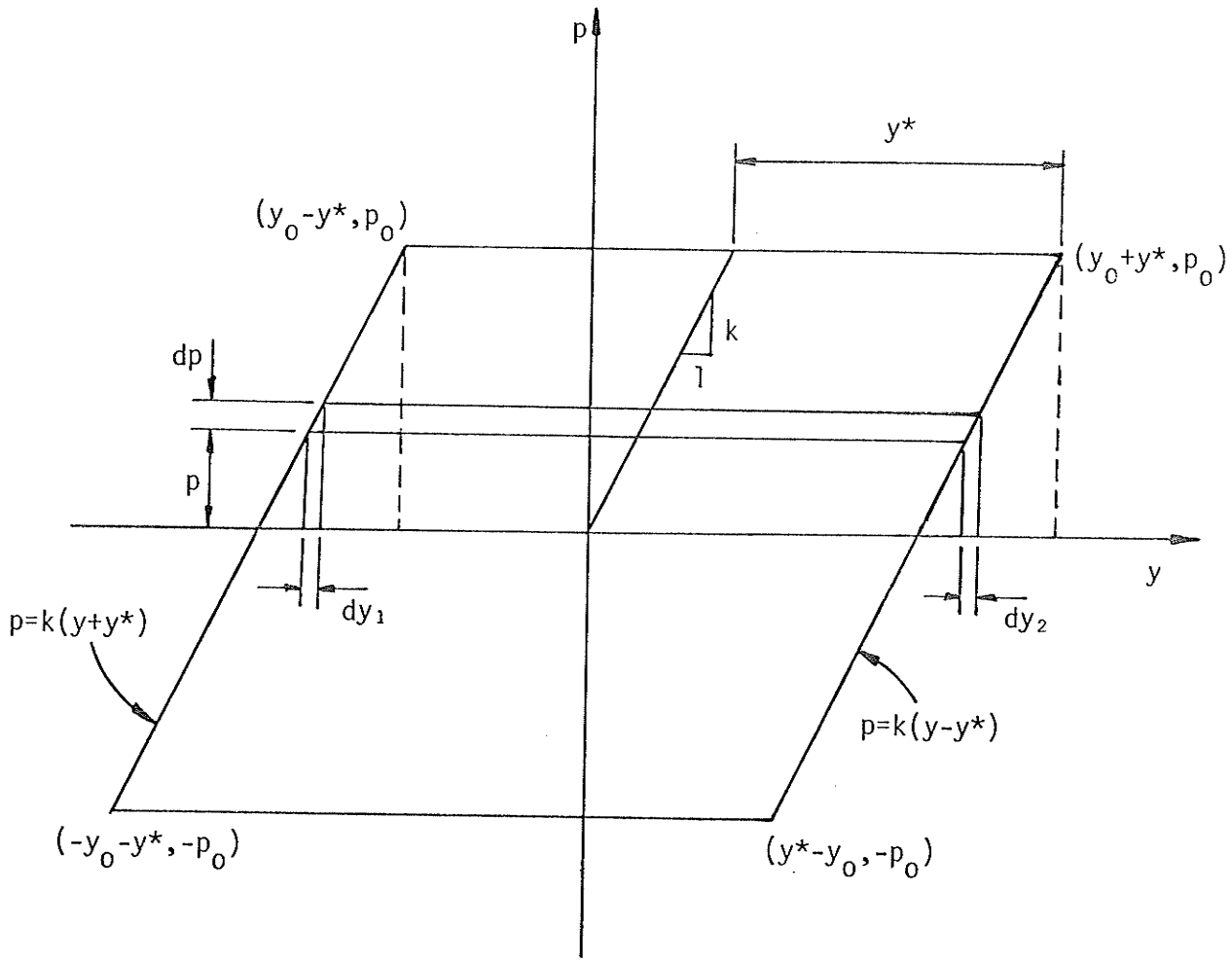

Figure F.3 Restoring Force Versus Displacement
(α = 0)

At the flat-top region, the probability of p having a value of p_o is equal to the probability of y having a value in the region from $y = y_o - y^*$ to $y = y_o + y^*$. Mathematically,

$$pr(p_o) = \int_{y_o - y^*}^{y_o + y^*} pr(y)dy \ .$$

Substituting equation (4.1) into the above equation and integrating, the equation becomes, after normalizing

$$pr(p_o) = \frac{1}{4} \left[\text{erfc} \left(\frac{y_o - y^*}{\sqrt{2}\,\sigma_y}\right) - \text{erfc} \left(\frac{y_o + y^*}{\sqrt{2}\,\sigma_y}\right)\right] , \qquad \text{(F.9)}$$

where erfc is the complimentary error function. The same expression can be obtained for $pr(-p_o)$. Combining equations (F.8) and (F.9), the probability density function of p for the elasto-plastic case becomes

$$pr(p) = \begin{cases} \frac{A}{2} \left[e^{I_1} + e^{I_2}\right] , & |p| < p_o \\ \frac{1}{4} \left[\text{erfc} \left(\frac{y_o - y^*}{\sqrt{2}\,\sigma_y}\right) - \text{erfc} \left(\frac{y_o + y^*}{\sqrt{2}\,\sigma_y}\right)\right] , & p = \pm p_o \ . \end{cases} \qquad \text{(F.10)}$$

A P P E N D I X G

PHYSICAL-ANALOG MODEL OF A BILINEAR HYSTERETIC ELEMENT

APPENDIX G

PHYSICAL-ANALOG MODEL OF A BILINEAR HYSTERETIC ELEMENT

A physical-analog model was constructed to validate the theoretical results for a bilinear hysteretic element. The block diagram of this model is shown in Figure G.1. The input signal was provided by a random signal generator. This signal was fed to an electromagnetic shaker and the resulting random displacement became the input to the hysteretic element. A capicitance transducer was installed as shown to pick up the displacement input voltage signal. This signal was fed to a solid state circuit in which the hysteretic effect was produced and different values of p_o, k and α could be selected. An analog differentiator was also included in this circuit. The outputs of this circuit were two voltages, one, v_p, proportional to the required bilinear restoring force and the other, $v_{\dot{y}}$, proportional to the velocity. The restoring force signal was further processed in an amplifier to produce a current, i_p, proportional to the restoring force signal. Thus, a mechanical hysteretic force was produced by allowing the current to flow in a coil placed in an electromagnetic field. This force was measured by a piezoelectric force transducer and the resulting signal passed to one input of a multiplier and time averager. The velocity signal formed the other multiplier input. A simple switching arrangement permitted the quantities $\overline{p\dot{y}}$, $\overline{pp}$ and $\overline{\dot{y}\dot{y}}$ to be measured and the power ratio to be evaluated. It is noted that the power ratio, being a normalized factor, is dimensionless and calibration of force and velocity is not required.

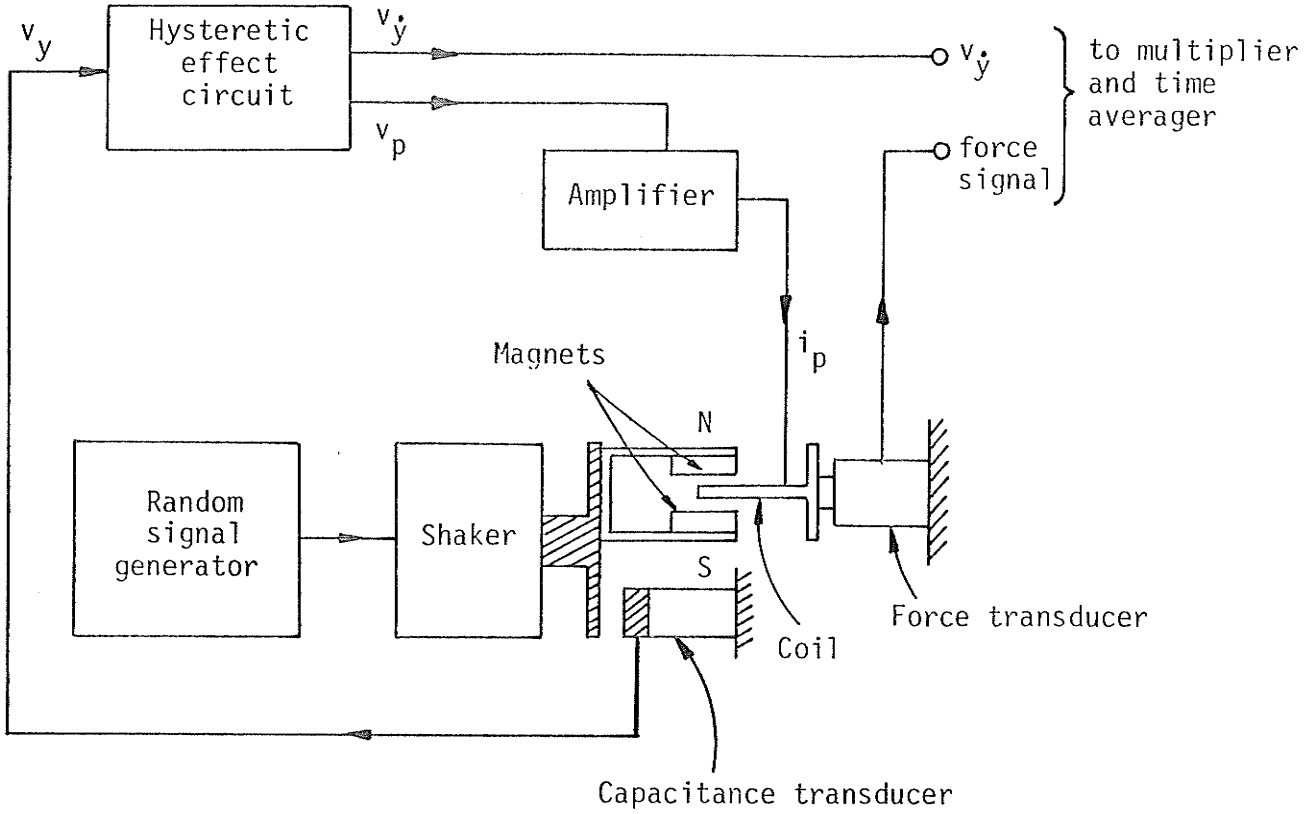

Figure G.1 Block Diagram of Physical-Analog Model of Bilinear Hysteretic Element

The hysteretic effect circuit is shown in Figure G.2. The input signal is multiplied by a factor k_1, the value of which is controlled by the variable resistance VR1 as shown on the left part of the figure. The diodes, D_1 and D_2, and the capacitor shown in the central part of the figure form the hysteresis generating portion of the circuit. A simplified explanation of the circuit functions is as follows. The output voltage of amplifier A_2 is a linear version of the voltage, v_y, which, in turn, is proportional to displacement, y. Thus, if the displacement is assumed to be increasing linearly with time the voltage at the "+ ve" input to amplifier A_3 will follow providing only that the total leakage current on the 2.2 μF capacitor is negligible. Under these conditions, a straight-line relationship between the output of A_3 and the input v_y is given with the constant of proportionality k_1, being set by VR1 [similar to A-B, Figure G.3(a)]. As the magnitude of the output voltage of A_2 increases, a point is reached where either D_1 or D_2 conducts. At this point no further increase in voltage occurs at the output of A_3 and the 2.2 μF capacitor is charged to the voltage difference between the switch-on voltage of the diode and the output voltage of A_2. As a result, the output voltage of A_3 remains constant at the bias (switch-on) voltage of the diode [similar to B-C, Figure G.3(a)]. If now the direction of the linearly changing displacement is reversed the diode ceases to conduct and the straight-line relationship between v_y and the output of A_3 is re-established [similar to C-D, Figure 6.3(a)]. Thus, so long as the bias voltage of either diode is not exceeded, a straight-line relationship (C to E) will be maintained. The diodes are of course reversely connected and are oppositely biased through ampli-

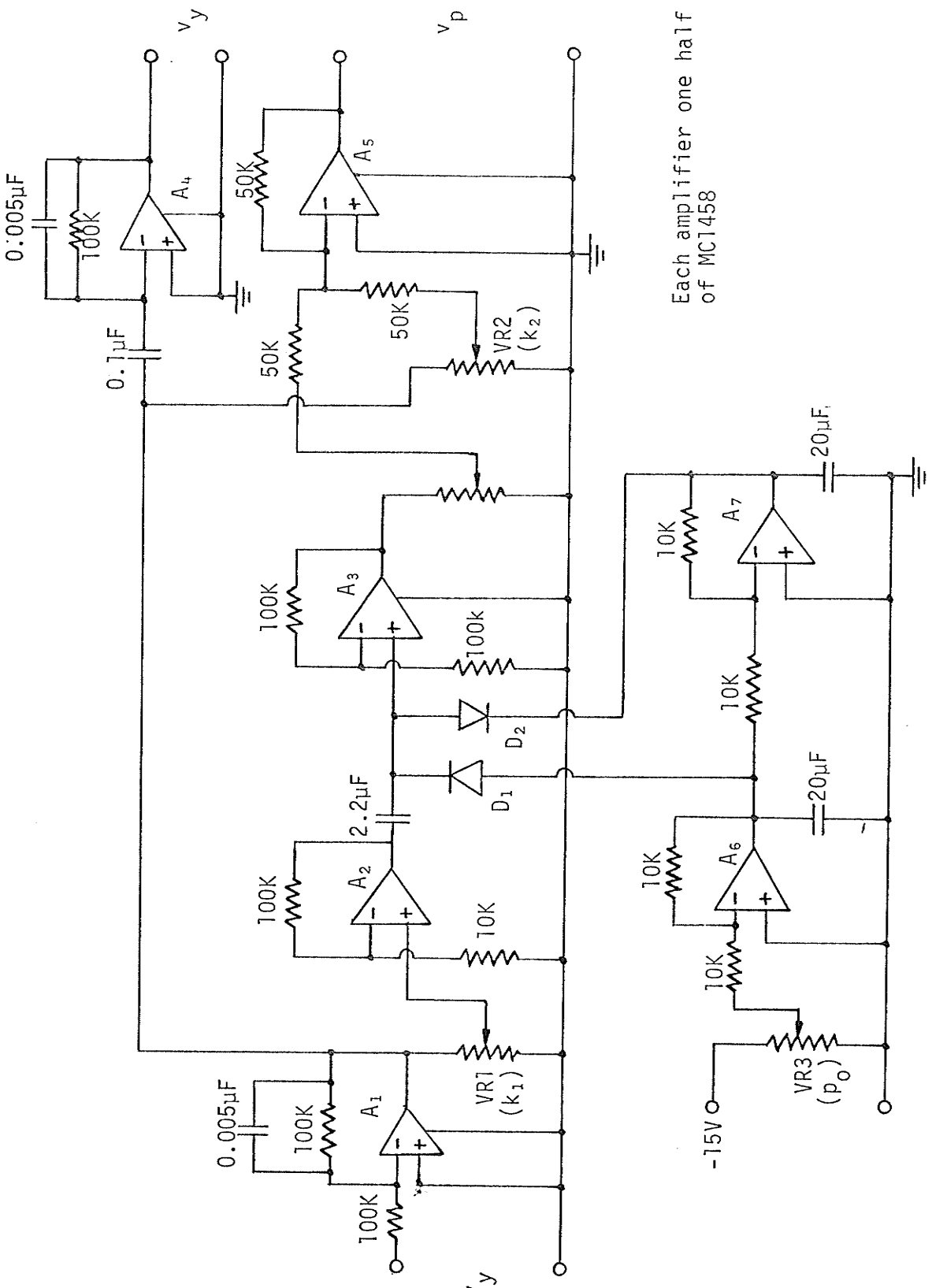

Figure G.2 Hysteretic Effect Circuit

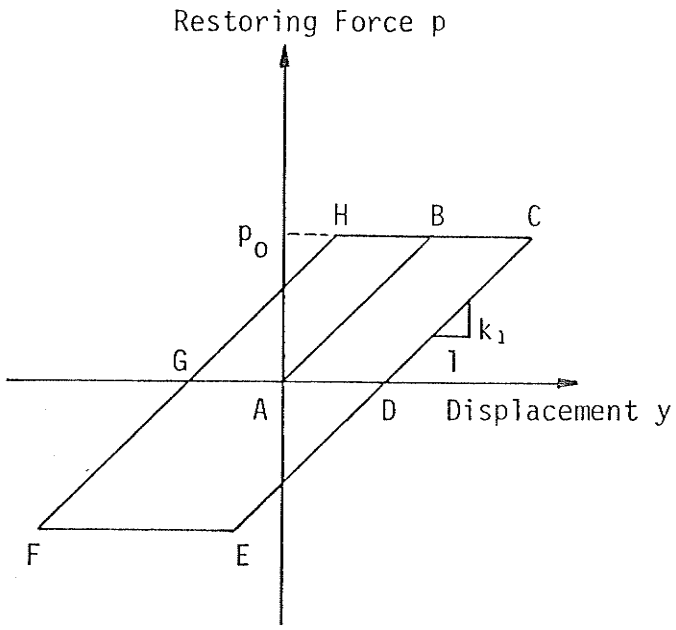

(a) Initial p-y Relationship

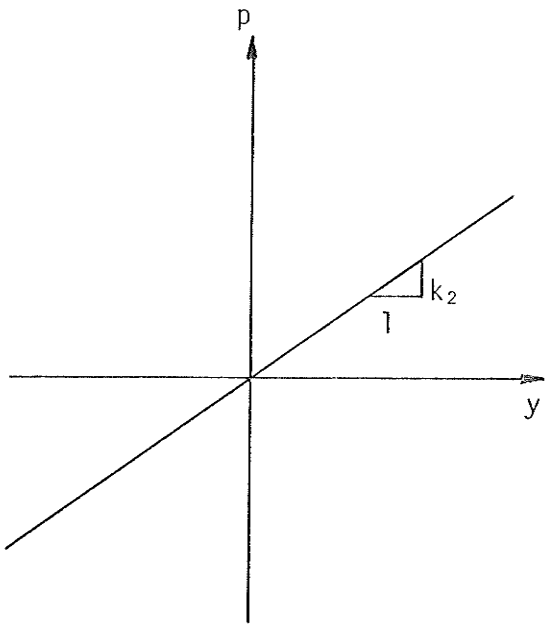

(b) Additional Linear Stiffness

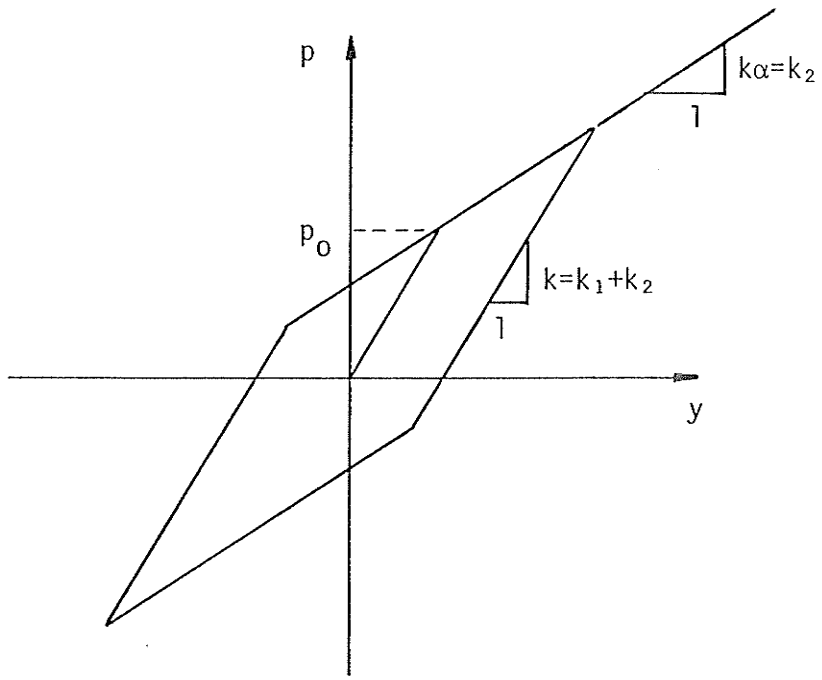

(c) Output p-y Relationship

Figure G.3 Generation of Bilinear Hysteretic p-y Relationship

fiers A_6 and A_7. In this way, the required positive and negative "yield" points are provided. Control of the "yield" value, p_o, is given by the potential divider VR3 connected to the -15 volt supply line. This central part of the circuit (Figure G.2) produces the basic hysteretic relationship [Figure G.3(a)] between displacement, represented by v_y, and the output voltage of A_3.

The primary limitations of this simple circuit are, firstly, it will not function at extremely low frequencies and secondly, the dynamic range is limited by the maximum linear voltage swing permitted by the operational amplifiers A_1 and A_2. The first of these limitations is caused by the non-zero discharge rate of the 2.2 μF capacitor caused by the leakage resistances of D_1 and D_2 and the input circuit of A_3. The time constant was measured and found to be approximately 15 seconds and hence phase and gain errors are small down to a frequency of 0.1 Hz. The second limitation, limited linear voltage swing, set a limit on the maximum range of yielding [B-C, Figure G.3(a)] that could be achieved. This is the origin of the limitation quoted in Section 4.3.

The relationship between the input, v_y and the output of A_3 is hysteretic and of the form shown in Figure G.3(a). To provide a general bilinear hysteretic mechanism, the original input signal is multiplied separately by a factor k_2, a value controlled by the variable resistance VR2 shown on the right part of Figure G.2. This operation alone, gives rise to a $(p - y)$ relationship as shown in Figure G.3(b). When this effect is combined with that from the first stage, a general bilinear hysteretic mechanism is produced, as shown in Figure G.3(c).

The resulting force-displacement relationship has a first slope

of (k_1+k_2) and a second slope k_2. It may readily be seen that in this case (k_1+k_2) is equivalent to k and k_2 equivalent to $k\alpha$, where k and α are defined in Chapter 4. To provide the required velocity information the input, v_y, is differentiated with respect to time (using amplifier A_4 of Figure G.2) to provide the velocity proportional signal, $v_{\dot{y}}$.

To avoid the difficulties associated with excessive gain at spuriously high frequencies, "roll-off" capacitors were provided on amplifiers A_1 and A_2. Thus, due to these capacitors, the two amplifiers have upper frequency break-points of approximately 300 Hz.

Overall, the circuit of Figure G.2 gave a means of producing an hysteretic effect which could be controlled over a wide range of parameter values by the adjustment of VR1, VR2 and VR3. The useful frequency range was 0.1 Hz to 30 Hz and when combined in the circuit of Figure G.1 produced a similar, widely controllable, hystertic force. An indication of the performance of the system just described is given in Figure G.4 which shows an oscillogram of the hysteretic effect produced. In this case the input, v_y, is a random, Gaussian time function.

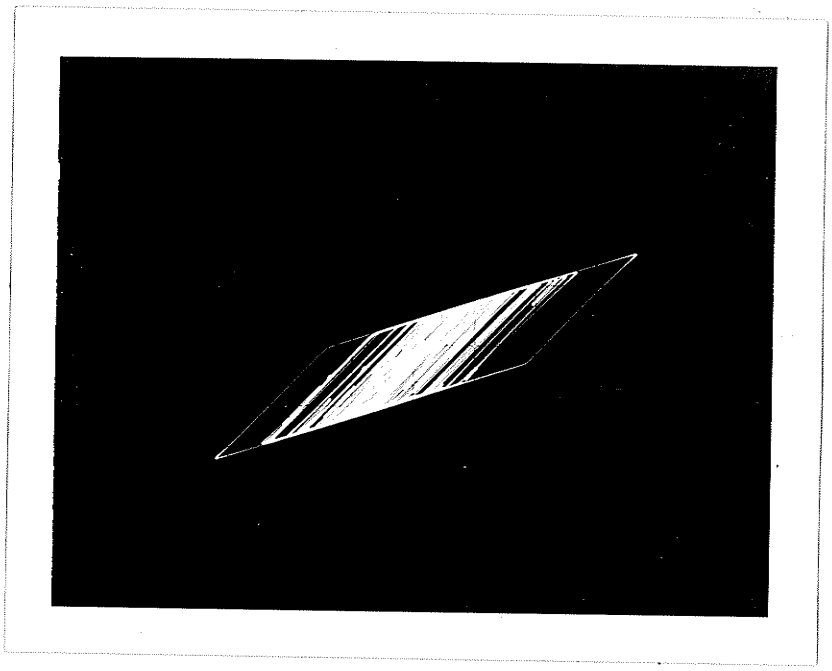

Figure G.4 Oscillogram of the Hysteretic Effect Produced

APPENDIX H

DIGITAL SIMULATION PROGRAM OF A BILINEAR HYSTERETIC ELEMENT

APPENDIX H

DIGITAL SIMULATION PROGRAM OF A BILINEAR HYSTERETIC ELEMENT

A digital simulation program was written for the evaluation of the power ratio of a bilinear hysteretic element subjected to excitation in the form of displacement. The program was coded in BASIC for the HP-9830 desk-top computer. To suit the limited storage capacity of the HP-9830, displacement input data was grouped into a number of records, each contained a maximum of 256 data. For simplicity of explanation, the processing of only one record of data is presented here.

The flow chart of the program is shown in Figure H.1. The program starts by reading the values of the parameters p_o, k and α of the element, the number of displacement input data N in the record and the time interval ΔT between adjacent data. Random displacement input data must be supplied by the user. Data of sinusoidal, triangular and square input waveform may be generated as desired. The constant A and B are defined as shown in Figure H.1.

Description of the program is aided by reference to Figure H.2, which shows the three deformed states of a bilinear hysteretic element. The first state is the forward yielding state. Here, the element yields while the displacement is increasing. The equation which governs the force and displacement is $p = Ay + B$. The second state is the non-yielding state in which the equation governing the force and displacement is $p = ky + p_1 - ky_1$, where (p_1, y_1) is an immediate past point on the line with known coordinates. The third is the backward yielding state, in

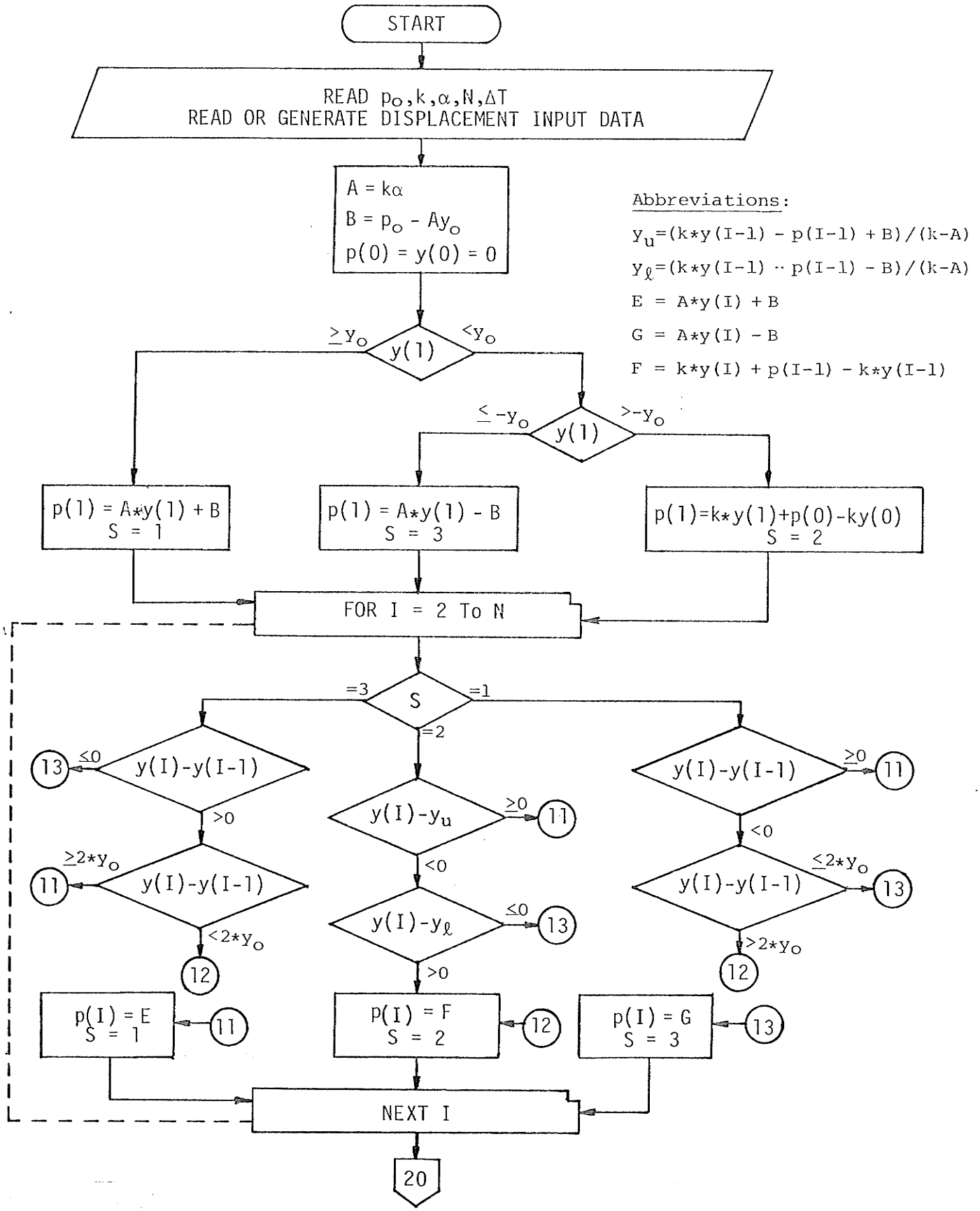

Figure H.1 (a) Flow Chart of Bilinear Hysteretic Element Simulation Program

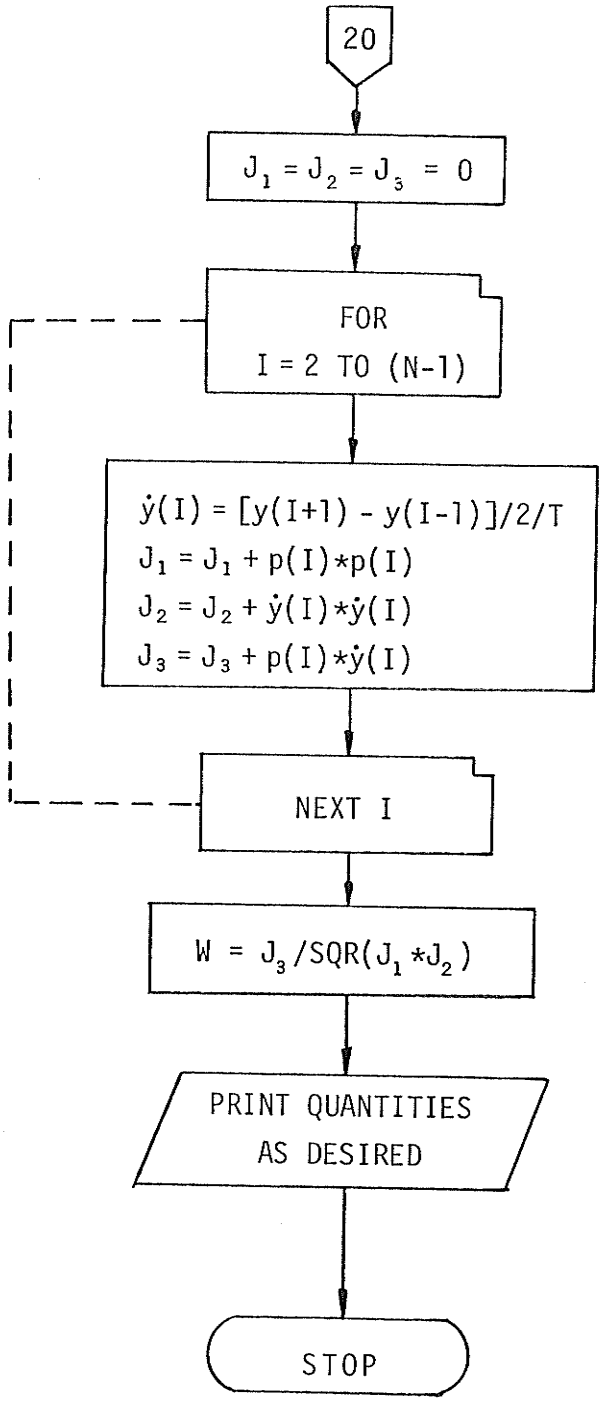

Figure H.1 (b) Flow Chart of Bilinear Hysteretic Element Simulation Program (Continued From Figure H.1(a))

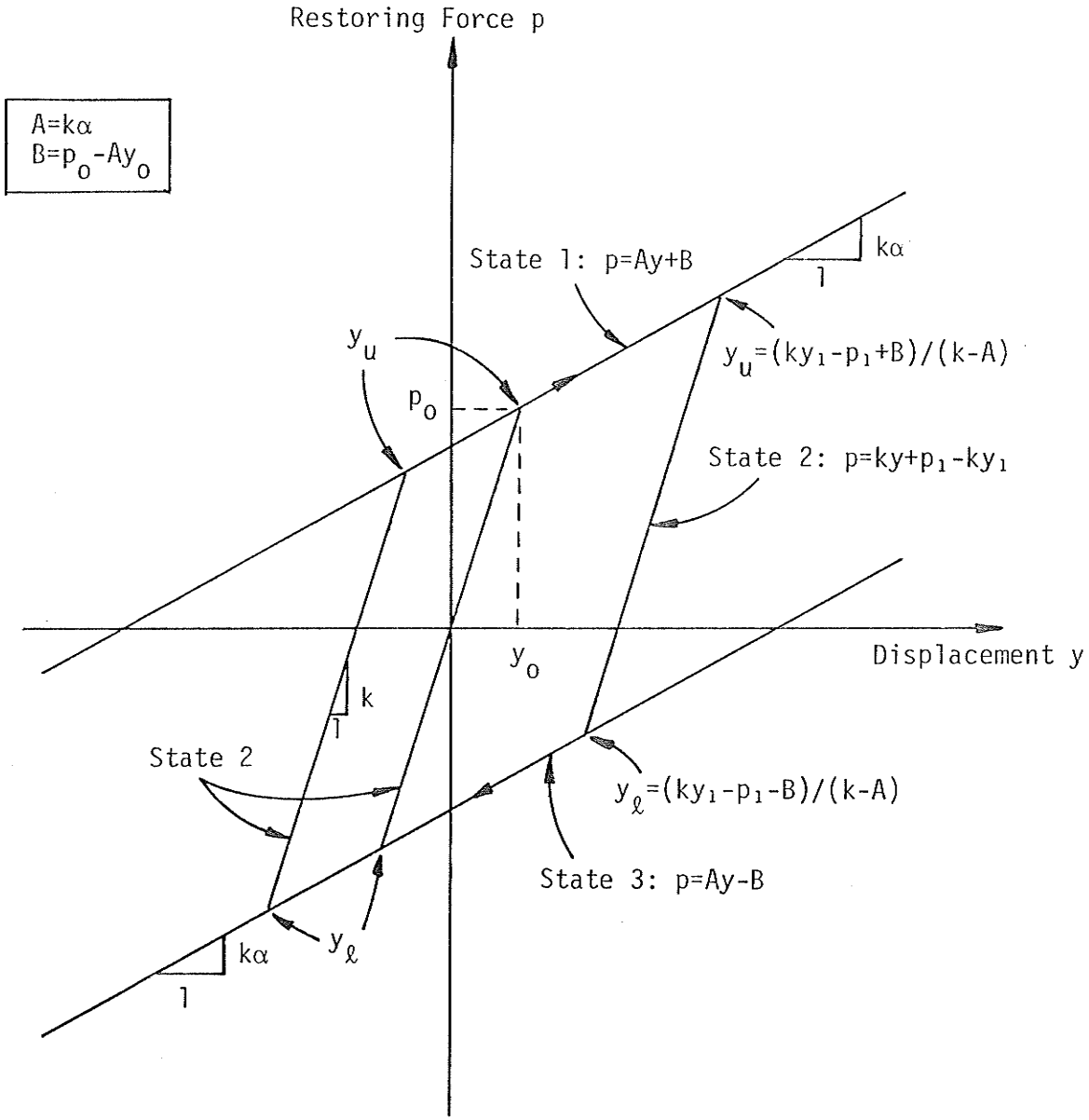

Figure H.2 Three Deformed States of a Bilinear Hysteretic Element

which case the element yields while the displacement is decreasing. The corresponding equation in this state is $p = Ay - B$. The displacement coordinate for the point of intersection between the equations of states 1 and 2 is $y_u = (ky_1 - p_1 + B)/(k - A)$, and that for the point of intersection between equations of states 3 and 2 is $y_\ell = (ky_1 - p_1 - B)/(k - A)$.

To start the calculation, it is assumed that the initial values of displacement y(0) and force p(0) are zero. The first displacement data y(1) is then examined (see Figure H.1). If y(1) is greater than or equal to y_o, the element will be in the forward yielding state (S = 1). If y(1) is less than or equal to $-y_o$, the element will be in the backward yielding state (S = 3). For other values of y(1), the element will stay in the non-yielding state (S = 2). In each of these cases, the value of p(1) can be calculated using the value of y(1) and the appropriate equation of each state. A repetitive loop is set up to continue the calculation, starting from the second displacement data.

Consider the I-th cycle of the loop. The value of S for the previous cycle is examined. For S equals to 1, the previous state of the element is forward yielding. Hence, if y(I) is greater than y(I-1) the element will remain in the first state. If y(I) is less than y(I-1) by more than $2y_o$, the element will be in the third state. Otherwise, the element will be in the second state. The value of p(I) is calculated for the appropriate state and the new value of S is noted.

If the previous value of S is 2, the previous state of the element is non-yielding. If, in this case, the value of y(I) is greater than or equal to y_u, the element will be in the first state. If y(I) is less than y_ℓ, the element will be in the third state. Otherwise, the element will remain in the second state. Appropriate values of p(I) and S are evaluated.

If the previous value of S is 3, the previous deformed state of the element is backward yielding. In this case, if y(I) is less than y(I-1), the element will remain in the third state. If y(I) is greater than y(I-1) by $2y_o$, the element will be in the first state. Otherwise, the element will be in the second state. Appropriate values of p(I) and S are evaluated.

The same procedure is repeated until all the displacement data are processed. As a result, values of restoring force correspond to every value of displacement are found.

The next step is to form the velocity time series from the displacement data. The I-th value of velocity is given by $\dot{y}(I) = \frac{y(I+1) - y(I-1)}{2\ \Delta T}$. By using a repetitive loop for values of I from 2 to (N-1), the velocity time series is obtained. Also, the quantities $J_1 = \Sigma p(I)*p(I)$, $J_2 = \Sigma \dot{y}(I)*\dot{y}(I)$ and $J_3 = \Sigma p(I)*\dot{y}(I)$ are obtained using the same loop. The power ratio is given by $W = J_3/SQR(J_1*J_2)$.

A P P E N D I X I

DIGITAL SIMULATION PROGRAM OF A BILINEAR HYSTERETIC SYSTEM

APPENDIX I

DIGITAL SIMULATION PROGRAM OF A BILINEAR HYSTERETIC SYSTEM

A digital simulation program was developed for the evaluation of power ratio of a bilinear hysteretic element coupled to a mass as in Figure 5.1. This program is thus the extension to the program as described in Appendix H for an hysteretic element, adding to it the effect of a mass. The program was coded in BASIC for the HP-9830 desk-top computer. As before, forcing input data were grouped into a number of records, each contained a maximum of 256 data. For simplicity, the version which processes only one record of data, and in which the integration time step is equal to the forcing time interval, is presented here.

The flow chart of the program is shown in Figures I.1 through I.4. The program starts by reading the values of parameters p_o, k, α and m of the model, the number of forcing input data N in the record and the time interval ΔT between adjacent data (equals to the integration time step). Random forcing input data must be supplied by the user. Data of sinusoidal, triangular and square input waveform can be generated in the program as desired. To start the calculation, it is assumed that the process starts from rest, so that the initial values of displacement, velocity, restoring force and input forcing are set to zero as shown in Figure I.1. The model is initially at the non-yielding state, S = 2 (refer to Figure H.3, Appendix H for the meanings of various deformed states) and the stiffness coefficient is k. A repetitive loop is established to calculate the system responses in a step-by-step manner.

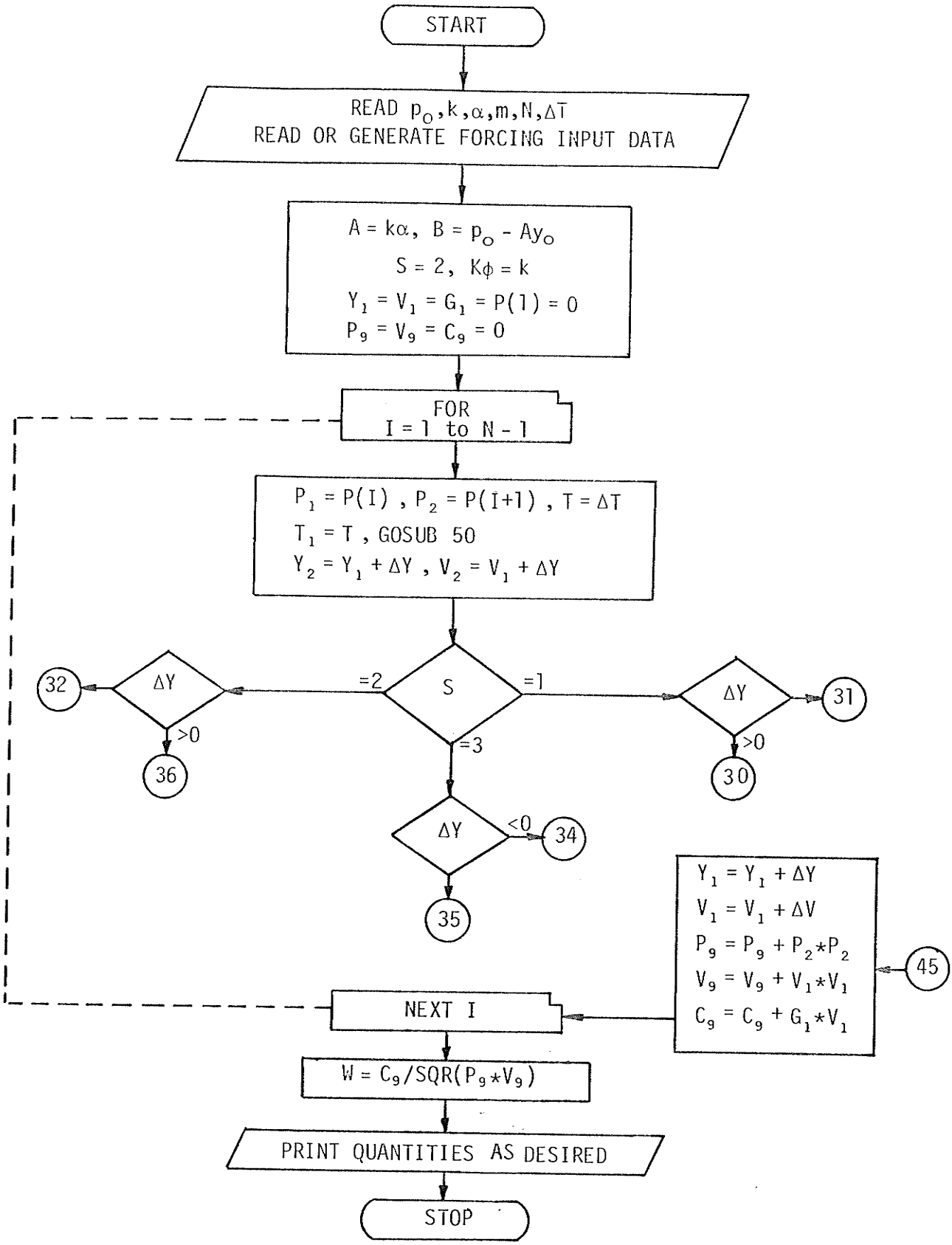

Figure I.1 Flow Chart of Bilinear Hysteretic System Simulation Program

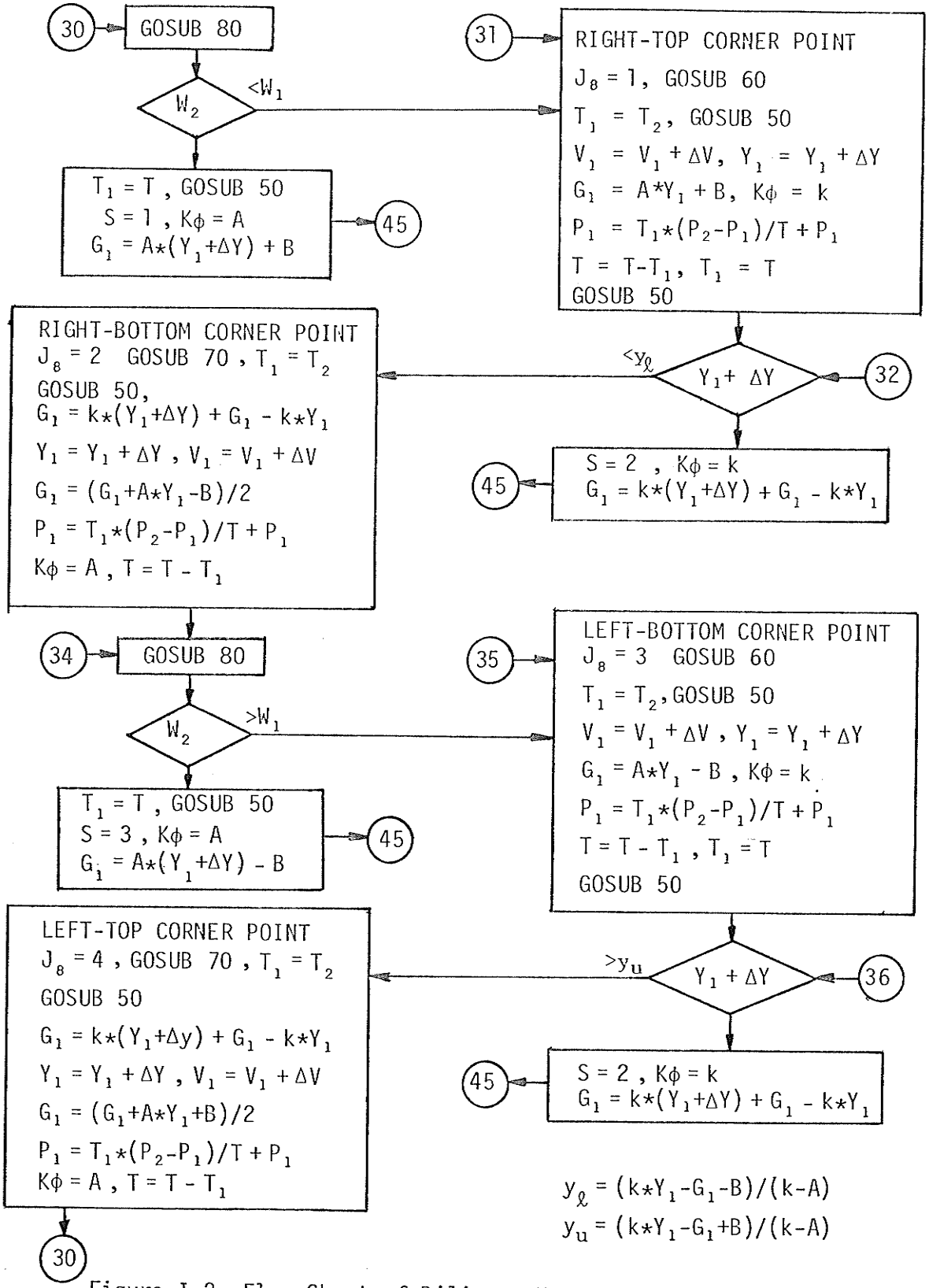

Figure I.2 Flow Chart of Bilinear Hysteretic System Simulation Program (continued from Figure I.1)

SUBPROGRAM 50 - NUMERICAL INTEGRATION

$Q_3 = 3*M$, $P_3 = 6*M/T_1$

$K_3 = 6*M/T_1/T_1$

$A_1 = (P_1-G_1)/M$

$\Delta K = K\phi + K_3$

$\Delta P = T_1*(P_2-P_1)/T + V_1*P_3 + A_1*Q_3$

$\Delta Y = \Delta P/\Delta K$

$\Delta V = 3*\Delta Y/T_1 - 3*V_1 - T_1*A_1/2$

RETURN

SUBPROGRAM 60 - LOCATE RIGHT-TOP AND LEFT-BOTTOM STATE-CHANGE POINTS BY TRIAL AND ERROR

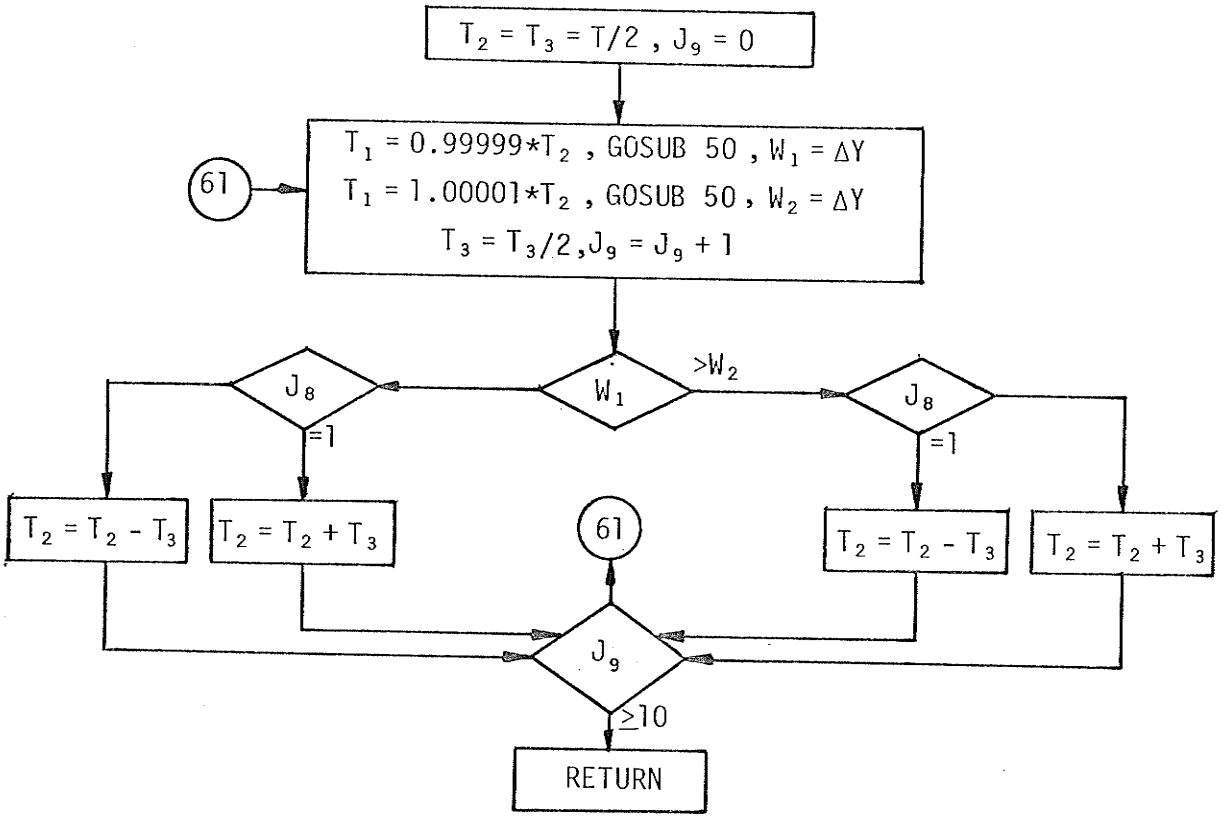

Figure I.3 Flow Chart of Bilinear Hysteretic System Simulation Program (continued from Figure I.2)

SUBPROGRAM 70 - LOCATE RIGHT-BOTTOM AND LEFT-TOP STATE-CHANGE POINTS BY TRIAL AND ERROR

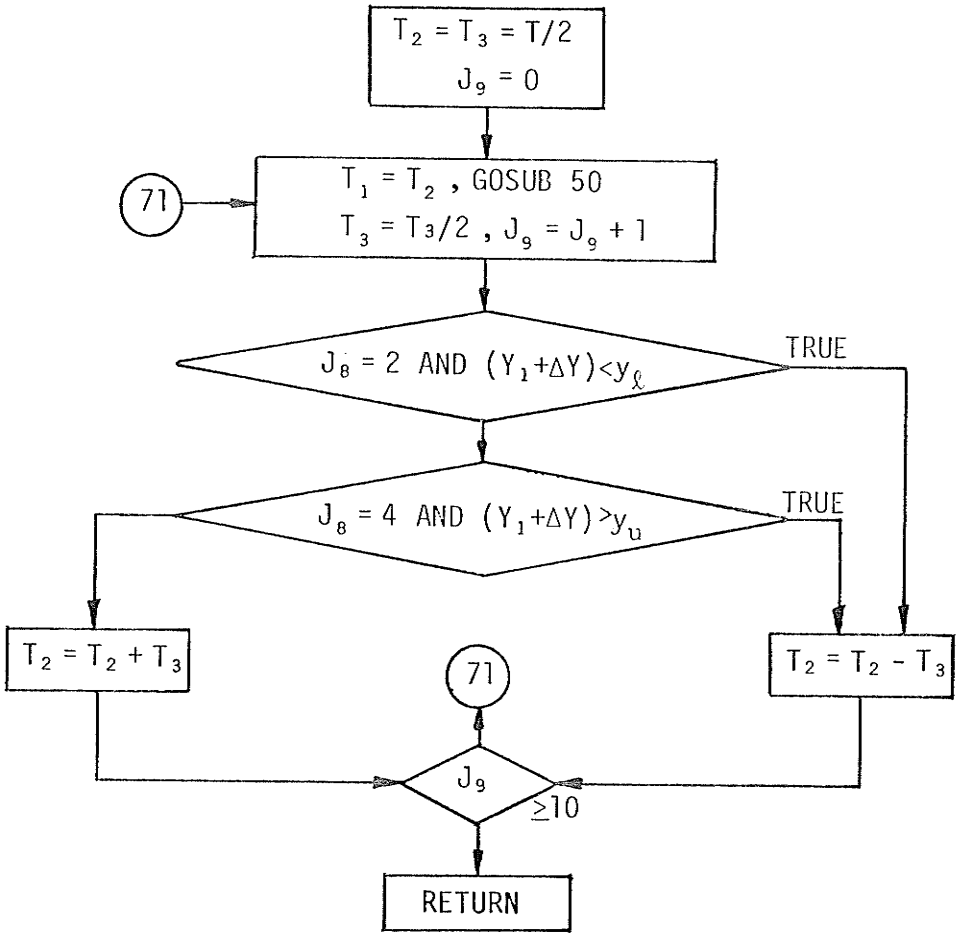

SUBPROGRAM 80 - TEST IF REMAINING IN THE YIELDING STATE

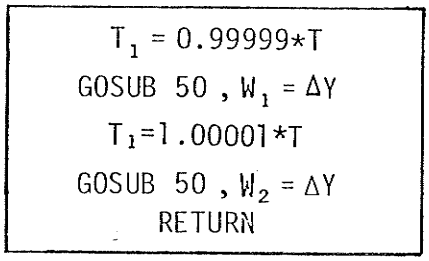

Figure I.4 Flow Chart of Bilinear Hysteretic System Simulation Program(continued from Figure I.3)

Consider the I-th cycle of operation. The values of forcing at the beginning and the end of the time step are noted. Subprogram 50 is then called to calculate the incremental displacement ΔY and velocity ΔV for the step [6]. Responses at the end of the time step are obtained by adding the incremental responses to those at the beginning of the step. The value of S for the previous cycle is examined.

If the value of S is 1, the previous state of the element is forward yielding. If ΔY for this step is positive, program control transferred to step 30, otherwise, control transferred to step 31. At program step 30, (Figure I.2), subprogram 80 is called to test if the forward yielding state is maintained at the end of the step, i.e. if W_1 is less than W_2 (W_1 is ΔY calculated at $T_1 = 0.99999T$ and W_2 is ΔY calculated at $T_1 = 1.00001T$), then the end of the step remained at state 1. The step is completed by storing the value of S, the stiffness at the new deformed state, KØ, and the values of restoring force G_1, displacement, Y_1, and velocity, V_1. These become the initial values of the next step. Values of force squared, velocity squared and restoring force times velocity are calculated and accumulated for each step. If W_2 is less than W_1, then there is a change of state in this step. Subprogram 60 is called to locate the right-top state-change point (J8 = 1) by trial and error. In this subprogram, the original time step is halved, and values of W_1 and W_2 are calculated as before. Whether state-change will occur before or after the present time step depends upon the values of W_1, W_2 and J8 and a quarter (one-eighth, one-sixteenth and so on for the latter cycles) of the original time step is either added to or subtracted from the present time step to form the new time step for the next cycle. The process is

repeated ten times, and the resulting values of time step is found to be within 0.3 percent of the true state-change time step. Using the state-change time just calculated, the forcing and responses at the state-change point are evaluated. These are then the initial values of the unfinished time step. Subprogram 50 is called to calculate ΔY and ΔV of the remaining step. If $Y_1 + \Delta Y$ is greater than y_ℓ (derived from Figure H.3), then the end of the step will stay at state 2, and the step is completed. If $Y_1 + \Delta Y$ is less than y_ℓ, then there is a further change of state, and subprogram 70 is called to locate the state-change point. This subprogram is similar to subprogram 60, it gives the state-change time after 10 cycles of trial and error operation. The values of forcing and responses at the state-change point are evaluated. Subprogram 80 is called to test if the end of the time step stays in the backward yielding state (state 3), and the process is continued for as many state-change points as may have in a single time step.

If, for the I-th cycle, the value of S of the previous cycle is 2, program control is transferred to step 36 for ΔY greater than zero, otherwise, control is transferred to step 32. As many state-change points may be located within the time step. Once the end of the time step is reached, values of responses are recorded as the initial values of the next cycle.

Similarly, if the value of S of the (I-1)th cycle is 3, program control is transferred to step 34 for ΔY less than zero, and transferred to step 35 otherwise.

After all cycles are completed, the power ratio of the model when subjected to the given forcing excitation, is given by W = C9/SQR(P9*V9).